BABAR Analysis Document #150, Version 003

B.A.D. 150

Draft Version 3

October 18, 2001

Exclusive Reconstruction of Hadronic B Decays to Open Charm

BReco AWG

October 18, 2001

Abstract

With the data recorded by the *BABAR* detector near $\sqrt{s} = 10.58$ GeV, we have fully reconstructed a variety of hadronic final states containing D^{*-}, D^{*0}, D^0 and D^+ mesons. In this paper, our B candidate reconstruction and selection techniques are described.

Contents

1 Introduction

This document reports our efforts to fully reconstruct B meson decays into a variety of channels containing a D^{*+}, D^{*0}, D^{+}, or D^{0} and a π^{-}, ρ^{-}, or a_1^{-}. These are the dominant modes leading to open charm in the final state, all being governed by a tree-level diagram with an external W^{-} emerging as the light hadron state.

The purpose of reconstructing B decays in these modes is to provide a large sample of $\Upsilon(4S)$ events where one reconstructed B gives a clean tag of the state of the recoil B in the event, with a purity of around 90%. Such a sample will be used in studies of B lifetimes, B^0 mixing, and as a means of determining, from the data itself, the effective tagging efficiency through use of information about the decay products of the recoil B. These studies are described elsewhere.

The channels currently under study are listed in Table 1. [1] The D^{*+} is reconstructed in the mode $D^0\pi^+$, the D^{*0} into $D^0\pi^0$ mode. The D^0 is found in the modes $K^-\ \pi^+$, $K^-\ \pi^+\ \pi^0$, $K^0_S\ \pi^+\ \pi^-$, and $K^-\ \pi^+\ \pi^+\ \pi^-$. For the D^+, the channels $K^-\ \pi^+\ \pi^+$ and $K^0_S\ \pi^+$ are included. B candidate reconstruction is based on standard selection techniques and background suppression methods, implemented using the `CompositionTools` package. The data used for the current study was obtained using the *BABAR* detector, operating in the PEP-II storage ring at energies near $\sqrt{s} = 10.58$ GeV. They constitute a sample equivalent to approximately $20.7 \pm 0.3\,\mathrm{fb}^{-1}$ on resonance recorded over the period from October, 1999 to December, 2000.

B Mode
$\overline{B}^0 \to D^{*+}\pi^-$
$\overline{B}^0 \to D^{*+}\rho^-$
$\overline{B}^0 \to D^{*+}a_1^-$
$\overline{B}^0 \to D^{+}\pi^-$
$\overline{B}^0 \to D^{+}\rho^-$
$\overline{B}^0 \to D^{+}a_1^-$
$B^- \to D^{*0}\pi^-$
$B^- \to D^{0}\pi^-$

Table 1: B decay channels examined in this analysis.

This report is organized as follows: Section 2 will describe the data and Monte Carlo samples and the event pre-selection techniques, Section 3 will provide a detailed description of the final candidate selection requirements, Section 4 will summarize the observed signals in B^0 channels, Section 5 will do the same for B^+ modes, and Section 6 will draw conclusions.

[1] Here, and throughout this document, we use the convention that a particular candidate state also implies the charge conjugate state is included.

2 Data Sample and Pre-Selection Criteria

2.1 Data Samples

This section describes the data samples used for this selection and to study backgrounds, as well as the Monte Carlo event samples used to study and optimize the selection. The data sample is referred to as the "TagMix Run 1" sample since it is used for a variety of time-dependant studies, including measurements of Δm_d, Γ_B, and the measurement of tagging dillutions in the combined fit with CP modes to extract $\sin 2\beta$.

2.1.1 Good Run Criteria

"Good runs" are selected using the following information recorded in the electronic logbook and OPR book-keeping database [9]:

- the run type should be "Colliding Beams",
- all subdetectors should be "on",
- the global data quality entered by the Data-Quality shift taker should be "good",
- the recorded luminosity should be non-zero, and
- the OPR processing status should be "done".

Some further checks are made on the self consistency of the electronic logbook information for a run, and by checking some OPR monitoring plots.

2.1.2 Run 1 Data Sample

The Run 1 data sample consists of 3371 runs in the range 9931–17106, for a total integrated luminosity of about $20.7\,\text{fb}^{-1}$ on resonance. This sample is not homogeneous, but can be divided into a few reasonably homogeneous sub-samples. The main effects to consider are the center of mass energy and the quality of the silicon vertex detector's (SVT) internal alignment.

Table 2 summarizes the main statistics for each sub-sample. Figure 1 shows the run-by-run offsets of the center of mass energy relative to the average values for a sub-sample of the Run 1 data.

Some of the plots in this note refer to a typical run: we choose run 12917 from sub-sample `good-2000-b1-s5-r8D-on2`. Table 3 summarizes the main parameters of this run.

2.1.3 Monte Carlo Samples

The Monte Carlo samples used in this report are taken from productions based on the releases 8.6.5 and 8.8.0. The background events mixed into these samples were taken from a sample of random triggers representative of the Run 1 data set.

Block	Set	List	Release / Alignment	Comment	$\int \mathcal{L}dt$ (fb^{-1})
1999-1	0	`good-1999-b1-s0-r8B-on0`	8.6.4d / A	DCH HV 1900V	426
2000-1	0	`good-2000-b1-s0-r8B-on0`	8.6.4d / C	DCH HV 1900V	607
	1	`good-2000-b1-s1-r8C-off0`	8.6.5a / C		139
		`good-2000-b1-s1-r8C-on1`	8.6.5a / C		545
	2	`good-2000-b1-s2-r8A-on1`	8.6.3c / C		1561
		`good-2000-b1-s2-r8A-off1`	8.6.3c / C		175
	3	`good-2000-b1-s3-r8C-on1`	8.6.5a / C	bad timing	268
	4	`good-2000-b1-s4-r8A-off1`	8.6.3c / D		109
		`good-2000-b1-s4-r8A-on2`	8.6.3c / D		707
	5	`good-2000-b1-s5-r8D-on2`	8.6.5b,e / E		1650
		`good-2000-b1-s5-r8D-off2`	8.6.5b,e / E		311
		`good-2000-b1-s5-r8D-on3`	8.6.5b,e / E		397
	6	`good-2000-b1-s6-r8A-on3`	8.6.3c / D		2174
		`good-2000-b1-s6-r8A-off3`	8.6.3c / D		448
		`good-2000-b1-s6-r8A-on4`	8.6.3c / D		2241
2000-2	0	`good-2000-b2-s0-r8A-on4`	8.6.3c / D	DCH HV at 1960 V	289
	1	`good-2000-b2-s1-r8A-on4`	8.6.3c / E		824
		`good-2000-b2-s1-r8A-off4`	8.6.3c / E		370
		`good-2000-b2-s1-r8A-on5`	8.6.3c / E		697
	2	`good-2000-b2-s2-r8D-on5`	8.6.5b,e / E	new IFR gas mix	845
	3	`good-2000-b2-s3-r8D-on5`	8.6.5b,e / E	DCH in FADC mode	1721
		`good-2000-b2-s3-r8D-off5`	8.6.5b,e / E		516
		`good-2000-b2-s3-r8D-on6`	8.6.5b,e / E		2524
		`good-2000-b2-s3-r8D-off6`	8.6.5b,e / E		395
	4	`good-2000-b2-s4-r8E-on7`	8.8.0e,g / E		2087

Table 2: Summary statistics for the sub-samples of the Run 1 dataset. Only good runs are included. Average center of mass energies are calculated from the PEP-II beam energies, relative to the nominal $\Upsilon(4S)$ mass of $10.580\,\mathrm{GeV}/c^2$.

2.2 Event Pre-Selection

Pre-selection starts from events assigned to the `isPhysicsEvents` stream in online prompt reconstruction (OPR). This stream includes events assigned to any of the physics sub-streams by the background filter (BGF). We do not make any explict requirement that events belong to the `BGFMultiHadron` sub-stream, but in practice, our requirements on charged track multiplicity and event shape are tighter than those for the `BGFMultiHadron` list (3 or more tracks, $R_2 < 0.98$). One subtlety to consider is that the track definition used by the background filter is not strictly looser than the definitions used in analysis, because it is based only on drift chamber information. A second pass of the preselection process consists in the production of ntuples for the final selection, with a tighter (but not yet final) selection.

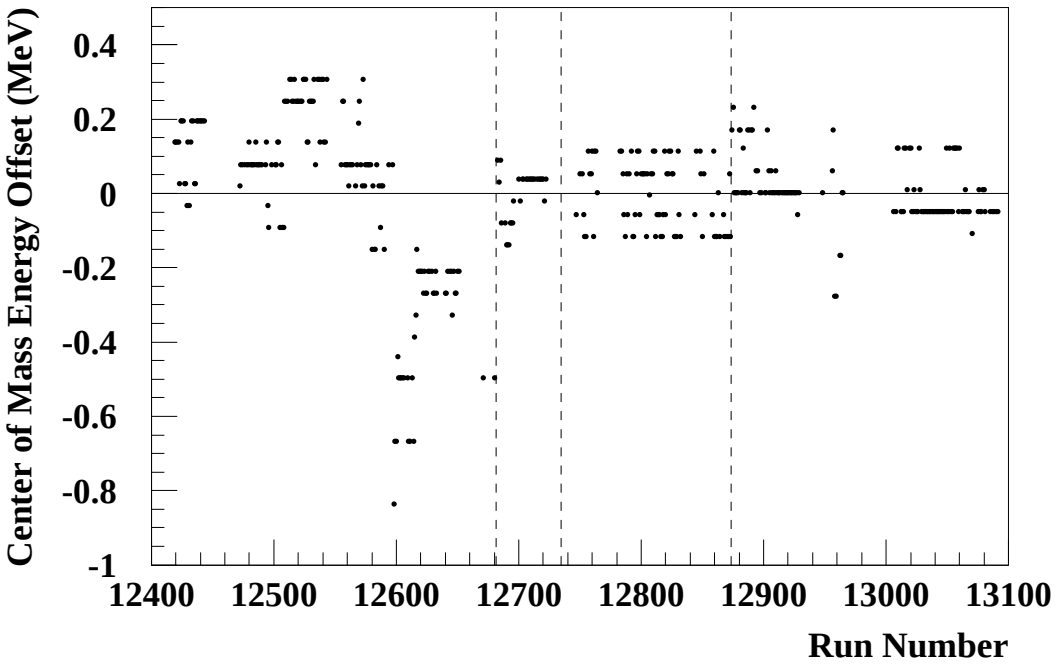

Figure 1: Run by run offsets of the center of mass energy calculated from the PEP-II beam energies relative to the average center of mass energies for a sub-sample of the runs included in Table 2

HER Energy	8.9711 GeV
LER Energy	3.1193 GeV
CM Energy	10.580 GeV
Integrated Luminosity	12.7 pb^{-1}
`isPhysicsEvents`	199,648

Table 3: Parameters of the typical run 12917, recorded from 8:06–11:06am on April 23, 2000.

2.2.1 Reconstruction Lists

The particles observed in the detector from the decay modes used in this selection are $K^{\pm}$, $\pi^{\pm}$, $e^{\pm}$, $\mu^{\pm}$, and γ. The basic objects corresponding to these particles and reconstructed in the detector are organized into the following lists[2], according to whether they are charged or neutral [10]:

- `ChargedTracks`: All tracks reconstructed in the drift chamber and/or the vertex detector, with parameters determined using a $\pi^{\pm}$ mass hypothesis.
- `GoodTracksVeryLoose`: A subset of the `ChargedTracks` list containing tracks with:
  1. a maximum momentum measured in the lab frame of 10 GeV/c, and

[2]List definitions differ slightly from release used for expedited skims (used for production of first 18.5 fb^{-1}) and full skims (used for production of last 2.2 fb^{-1}). In cases where there is a difference, the value used for the expedite skims is listed in parenthesis.

2. a distance of closest approach to the per-run nominal beam spot centroid of $\sqrt{\Delta x^2 + \Delta y^2} < 1.5$ cm, and $|\Delta z| < 10$ cm.

- `GoodTracksLoose`: A subset of the `GoodTracksVeryLoose` list containing tracks with:

  1. a minimum transverse momentum of 100 MeV/c, and
  2. at least 12 (20) hits recorded in the drift chamber, out of a possible maximum of 40 hits for tracks perpendicular to the beam pipe.

- `GoodTracksTight`: A subset of the `GoodTracksLoose` list containing tracks with:

  1. a minimum transverse momentum of 100 MeV/c,
  2. at least 20 hits recorded in the drift chamber, and
  3. a distance of closest approach to the per-run nominal beam spot centroid of $\sqrt{\Delta x^2 + \Delta y^2} < 1.0$ cm, and $|\Delta z| < 3.0$ cm.

  This list is exclusively used for reconstructing the primary vertex of the event, widely used for kinematic fitting of π^0 candidates.

- `CalorNeutral`: All "bumps" (local maxima of calorimeter energy deposit) not matched with any track, with parameters determined using a photon mass hypothesis.

- `GoodPhotonLoose`: A subset of `CalorNeutral` list with the following additional requirements:

  1. a minimum energy of 30 MeV,
  2. an upper cut on the lateral moment at 0.8.

- `GoodPhotonDefault`: A subset of `GoodPhotonLoose` list but with a minium energy of 100 MeV.

Figure 2 compares some inclusive charged-track distributions for the successively tigher track requirements. Figure 3 shows similar distributions for neutral calorimeter bumps.

2.2.2 Composition Lists

The composite particles used in this selection are: π^0, K^0_S, ρ^0, ρ^+, a_1^+, D^0, D^+, D^{*0} and D^{*+}. We identify candidates for each of these composites by combining entries in the reconstruction lists, and possibly other composite lists, and requiring that the resulting combinations pass loose kinematic cuts (applied to four-vector sums, without any refitting to include geometric or kinematic constraints, except for the case of π^0 candidates). Table 4 summarizes the different decay modes represented by the composite lists used in this selection.

π^0 Lists

The π^0 selection starts combining pairs of entries in the `GoodPhotonLoose` (`CalorNeutral`) list to define the `pi0VeryLoose` list, defined with the following requirements:

1. both bumps having a minimum energy of 30 MeV,

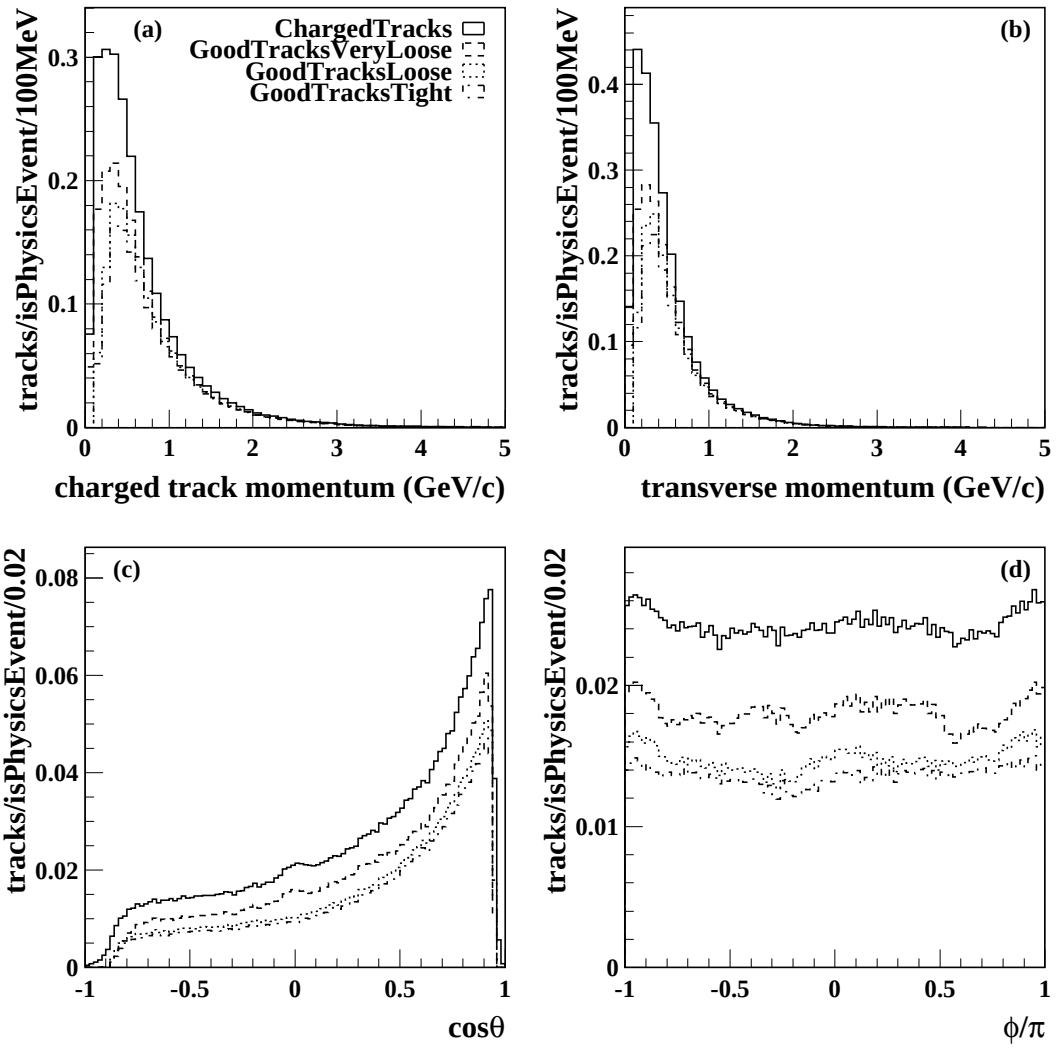

Figure 2: Distributions of (a) total momentum, (b) transverse momentum, (c) cosine of polar angle, and (d) azimuthal angle (all measured in the lab frame) for the charged track lists: `GoodTracks`, `GoodTracksVeryLoose`, `GoodTracksLoose`, `GoodTracksTight`. The plots are made from a typical run (number 12917) and normalized to display tracks/`isPhysicsEvent`/bin. The cut $R_2 < 0.45$ has been applied in these plots.

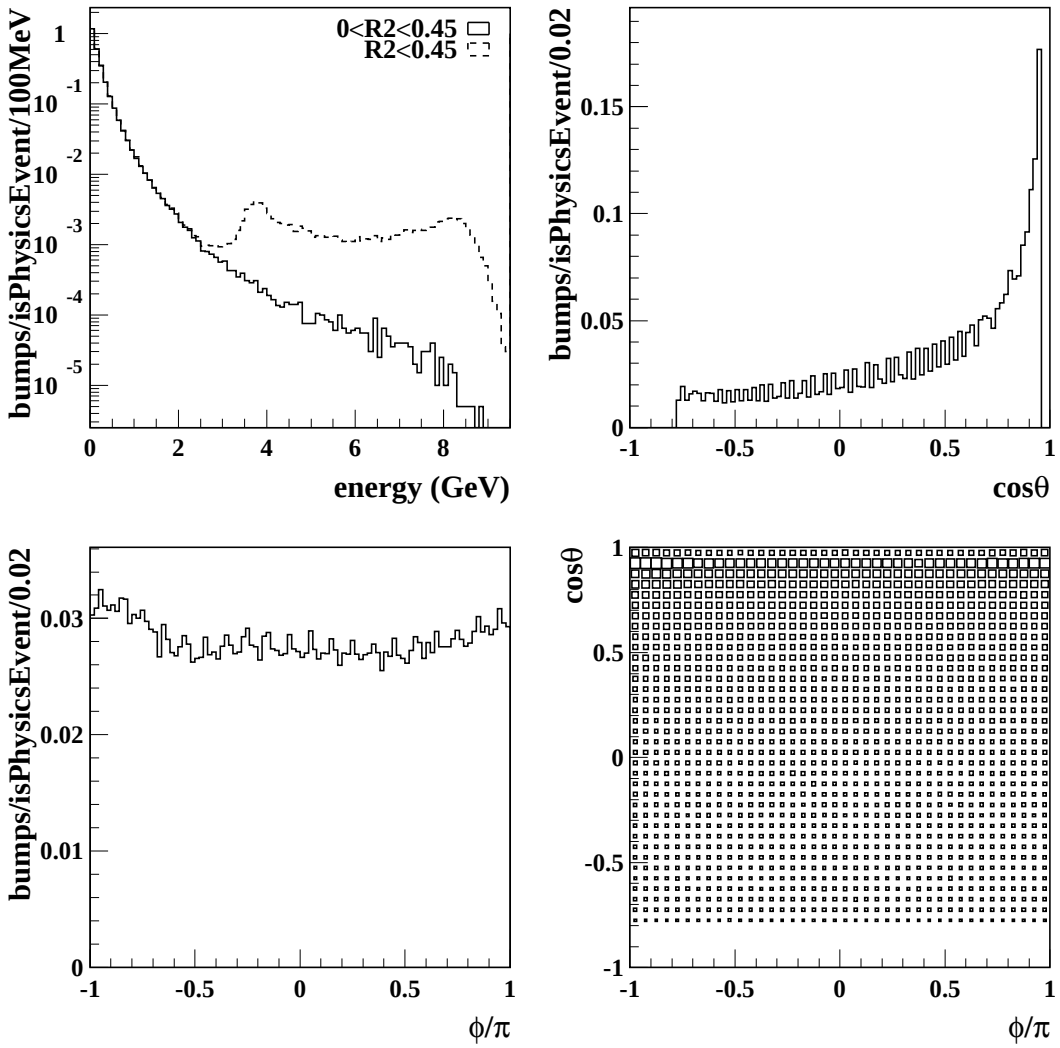

Figure 3: Distributions of (a) total energy, (b) cosine of polar angle, (c) azimuthal angles, and (d) a scatter plot of polar versus azimuthal angle for the neutral calorimeter bumps in the `CalorNeutral` list. The plots are made from a typical run (number 12917) and normalized to display bumps/isPhysicsEvent/bin. The cut $0 < R_2 < 0.45$ has been applied in these plots. The dashed histogram in (a) shows energy spectrum *without* excluding $R_2 = 0$.

Decay Mode	Parent Mass [MeV/c^2]	Branching Ratio [%]
$D^{*+} \to D^0\pi^+$	2009.93	68.3%
$D^{*+} \to D^+\pi^0$		30.6%
$D^{*0} \to D^0\pi^0$	2006.7	61.9%
$D^0 \to K^-\pi^+$	1864.51	3.91%
$D^0 \to K^-\pi^+\pi^0$		13.07%
$D^0 \to K^-\pi^+\pi^+\pi^-$		8.5%
$D^0 \to K^0_S\pi^+\pi^-$		2.7%
$D^+ \to K^-\pi^+\pi^+$	1869.3	9.0%
$D^+ \to K^0_S\pi^+$		1.45%
$\rho^+ \to \pi^+\pi^0$	770	100.0%
$\rho^0 \to \pi^+\pi^-$	770	100.0%
$K^0_S \to \pi^+\pi^-$	497.67	68.61%
$\pi^0 \to \gamma\gamma$	134.976	98.8%

Table 4: Decay modes represented in the composition lists which are used by this event selection. The mass values and branching ratios are those used in the Monte Carlo, which are consistent with Reference [1]. For the states which proceed via intermediate resonances ($D^0 \to K^-\pi^+\pi^0$, $D^0 \to K^0_S\pi^+\pi^-$, $D^0 \to K^-\pi^+\pi^+\pi^-$ and $D^+ \to K^-\pi^+\pi^+$) the branching ratios are summed over resonant and non-resonant contributions in the Monte Carlo, and include intermediate branching ratio factors for resonance decay into the final state shown in the table.

2. a pair invariant mass in the range of 90–165 (90–170) MeV/c^2, computed at the detector origin and assuming both entries are photons, and

3. both bumps having a lateral shower shape consistent with the expected pattern of energy deposits for an electromagnetic shower, as determined by a cut of LAT < 0.8.

From this common list several other lists are defined applying tighter selection criteria:

`pi0Loose` the sum of the two photon energies is at least 200 MeV, and the invariant mass in the range 100–160 (90–170) MeV/c^2;

`pi0LooseMass` same as `pi0Loose` but applying a mass constraint to the π^0 candidate, assuming the primary vertex as origin for the photons. No additional selection criteria to those applied to the `pi0Loose` list are imposed. This list does not exist in the production release of the expedite skims.

`pi0DefaultMass` same as `pi0LooseMass` but tighter mass window (before kinematic fitting), 115–150 MeV/c^2 (90–170 MeV/c^2).

`pi0SoftLoose` the sum of the two photon momenta in the $\Upsilon(4S)$ frame is between 70 and 450 MeV/c (0–450 MeV/c), and the invariant mass in the range 100–160 MeV/c^2 (90–170 MeV/c^2);

`pi0SoftDefaultMass` starting from `pi0SoftLoose`, applies a mass contraint to the candidate, assuming the primary vertex as origin for the photons, and the mass window before kinematic fitting is required to lie between 115 and 150 MeV/c^2 (90–170 MeV/c^2).

In production release of the full skim, entries in the `pi0LooseMass` are combined in a common list, `pi0AllLoose`, with the merged π^0 candidates contained in the `pi0MergedDefault`. In this 'smart' merging, only composite π^0 candidates with energy exceeding 1 GeV and overlaping with any of the merged π^0 are considered for replacement by the overlapping merged π^0. A `pi0AllDefault` list is also defined starting from `pi0AllLoose` and with a mass window between 115 and 150 MeV/c^2.

Figure 4 shows the invariant mass and energy distribution for entries in the `pi0Loose` list and χ^2 probability of mass-constraint fit in `pi0DefaultMass` list for a typical run. The energy and momenta of π^0 candidates in this list are recalculated with a constraint on the π^0 mass (using the value in Table 4) calculated at the nominal per-run beam spot position. This refitting technique improves the energy resolution of the π^0 candidates from 3.0% to 2.5% [3]. About 80% of all π^0's produced in generic Monte Carlo have both photons within the calorimeter's geometrical acceptance[3]. The fraction of π^0's within the acceptance which are included in the `pi0DefaultMass` list varies with π^0 energy: it is 65-70% from 0.5–2.0 GeV, and then falls linearly down to 25% at about 5 GeV due to a large fraction of overlapping showers [3]. Thus, for the B decays studies reported here, we consider only π^0 candidates formed from separated clusters, since there are few merged pions in the the available kinematic range.

K^0_S Lists

The K^0_S candidates used in this selection are collected into a `KsDefault` (`KsLoose`) list consisting of pairs of `ChargedTracks` entries with an invariant mass, computed from the vertex for the two tracks obtained in one iteration of the `GeoKin` (`VtxLeastChi2Vertex`) algorithm, to lie within $\pm$25 MeV/c^2 of the nominal K^0_S mass (462–535 MeV/c^2). Figure 5 shows the invariant mass and energy distributions of K^0_S candidates in this list for a typical run. The average efficiency for K^0_S's produced in generic $B\overline{B}$ decays with momenta greater than ?? GeV/c to be selected in the `KsDefault` list is estimated to be ??% from Monte Carlo [2].

D^0 Lists

The D^0 candidates used in this selection are reconstructed in several modes (see Table 4) and collected into a single `D0HardDefaultFlipSign` (`D0HardLoose`) list. The following cuts are applied for each mode:

- $D^0 \to K^-\pi^+$: pairs of entries in the `GoodTracksVeryLoose` (`GoodTracksLoose`) list having an invariant mass within $\pm$40 MeV/c^2 of the nominal D^0 mass (range [1.704,2.024] GeV/c^2);
- $D^0 \to K^-\pi^+\pi^0$, $\pi^0 \to \gamma\gamma$: pairs of entries in the `GoodTracksVeryLoose` (`GoodTracksLoose`) list combined with an entry from the `pi0AllDefault` (`pi0Loose`) list having an invariant mass within $\pm$70 MeV/c^2 of the nominal D^0 mass (range [1.704,2.024] GeV/c^2);
- $D^0 \to K^-\pi^+\pi^+\pi^-$: sets of entries from the `KMicroNotPion` (see section 3.2) (`GoodTracksVeryLoose`) and `GoodTracksVeryLoose` lists with an invariant mass within $\pm$40 MeV of the nominal D^0 mass (range [1.764,1.964] GeV/c^2);

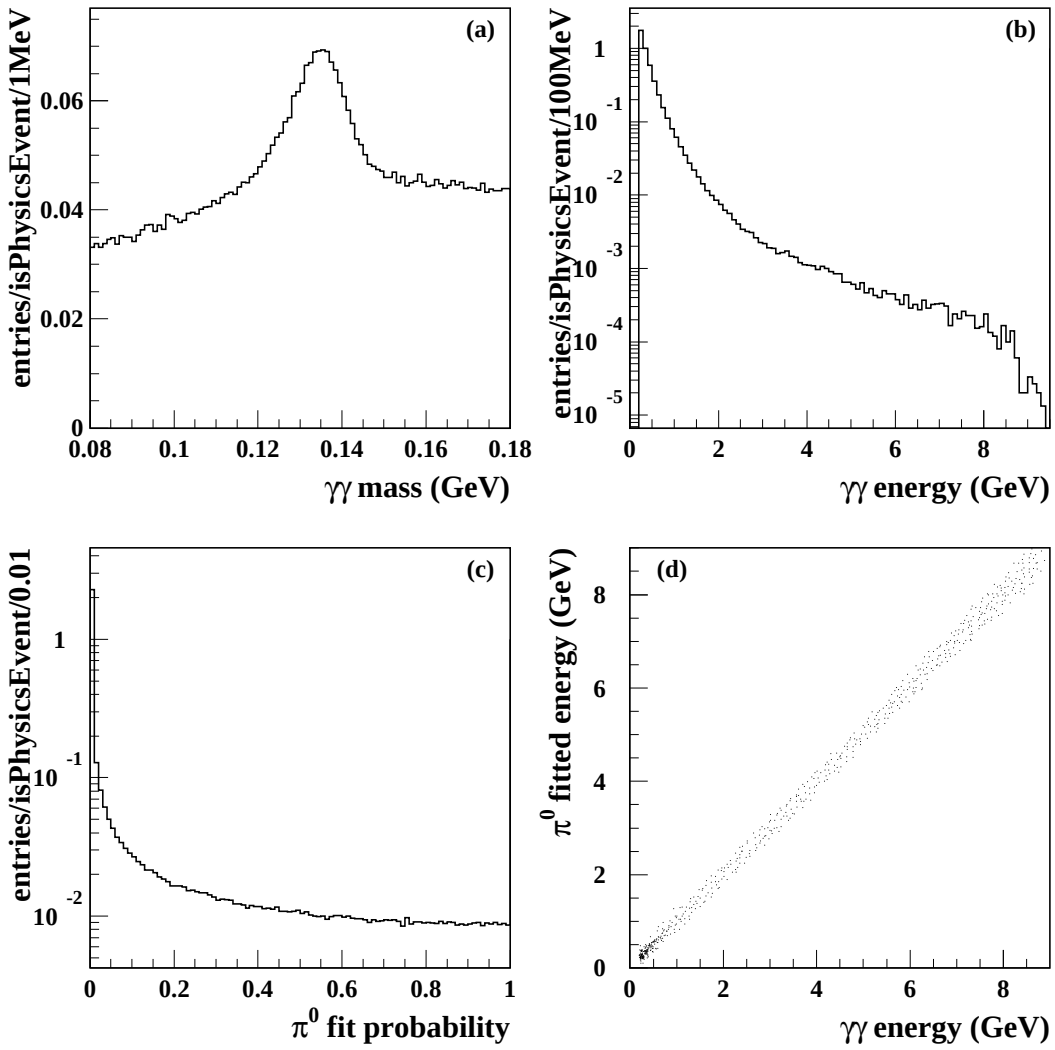

Figure 4: Distributions of (a) invariant mass, (b) total energy for pairs of neutral calorimeter clusters found in the `pi0Loose` list, (c) mass-constraint fit χ^2 probability in the `pi0DefaultMass` list, and (d) a scatter plot of energies comparison from a typical run (number 12917). The plots are normalized to show entries/isPhysicsEvent/bin.

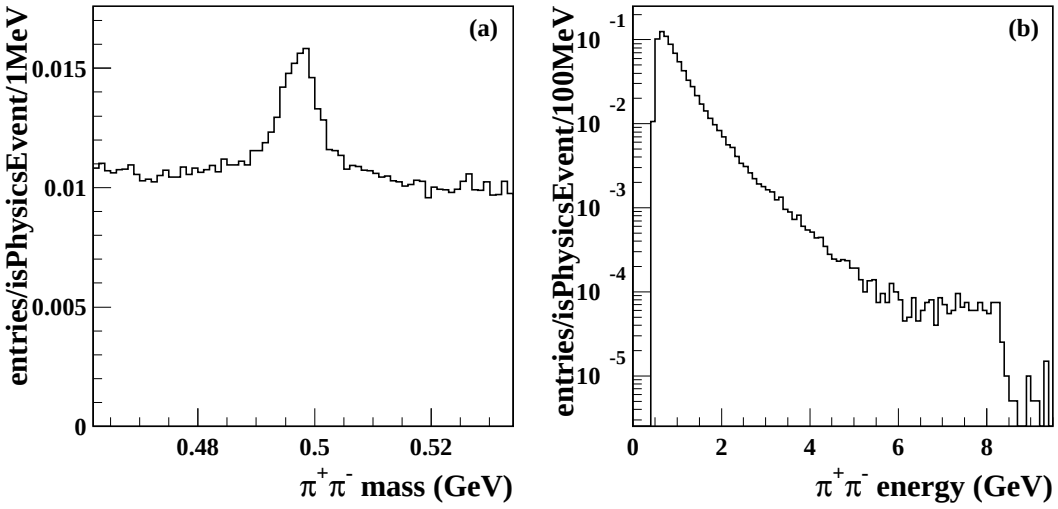

Figure 5: Distributions of (a) invariant mass and (b) total energy for pairs oppositely charged tracks found in the `ChargedTrack` list, from a typical run (number 12917). The plot are normalized to show entries/`isPhysicsEvent`/bin.

- $D^0 \to K^0_S\pi^+\pi^-$, $K^0_S \to \pi^+\pi^-$: pairs of entries in the `GoodTracksVeryLoose` (`GoodTracksLoose`) list combined with an entry from the `KsDefault` (`KsLoose`) list having an invariant mass within ± 40 MeV/c^2 of the nominal D^0 mass (range [1.704,2.024] GeV/c^2).

In addition, all D^0 candidates must have momentum in the $\Upsilon(4S)$ frame greater than 1.3 GeV/c. All invariant masses are calculated from four-momenta addition of the decay-product tracks. The nominal D^0 mass is given in Table 4. Figure 6 compares the invariant mass distributions measured in data for candidates reconstructed in each of these modes.

Figure 6: Invariant mass distributions of D^0 candidates in the `D0HardLoose` list reconstructed as (a) $D^0 \to K^-\pi^+$, (b) $D^0 \to K^-\pi^+\pi^0$, $\pi^0 \to \gamma\gamma$, and (c) $D^0 \to K^-\pi^+\pi^+\pi^-$. The plots are generated from the ZZ subsample and normalized as decays/event/bin.

D^+ Lists

The D^+ candidates used in this selection are reconstructed in several modes (see Table 4) and collected into a single `DcHardDefault` (`DcLoose`) list. The following cuts are applied for each mode:

- $D^+ \to K^-\pi^+\pi^+$: sets of entries from the `KMicroNotPion` (`GoodTracksLoose`) and `GoodTracksVeryLoose` (`GoodTracksLoose`) lists having an invariant mass within ± 40 MeV/c^2 of the nominal D^+ mass (range [1.7,2.1] GeV/c^2);

- $D^+ \to K^0_S\pi^+$: an entry in the `KsDefault` (`KsLoose`) list and combined with an entry in the `GoodTracksVeryLoose` (`GoodTracksLoose`) list having an invariant mass within ± 40 MeV/c^2 of the nominal D^+ mass (range [1.7,2.1] GeV/c^2).

In addition, all D^+ candidates must have momentum in the $\Upsilon(4S)$ frame greater than 1.3 GeV/c. All invariant masses are calculated from four-momenta addition of the decay-product tracks. The nominal D^0 mass is given in Table 4.

D^{*+} Lists

D^{*+} candidates in the mode $D^0\pi^+$ are reconstructed as combinations of an entry in the `D0HardDefaultFlipSign` (`D0HardLoose`) list and an entry in the `GoodTracksVeryLoose` list ("soft pion"). Combinations passing the following cuts are added to a `DstarHardDefault` (`DstarHardLoose`) list:

- a maximum soft π^+ momentum of 450 MeV/c in the $\Upsilon(4S)$ frame,
- an invariant mass within 500 MeV/c^2 of the nominal D^{*+} mass (see Table 4), and
- a mass difference, $\Delta m \equiv m(D^0\pi^+) - m(D^0)$, in the range 139–150 (130–160) MeV/c^2.
- 'right-sign' correlation between the charge of the soft pion and the kaon from the D^0 decay, where applicable.

D^{*+} candidates in the mode $D^+\pi^0$ are reconstructed as combinations of an entry in the `DcHardDefault` (`DcLoose`) list and an entry in the `pi0SoftDefaultMass` list ("soft pion"). Combinations passing the following cuts are added to a `DstarHardDefault` (`DstarHardLoose`) list:

- a maximum soft π^0 momentum of 450 MeV/c in the $\Upsilon(4S)$ frame,
- an invariant mass within 500 MeV/c^2 of the nominal D^{*+} mass (see Table 4), and
- a mass difference, $\Delta m \equiv m(D^+\pi^0) - m(D^+)$, in the range 130–160 MeV/c^2.
- 'right-sign' correlation between the charge of the soft pion and the kaon from the D^0 decay, where applicable.

D^{*0} Lists

D^{*0} candidates in the mode $D^0\pi^0$ are reconstructed as combinations of an entry in the `D0HardDefaultFlipSign` (`D0HardLoose`) list and an entry in the `pi0SoftDefaultMass` list ("soft pion"). Combinations passing the following cuts are added to a `Dstar0HardDefault` (`Dstar0Loose`) list:

- π^0 momentum less than 450 MeV/c in the $\Upsilon(4S)$ frame
- an invariant mass within 500 MeV/c^2 of the nominal D^{*0} mass (see Table 4), and
- a mass difference, $\Delta m \equiv m(D^0\pi^0) - m(D^0)$, in the range 130–160 MeV/c^2.

ρ^0 and ρ^+ Lists

Oppositely charged tracks from the `GoodTracksVeryLoose` (`GoodTracksLoose`) list that lie within ± 160 (± 300) MeV/c^2 of the nominal ρ^0 mass are collected on the `rho0Tight` (`rho0Default`) list. The ρ^+ list `rhoCHardTight` (`rhoCDefault`) is a collection formed from paired entries on the `GoodTracksVeryLoose` (`GoodTracksLoose`) and `pi0AllLoose` (`pi0DefaultMass`) lists lying within ± 160 (± 320) MeV/c^2 of the nominal ρ^+ mass, and momentum in $\Upsilon(4S)$ frame higher than 500 (0) MeV/c^2.

a_1^+ Lists

Candidates for $a_1^+ \to \rho^0\pi^+$ are collected on the `a1CHardTight` (`a1CDefault`) list, by combining entries from the `rho0Tight` (`rho0Default`) and `GoodTracksVeryLoose` (`GoodTracksLoose`) lists. An invariant mass between 1.0 and 1.6 GeV/c^2 is required, with momentum in $\Upsilon(4S)$ frame higher than 500 (0) MeV/c^2.

2.2.3 B^0 and B^+ Skims

Decay Mode	Branching Ratio [10^{-3}]
$B^0 \to D^{*-}\pi^+$	2.7
$B^0 \to D^{*-}\rho^+$	7.0
$B^0 \to D^{*-}a_1^+$	12.2
$B^0 \to D^-\pi^+$	3.0
$B^0 \to D^-\rho^+$	8.2
$B^0 \to D^-a_1^+$	6.0
$B^+ \to \overline{D}^{*0}\pi^+$	5.0
$B^+ \to \overline{D}^{*0}\rho^+$	14.7
$B^+ \to \overline{D}^{*0}a_1^+$	18.3
$B^+ \to \overline{D}^0\pi^+$	4.8
$B^+ \to \overline{D}^0\rho^+$	13.2
$B^+ \to \overline{D}^0a_1^+$	4.2

Table 5: B decay modes represented in the composition lists which are used by this event selection. The branching ratios are those used in the Monte Carlo, which are consistent with Reference [1].

Common lists are constructed, `B0ToDLightDefault` (`B0ToDDstarLoose`) for neutral B's and `BchToDLightDefault` (`BchToDDstarLoose`) for charged B's, using the decay modes listed in Table 5, for pairs of entries from the `DstarHardDefault` (`DstarHardLoose`), `Dstar0HardDefault` (`Dstar0Loose`), `DcHardDefault` (`DcLoose`), `D0HardDefaultFlipSign` (`D0HardLoose`), `rhoCHardTight` (`rhoCDefault`), `a1CHardTight` (`a1CDefault`) and `GoodTracksVeryLoose` (`GoodTracksLoose`) lists, with the following additional requirements on the B candidate:

- the raw mass lies in the range 5.0 to 5.5 GeV/c^2, and
- the reconstructed energy lies within ± 300 MeV of one-half the center-the-mass energy.

In the production release of the expedite skims, a total of 48 separate tag bits are defined for each of the complete B decay chains. In the full skims, only 12 tags bits are defined, one for each B mode. The final pre-selected datasets are based on the two composition lists, `B0ToDLightDefault` (`B0ToDDstarLoose`) and `BchToDLightDefault` (`BchDDstarLoose`), which are used as the basis for the `B0ToDLight` and `BchToDLight` (`BrecoBTag`) skims.

2.2.4 Ntuple Production

Ntuples for analysis are produced by running the `BRecoUser` [16] program, reading events flagged by the `B0ToDLight` and `BchToDLight` (`BrecoBTag`) skims. Table 6 summarizes the software versions that were used. The composition lists created when the tag bits is set are not stored in the event, so the ntuple creation job must recreate them. At this stage, vertex and kinematic fitting is performed [17, 18], to create the ntuple output variables:

- In selecting D^0 and D^+ candidates for B reconstruction, a single iteration vertex constraint fit using `GeoKin` [17]; in reconstructing the B parent, a combined mass and vertex constraint fit using `GeoKin` is applied to the D^0 and D^+;
- All $D^{*+} \to D^0\pi^+$ candidates are refitted with the beam-spot constraint to improve the soft pion angle measurement, using a fixed vertical beam spot sigma of 30 μm [17]; and
- A vertex fit using `GeoKin` is applied to the final B candidate.

Package	Version Tag
`AbsBTagging`	`V00-01-07`
`BRecoUser`	`V00-08-36`
`BTaggingTools`	`V00-01-26`
`BdbEvent`	`V01-00-23`
`BetaTools`	`V00-10-06-03`
`CompositionSequences`	`rf-120700`
`CompositionUtils`	`fmv121200`
`FastVtx`	`V03-03-07`
`NetTagger`	`V00-01-16`
`VertexingTools`	`V00-08-41`
`VtxFitter`	`V00-08-48`

Table 6: Versions of the packages used to create the Run 1 sample ntuples. Other packages used the versions in the `analysis-7` release.

3 Reconstruction of B Mesons

The final B reconstruction studies discussed in this report are based on the ntuples created from the skimmed samples `B0ToDLight` and `BchToDLight` (`BrecoBTag`). As described in section 2.2, the composition lists are used to select the candidates and to generate the

variables contained in the skimmed ntuples. The final analysis uses only a subset of the 48 possible decay chains and frequently makes tighter final cuts. We will repeat here, in a physics language more appropriate for a final presentation, the selection requirements for the B decay modes included in this study. A tabular summary of the final cuts is also provided, organized in a way to show a comparison with the pre-selection cuts. If the 'Final Analysis' column is blank in these comparisons, the cut is identical to the pre-selection. The additional cuts in the final selection are aimed at producing a result with a signal purity of around 90%, although further optimization in this direction is still required.

3.1 Track Selection

For most charged particles, we require the reconstructed track satisfy a minimal quality selection, `GoodTracksVeryLoose` (`GoodTracksLoose`) list. In order to reduce contributions from beam gas and beam wall backgrounds, tracks are required to satisfy a loose requirement of having a distance of closest approach within ± 10 cm in z and 1.5 cm in radius of the average beam spot position. The beam spot position is determined on a run-by-run basis. The transverse momentum is required to lie between 0.1 and 10 GeV/c. Finally, the particle is required to have penetrated the drift chamber, with at least (12) 20 assigned hits. In the case of the soft pion from the transition $D^{*+} \to D^0\pi^+$ or the daughters from a K^0_S decay (discussed below), these restrictions are removed, and any charged track is used (`ChargedTracks` list) in the reconstruction.

Criteria	Skim	Final Analysis
Default Track	`GoodTrackVeryLoose` (`GoodTrackLoose`)	
p_T	[0.0,10.] ([0.1,10.]) MeV/c	
d_0	< 1.5 cm	
z_0	$< 10.$ cm	
n_{DCH}	$> 12(20)$	
Soft Track	`ChargedTracks`	
No cuts		

Table 7: Summary of cuts for charged tracks.

3.2 Particle Identification

The SMS particle selector is used to identify kaons in D^0 and D^+ reconstruction. It permits to reject pions background in modes where it is needed to obtain a rough optimization of $S^2/(S+B)$. [3]

All selectors use likelihoods calculated with information given by these three subdetectors:

- *Silicon Vertex Detector*: measurement of dE/dX and the number of hits,
- *Drift Chamber*: measurement of dE/dX and the number of hits,

[3] A detailed optimization study is in progress.

- *DIRC*: value of the Cerenkov angle and the number of photons.

In B reconstruction to exclusive modes, two particular selectors are used:

- The SMS "Not A Pion" selector is used most of the time. For this selection, if a subdetector gives no information, the particle is assumed to be a kaon for this detector.
- The SMS "Tight" selector is used for modes with higher backgrounds such as $B^- \to D^{*0}\pi^-$, $D^0 \to K^-\pi^+\pi^0$ or $D^0 \to K^-\pi^+\pi^-\pi^+$. This algorithm requires that the likelihood calculated for the kaon hypothesis be greater than the pion and proton hypotheses. The effect of this selection on the decay mode $B^+ \to \overline{D}^{*0}\pi^+$, $D^0 \to K^-\pi^+\pi^0$ can be seen in Fig. 7.

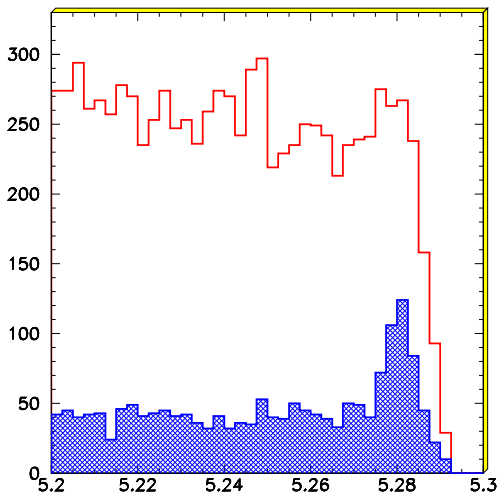

Figure 7: Effect of SMS "Tight" Selector on the reconstruction of the decay mode $B^- \to D^{*0}\pi^-$, $D^0 \to K^-\pi^+\pi^0$. Blank histogram: without any selection; colored histogram: SMS "Tight" selection required for the kaon in the decay $D^0 \to K^-\pi^+\pi^0$

3.3 π^0 Reconstruction

The π^0 are formed by combining pairs of photon candidates taken from the `GoodPhotonLoose` (`CalorNeutral`) list. The `pi0AllLoose` (`pi0DefaultMass`) and `pi0SoftDefaultMass` lists were used for skimming. For ntuple production, `pi0DefaultMass` and `pi0SoftDefaultMass` were used. The reconstructed $\gamma\gamma$ mass is shown in Fig.8. For those π^0 mesons produced by $\rho^+ \to \pi^+\pi^0$ or $D^0 \to K^-\pi^+\pi^0$, a cut at $E > 200$ MeV is applied to the π^0 energy. For the π^0 from $D^{*0} \to D^0\pi^0$ and $D^{*+} \to D^+\pi^0$, the π^0 is required to have momentum less than 450 MeV/c in the $\Upsilon(4S)$ frame. The selection efficiency, determined from generic $B\overline{B}$ events in SP3 Monte Carlo, increases from about 40% at threshold to 55% for π^0's with 2 GeV in energy. The variation in efficiency as a function of the π^0 energy is shown on Fig. 8.

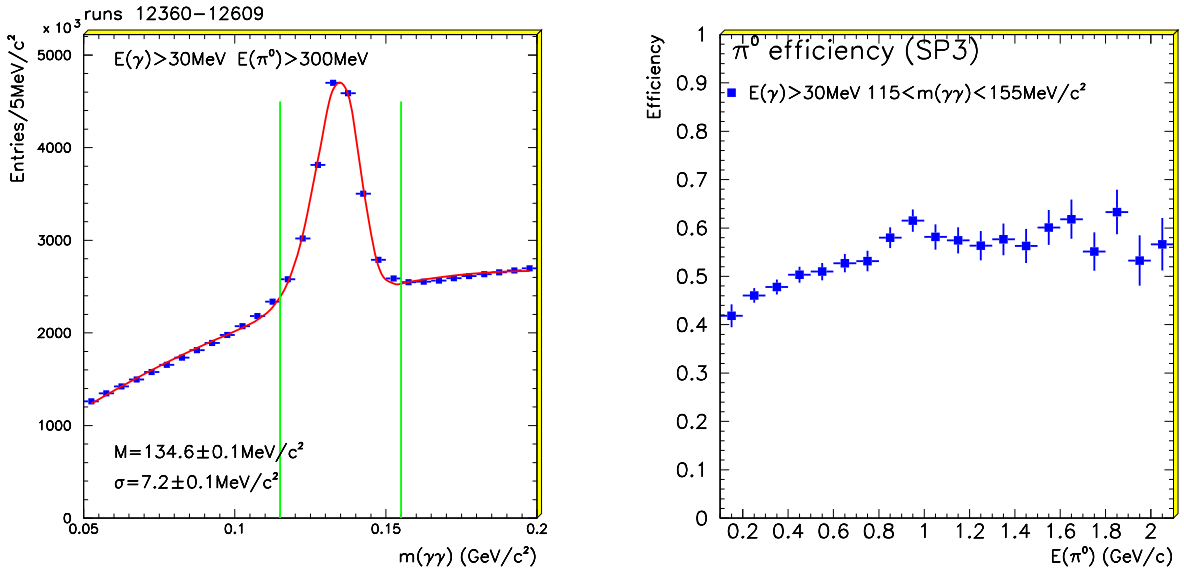

Figure 8: The $\gamma\gamma$ mass distribution in the data for $E(\pi^0) > 300$ MeV is shown on the left. The data points are overlaid with the result of a fit using a Novosibirsk function for the signal plus a 2^{nd}-order polynomial for the background. The vertical lines indicate the mass window used to select π^0 candidates. The π^0 selection efficiency as a function of the π^0 energy in shown on the right for generic $B\overline{B}$ events in the SP3 Monte Carlo.

3.4 K^0_S Reconstruction

The K^0_S candidates are formed from pairs of oppositely charged tracks without restrictions on p_T or distance of closest approach to the beam spot centroid (`ChargedTracks` list). A vertex fit is performed using GeoKin, where a χ^2 probability greater than 0.1% is required. The invariant mass computed at this vertex location is required to lie in with ± 25 MeV/c^2 of the nominal K^0_S mass. The opening angle, α, between the flight directionand the momentum vector for the K^0_S candidate must be smaller than 200 mrad. Finally, the transverse flight distance from the primary vertex in the event, r_{xy}, is required to be greater than 2 mm. The π^+ π^- mass distribution for candidates passing these requirements is shown in Figure 9. The fitted mass is zzz, consistent with the nominal value. The resolution is observed to be zzz, in agreement with Monte Carlo estimates of zzz. The efficiency for a K^0_S to satisfy these requirements is shown in Figure 9. A mass constraint fit is applied to those K^0_S candidates passing these requirements, for use in subsequent reconstruction of charm mesons.

3.5 Charm Meson Reconstruction

D^0 Candidates

D^0 candidates are reconstructed in the modes $D^0 \to K^-\pi^+$, $D^0 \to K^-\pi^+\pi^0$, $D^0 \to K^-\pi^+\pi^-\pi^+$, and $D^0 \to K^0_S\pi^+\pi^-$. We require that the daughter tracks used in the $D^0 \to K^-\pi^+$ mode have a minumum momentum of 200 MeV/c. For $D^0 \to K^-\pi^+\pi^0$ $D^0 \to K^-\pi^+\pi^-\pi^+$, and $D^0 \to K^0_S\pi^+\pi^-$ modes in channels other than $\overline{B}^0 \to D^{*+}\pi^-$ and $D^{*+}\rho^-$,

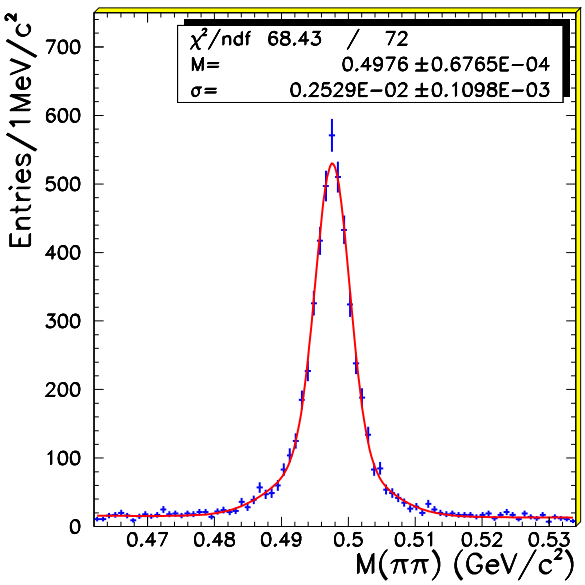

Figure 9: Distribution of π^+ π^- invariant mass for K^0_S candidates, after cuts on the flight angle α and the transverse flight distance.

Criteria	Skim	Final Analysis
Default K^0_S	`KsDefault` (`KsLoose`)	`KsDefault`
Vertex Fitter	GeoKin (VtxLeastChiVertexer)	GeoKin
$m(\pi^+\pi^-)$	$m(K^0_S) \pm 25(36)$ MeV/c^2	
χ^2		> 0.001
α		< 200 mrad
r_{xy}		> 2 mm

Table 8: Summary of cuts for K^0_S selection

the minimum charged track momentum is 150 MeV/c. Also, in these modes, we use the SMS "Not A Pion" particle selector to reject pion backgrounds for the kaon track in modes where background rejection is needed to obtain a rough optimization of $S^2/(S+B)$. D^0 candidates in the channels $\overline{B}^0 \to D^{*+}\pi^-$ and $D^{*+}\rho^-$ are required to have an invariant mass within $\pm 3\sigma$ of the fitted D^0 mass in the inclusive D^0 spectrum (Table 10) in the B candidate sample. In all other cases, the D^0 candidates are required to lie within $\pm 3\sigma$, calculated on an event-per-event basis, of the nominal D^0 mass. For $D^0 \to K^-\pi^+\pi^0$ mode, we only reconstruct the dominant resonant mode $D^0 \to K^-\rho^+$, $\rho^+ \to \pi^+\pi^0$ at this moment. This, the $\pi^+\pi^0$ invariant mass is required to lie within ± 150 MeV/c^2 of the nominal ρ mass and the angle between the π^+ and K^- in the $\pi^+\pi^0$ rest frame, $\theta^*_{K\pi}$, must satisfy $|\cos\theta^*_{K\pi}| > 0.4$. However, this choice of cuts is not optimal, which would require maximizing $S^2/(S+B)$ based on the Dalitz distribution [13, 14]. All D^0 candidates must have momentum greater than 1.3 GeV/c in the $\Upsilon(4S)$ frame. A vertex fit is performed using `GeoKin`, where a χ^2 probability greater than 0.1% is required.

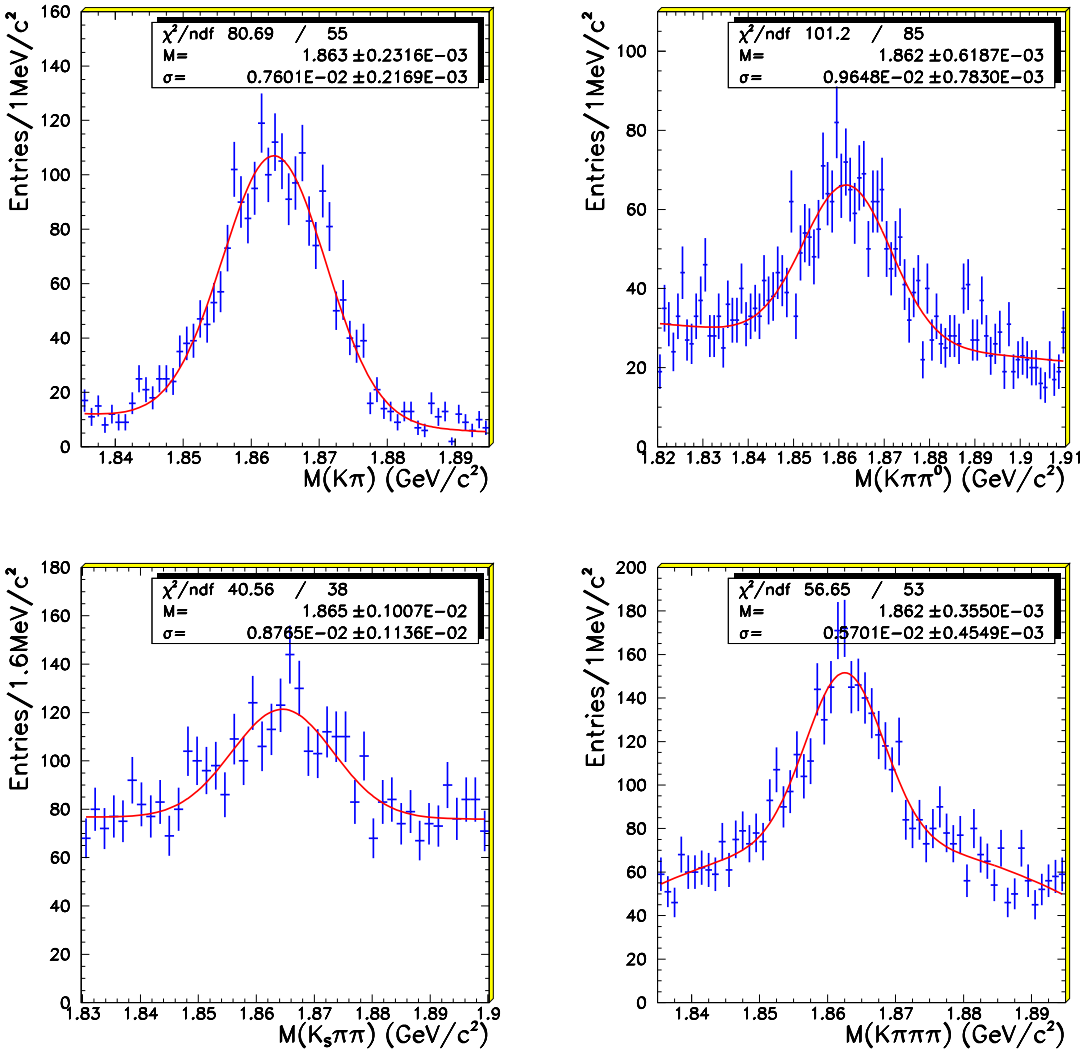

Figure 10: D^0 candidates selected for $D^0 \to K^-\pi^+$, $D^0 \to K^-\pi^+\pi^0$ $D^0 \to K^0_S\pi^+\pi^-$, and $D^0 \to K^-\pi^+\pi^-\pi^+$ modes.

Criteria	Skim	Final Analysis
Default D^0	`D0HardDefaultFlipSign` (`D0HardLoose`)	`D0DefaultVtx`
Vertex Fitter		`GeoKin`
χ^2		> 0.001
$p^*(D^0)$	> 1.3 GeV/c	
$D^0 \to K^-\pi^+$		
$m(K^-\pi^+)$	± 0.040 ([1.704,2.024]) GeV/c^2	$\pm 3\sigma^\dagger$ MeV/c^2
$p(K^-)$	> 100 MeV/c	> 200 MeV/c
$p(\pi^+)$	> 100 MeV/c	$> 200^\dagger$ MeV/c^2
$D^0 \to K^-\pi^+\pi^0$		
$m(K^-\pi^+\pi^0)$	± 0.070 ([1.704,2.024]) GeV/c^2	$\pm 3\sigma$ MeV/c^2
$p(K^-, \pi^\pm)$	> 100 MeV/c	> 150 MeV/c
$m(\pi^+\pi^0)$		$m(\rho) \pm 150$ MeV/c^2
$\lvert\cos\theta^*_{K\pi}\rvert$		> 0.4
$D^0 \to K^0_S\pi^+\pi^-$		
$m(K^0_S\pi^+\pi^-)$	± 0.040 ([1.704,2.024]) GeV/c^2	$\pm 3\sigma$ MeV/c^2
$p(\pi^\pm)$	> 100 MeV/c	> 150 MeV/c
$D^0 \to K^-\pi^+\pi^+\pi^-$		
$m(K^-\pi^+\pi^+\pi^-)$	± 0.040 ([1.764,1.964]) GeV/c^2	$\pm 3\sigma$ MeV/c^2
$p(K^-, \pi^\pm)$	> 100 MeV/c	> 150 MeV/c

† For modes other than $\overline{B}^0 \to D^{*+}\pi^-$ or $D^{*+}\rho^-$

Table 9: Summary of cuts for D^0 selection

Mode	m_D (MeV/c^2)	σ_{m_D} (MeV/c^2)
$D^0 \to K^-\pi^+$	1863.1 ± 0.5	6.8 ± 0.6
$D^0 \to K^-\pi^+\pi^0$	1863.1 ± 1.4	11.5 ± 1.4
$D^0 \to K_s\pi^-\pi^+$	1863.3 ± 1.0	8.1 ± 1.0
$D^0 \to K^-\pi^+\pi^-\pi^+$	1863.7 ± 0.5	6.2 ± 0.8

Table 10: D^0 fitted mass and widths.

D^+ Candidates

D^+ candidates are reconstructed in the modes $D^+ \to K^-\pi^+\pi^+$ and $D^+ \to K^0_S\pi^+$. We require that the kaon used in the $K^-\pi^+\pi^+$ mode have a minumum momentum of 200 MeV/c; the pions are required to have momentum greater than 150 MeV/c. For the $K^0_S\pi^+$ mode, the minimum charged track momentum is 200 MeV/c. We also use the SMS "Not A Pion" particle selector to reject pion backgrounds for the kaon track in modes where background rejection is needed to obtain a rough optimization of $S^2/(S+B)$. D^+ candidates are required to have an invariant mass within $\pm 3\sigma$, calculated on an event-by-event basis, of the nominal D^+ mass. All D^+ candidates must have momentum greater than 1.3 GeV/c in the $\Upsilon(4S)$ frame. A vertex fit is performed using `GeoKin`, where a χ^2 probability greater than 0.1% is required.

Criteria	Skim	Final Analysis
Default D^+	`DcHardDefault` (`DcLoose`)	`DcDefaultVtx`
Vertex Fitter		`GeoKin`
χ^2		> 0.001
$p^*(D^+)$	> 1.3 GeV/c	
$D^+ \to K^-\pi^+\pi^+$		
$m(K^-\pi^+\pi^+)$	± 0.040 ([1.7,2.1]) GeV/c^2	$\pm 3\sigma^\dagger$
$p(K^-)$	> 100 MeV/c	> 200 MeV/c
$p(\pi^+)$	> 100 MeV/c	> 150 MeV/c
$D^+ \to K^0_S\pi^+$		
$m(K^0_S\pi^+)$	± 0.040 ([1.7,2.1]) GeV/c^2	$\pm 3\sigma^\dagger$
$p(\pi^+)$	> 100 MeV/c	> 200 MeV/c

† Calculated on an event-by-event basis

Table 11: Summary of cuts for D^+ selection

D^{*+} Candidates

We form D^{*+} candidates by combining the a D^0 with a pion which has momentum greater than 70 MeV/c. `GeoKin` is used to perform a vertex fit for the D^{*+} using the constraint of the beam spot to improve the angular resolution for the soft pion. A fixed $\sigma = 30$ μm is used to model the beam spot spread in the vertical direction [17]. The fit is required to converge, but no cut is applied on the proability of χ^2. After fitting, selected D^{*+} candidates are required have Δm within $\pm 3\sigma$ of the measured nominal value. The width is taken to be a weighted average of the core and broad Gaussian distributions required to fit the Δm distribution.

D^{*+} candidates are also formed by combining the a D^+ with a π^0. The maximum momentum of the π^0 in the $\Upsilon(4S)$ frame is 450 MeV/c. The D^{*+} candidates are required have Δm within $\pm 3\sigma$ of the nominal mass-difference value.

Criteria	Skim	Final Analysis
Default D^{*+}	`DstarHardDefault` (`DstarHardLoose`)	`DstarDefaultVtx`
$D^{*+} \to D^+\pi^-$		
Vertex Fitter		`GeoKin`, beam spot
χ^2		constraint ($\sigma_y = 30$ μm), convergence
$m(D^0\pi^+) - m(D^0)$	[139,150] ([130,160]) MeV/c^2	$\pm 3\sigma$ MeV/c^2
$p^*(\pi^+)$	[70,450] MeV/c	

Table 12: Summary of cuts for D^{*+} selection

D^{*0} Candidates

D^{*0} candidates are reconstructed by combining a selected D^0 with a π^0 having momentum less than 450 MeV/c in the $\Upsilon(4S)$ frame. Selected D^{*0} candidates are required to have Δm

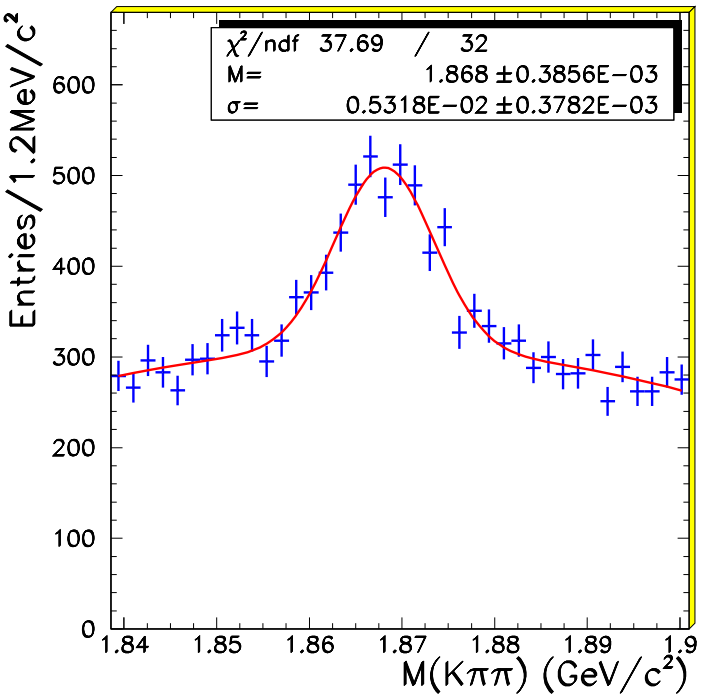

Figure 11: $D^+ \to K^-\pi^+\pi^+$ candidates selected.

within 4 MeV/c^2 of the nominal value. The Δm distribution, obtained from an inclusive sample of $D^0 \to K^-\pi^+$ decays, is shown in Fig. 14, for both a $b\overline{b}$ enriched ($p^*(D^0) < 2.5$ GeV/c) and a $c\overline{c}$ enriched sample ($p^*(D^0) > 2.5$ GeV/c).

Criteria	Skim	Final Analysis
Default D^{*+}	`Dstar0HardDefault` (`Dstar0Loose`)	`DstarDefaultVtx`
$D^{*0} \to D^0\pi^0$		
$m(D^0\pi^0) - m(D^0)$	[130,160] MeV/c^2	± 4 MeV/c^2
$p^*(\pi^0)$	[70,450] MeV/c	
$D^{*0} \to D^0\gamma$		

Table 13: Summary of cuts for D^{*0} selection

3.6 B Candidate Selection

B meson candidates are obtained by combining a D or D^* candidate, reconstructed as described in section 3.5, with a π, ρ or a_1 meson.

The pion momentum spectrum for the two-body decay $\overline{B}^0 \to D^{*+}\pi^-$ is shown in Fig. 15 For this analysis, the pion is required to have momentum greater than 500 MeV/c. No particle identification requirement is made for this track.

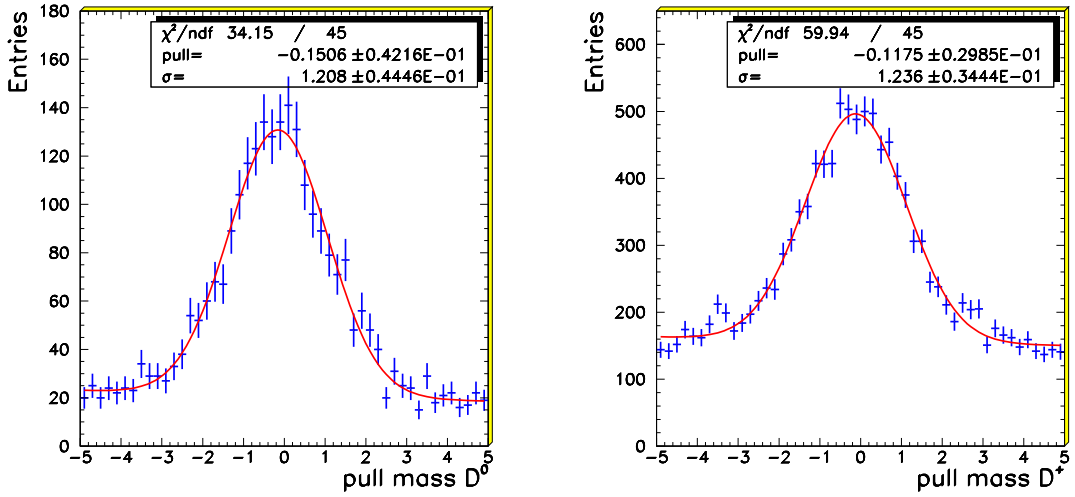

Figure 12: Pull distributions in mass for candidates in the modes $D^0 \to K^-\pi^+$ (left) and $D^+ \to K^-\pi^+\pi^+$ (right).

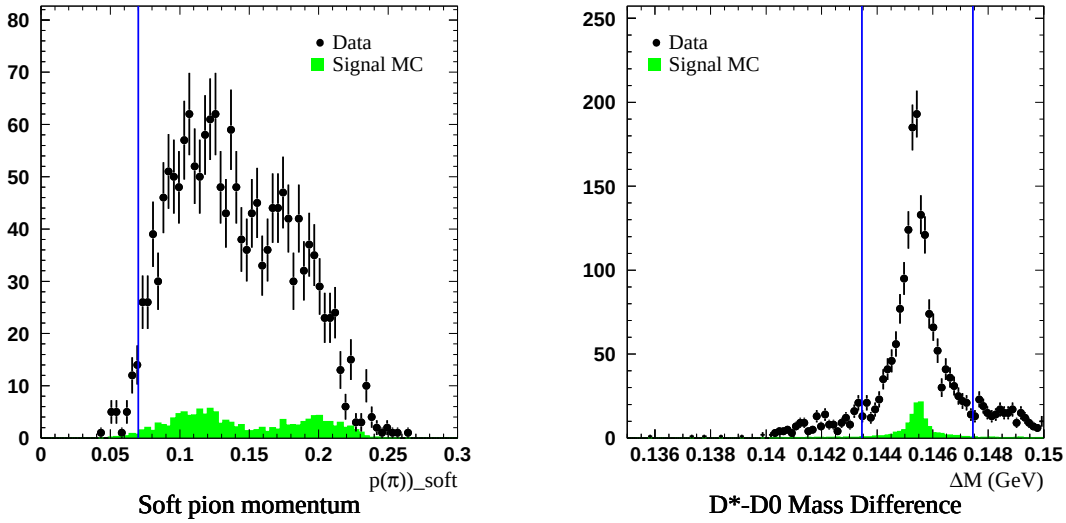

Figure 13: Distribution of soft pion momentum in the $\Upsilon(4S)$ frame (left) and $m(D^{*+}\pi^-) - m(D^0)$ mass distribution for D^{*+} candidates in the $\overline{B}^0 \to D^{*+}\pi^-$, $D^0 \to K^-\pi^+$ mode. Data includes selected D^{*+} candidates for all modes included in the B0toDStarX ntuples. Units in both plots are GeV. Vertical lines indicate selection criteria

For the $\overline{B}^0 \to D^{*+}\rho^-$ mode, ρ^+ candidates are formed by combining a π^0 meson and a charged pion both with momentum greater than 200 MeV/c. We require the ρ momentum to be greater than 1 GeV/c, and the $\pi^-\pi^0$ invariant mass to satisfy $|m(\pi^-\pi^0) - 770| < 150$ MeV/c^2. For the $\overline{B}^0 \to D^{*+}a_1^-$ mode, the a_1^- meson is selected by combining three charged pions, where the invariant mass must lie in the range 1.0 to 1.6 MeV/c^2. In addition, a

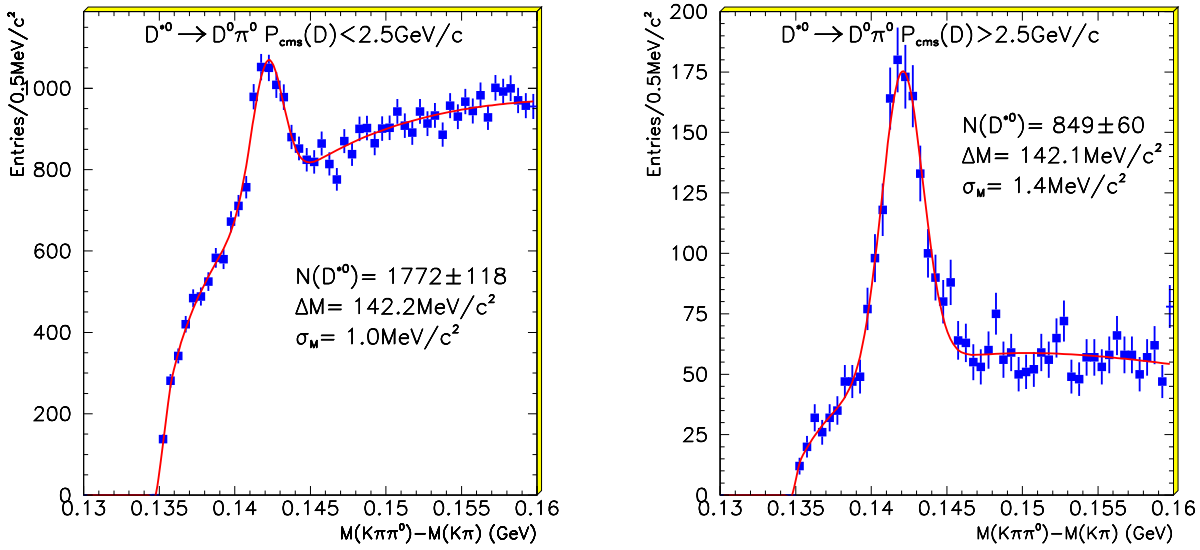

Figure 14: Δm distribution for $D^{*0} \to D^0\pi^0$ decays, where $p^*(D^0) < 2.5$ GeV/c (left) and $p^*(D^0) > 2.5$ GeV/c (right)

Mode	Δm (MeV/c^2)	$\sigma_{\Delta m}$ (MeV/c^2)
$D^{*+} \to D^0\pi^+$		
$D^0 \to K^-\pi^+$	145.45	0.8
$D^0 \to K^-\pi^+\pi^0$	145.54	1.1
$D^0 \to K^0_S\pi^+\pi^-$	145.45	0.9
$D^0 \to K^-\pi^+\pi^+\pi^-$	145.54	0.8
$D^{*0} \to D^0\pi^0$	142.2	1.0
$D^{*0} \to D^0\gamma$	142.2	5.2

Table 14: Δm signal widths used for D^* candidate selection.

vertex constraint fit to the a_1^- candidate is required to converge with $\chi^2 > 0.1\%$.

In the case of a correctly reconstructed B meson produced by the decay of an $\Upsilon(4S)$, within the experimental resolution, the measured sum of neutral and charged energies, E^*_{meas}, must be equal to the beam energy, E^*_{beam}, both evaluated in the $\Upsilon(4S)$ frame. We define ΔE to be the difference between the measured B candidate energy and beam energy in the $\Upsilon(4S)$ frame as:[5]

$$\Delta E \;=\; E^*_{meas} - E^*_{beam} \qquad (1)$$

The resolution on $\sigma_{\Delta E}$ varies from 20 to 40 MeV depending on mode. The list of the modes we have studied and the corresponding values of $\sigma_{\Delta E}$ are given in Tables 18 and 20.

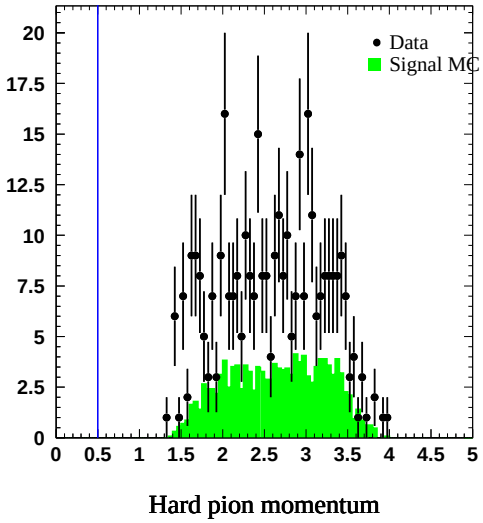

Figure 15: Spectrum of pion momentum in the two-body decay $\overline{B}^0 \to D^{*+}\pi^-$. The vertical line indicates the cut value.

We define an energy substituted B mass, $m_{\rm ES}$, as:

$$m_{ES}^2 \;=\; (E_{beam}^*)^2 - \left(\sum_i \vec{p}_i\right)^2 \tag{2}$$

where the $\vec{p}_i$ is the momentum of the ith daughter of the B candidate. The predicted resolution in $m_{\rm ES}$ is typically about 2.6 MeV/c^2 for most decay modes involving all-charged final states. This is about a factor of 10 better than the resolution in the reconstructed invariant mass. The resolution for $m_{\rm ES}$ is dominated by the beam energy spread rather than by the detector resolution, although there are examples where the measurement errors can contribute as well. It is largely uncorrelated with the error on ΔE [8].

The variables ΔE and $m_{\rm ES}$ are used to define a signal region and sidebands for background study. For all modes, the region between 5.2 and 5.3 GeV/c^2 in $m_{\rm ES}$ and between $\pm$300 MeV in ΔE is used to study the B candidates. The peak position, m_B, which should be the nominal B mass, and the resolution $\sigma_{m_{\rm ES}}$ are extracted from the distribution of $m_{\rm ES}$ after requiring ΔE be consistent with zero to within $\pm 2.5\sigma$. The resolution in ΔE is extracted from the ΔE distribution obtained by requiring $m_{\rm ES}$ lie within $\pm 2.5\sigma_{m_{\rm ES}}$ of m_B^0.

The signal region in the two dimensional plane $m_{\rm ES}$ versus ΔE is defined as a area $\pm 2.5\sigma$ wide centered at the nominal B mass, m_B^0, and $\Delta E = 0$. The sidebands outside this signal region are currently under study, both to demonstrate the appropriateness of our assumed background form and to better understand feeddown from other channels.

We allow only one candidate per event to appear in the $m_{\rm ES}$ versus ΔE distribution. Several different ways to choose the best candidate from among multiple candidates in the same event have been explored. The criteria selected in the end is to consider only the entry with the smallest absolute value for ΔE.

3.7 Background Rejection

The background composition in our signal region has significant contributions from both other $B\overline{B}$ events and continuum, and depends on the decay mode. In $\overline{B}^0 \to D^{*+}\pi^-$, for example, a study of 2 fb^{-1} of generic $B\overline{B}$ shows the most significant background to be from $c\overline{c}$ events.

To enrich the final sample with B signal and obtain a rough optimization of signal to background [4], we use two event shape techniques to reduce continuum background.

First, each event is required to satisfy $R_2 < 0.5$ where R_2 is the ratio of the second Fox-Wolfram moment to the zeroth moment determined using charged tracks and unmatched neutral showers in the $\Upsilon(4S)$ frame. This is designed to reject the jetlike continuum events over the more uniformly distributed $\Upsilon(4S)$ decays.

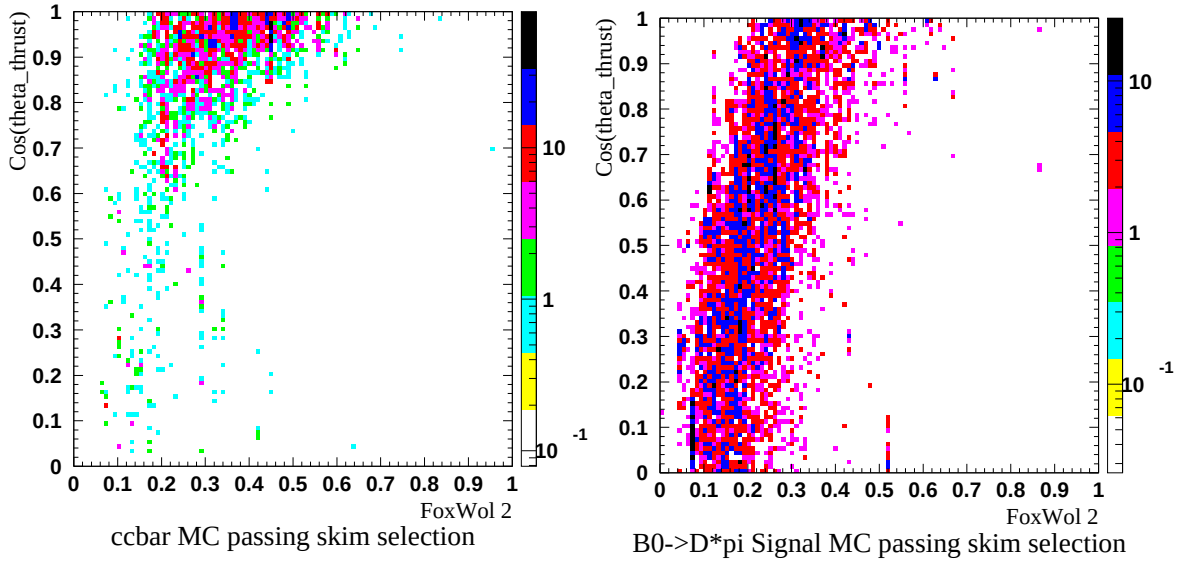

Figure 16: $\cos\theta_{th}$ vs. R_2 for Monte Carlo signal samples for generic $c\bar{c}$ and $\overline{B}^0 \to D^{*+}\pi^-$, $D^0 \to K^-\pi^+$. Although these variables are correlated, the thrust angle selection still has significant continuum background rejection power even after the R_2 selection is applied.

We further reduce backgrounds in some of the lower-purity modes by using a thrust-angle technique. The 'thrust angle', θ_{th}, is defined as the angle between the thrust axis of the particles which form the reconstructed B candidate and the thrust axis of the remaining tracks and unmatched clusters in the event, computed in the $\Upsilon(4S)$ frame. The two axes are almost completely uncorrelated in $B\overline{B}$ events, because the B mesons are almost at rest in the $\Upsilon(4S)$ rest frame, and the distribution in $|\cos\theta_{th}|$ given in Fig. 17 for the decay mode $\overline{B}^0 \to D^{*+}\pi^-$, $D^0 \to K^-\pi^+$. In continuum events, which are more jetlike, the two thrust axes tend to have small opening angles. Requiring $|\cos\theta_{th}| < 0.8$ typically removes about xx% of the continuum background while retaining 80% of the signal. The selection criteria $|\cos\theta_{th}|$ that depends on mode and is summarized in Table 15.

[4] A detailed optimization study is in progress.

Mode	$\lvert\cos\theta_{th}\rvert$ cut
$B^0 \to D^{*-}\pi^+$	No cut
$B^0 \to D^{*-}\rho^+$	No cut
$B^0 \to D^{*-}a_1^+$	No cut
$B^0 \to D^{-}\pi^+$	< 0.9
$B^0 \to D^{-}\rho^+$	< 0.8
$B^0 \to D^{-}a_1^+$	< 0.7
$B^+ \to D^{*0}\pi^+$	< 0.9

Table 15: Thrust angle cuts applied in the each B decay channel under study.

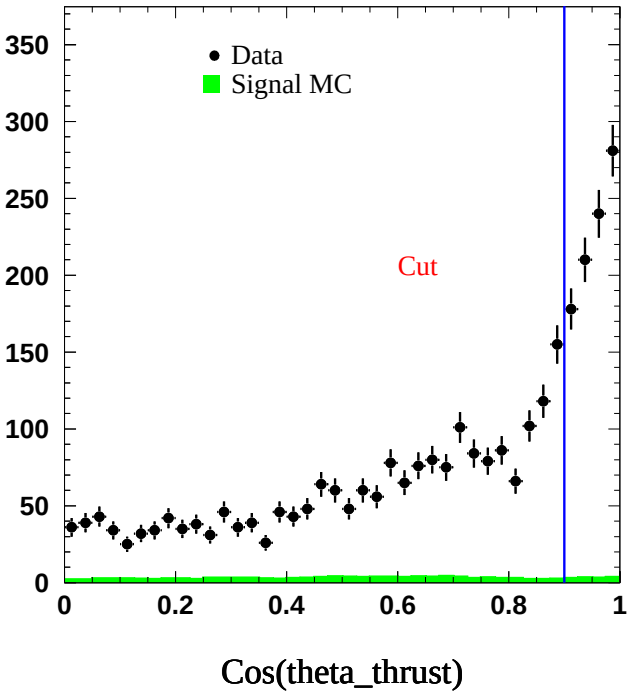

Figure 17: Distribution of the opening angle, θ_{th}, between thrust axes for the B candidate and the remaining tracks in the event for the mode $\overline{B}^0 \to D^{*+}\pi^-$, $D^0 \to K^-\pi^+$.

3.8 Background Fitting

The measurement of branching ratios, mixing and B lifetime require a good understanding of the shape of the background in the $m_{\rm ES}$ distribution. We expect the $m_{\rm ES}$ distribution from the ΔE sideband to provide important constraints about the background shape. However, this question is still under study both in data and Monte Carlo simulation. For the time being, we assume a background shape given by the ARGUS function, which parametrizes how phase space approaches zero as the candidate energy approaches E^*_{beam}:

$$f_{BG}(x) \;=\; Nx\sqrt{1-x^2}\exp(\kappa(1-x^2)) \qquad (3)$$

where $x = m_{\rm ES}/E^*_{beam}$, and the normalization and the shape are determined by the parameters N and κ. To determine the number of signal events from the $m_{\rm ES}$ distribution in the ΔE interval centered at zero, we make a fit using the ARGUS background function and a Gaussian signal with free mass, m_B, and width, $\sigma_{m_{\rm ES}}$. For projections of the signal as a function of ΔE a fit to the ΔE distribution is made using a linear background function plus a single Gaussian distribution with free mean and width, $\sigma_{\Delta E}$.

3.9 Monte Carlo Peaking Background Studies

Time-dependant measurements such as B mixing and lifetimes use the background fit to the $m_{\rm ES}$ distribution to estimate the signal probability on an event-by-event basis. For this reason, it is important to understand in some detail whether there is any background which is not well-described by the ARGUS fit. In particular, mis-reconstructed Bs can peak near the B mass and are therefore especially important to understand. As we will describe, there is a small but non-negligible peaking component to the backgrounds which comes from mis-reconstructed Bs. Here we will describe the methods we use to estimate the level of such "peaking background".

3.9.1 Generic Monte Carlo Peaking Background Studies

We use generic Monte Carlo to characterize background composition. Table 16 shows the statistics of the generic samples we used for these studies. Figures 18 through 30 show the ΔE and $m_{\rm ES}$ distributions for each individual decay chain. Each plot contans the distuibutions for the signal and the different background components. Figure 31 shows the distribution of all background to the B^0 events after subtracting the ARGUS bacground. A peaking component corresponding to approximately 1% of the signal is evident.

Sample	Events (M)
$B^0\overline{B}^0$	2.3
B^+B^-	3.1
$c\bar{c}$	5.5
uds	8.7

Table 16: Generic Monte Carlo samples used for background characterization studies.

3.9.2 Cocktail Monte Carlo Peaking Background Studies

Generic MC studies indicate that there is evidence for a small fraction of background which peaks in $m_{\rm ES}$, and its properties are therefore not accounted for in the $m_{\rm ES}$ sideband. Studies on MC ([15]) indicate that this background arises from misreconstructed B's. In the case of misreconstructed B^0 s, this is irrelevant: their time structure is identical to the signal. Only charged B's which are reconstructed as neutral B require special attention, as these do not mix and have a different lifetime than B^0 s..

The mechanism for the mis-reconstruction responsible for the peaking background is suspected to be soft pion exchagne. To characterize this component of the background in

the B^0 sample, we generated a "Cocktail" of Monte Carlo events which contains charged B decays to the modes which are suspected to be the cause of the feed-through. In particular, $B^+ \to D^{*0}\pi^-$ can be mis-reconstructed as $B^0 \to D^{*+}\pi^-$ if the soft π^0 from the D^{*0} is exchanged with another soft track in the event. If the momentum of the soft pions is similar, the mis-reconstructed B will show up in the signal region. We include in the coctail the modes listed in 17

Mode
$B^+ \to D^{*0}\pi^+$
$B^+ \to D^{*0}\rho^+$
$B^+ \to D^{*0}a_1^+$
$B^+ \to D^0\pi^+$
$B^+ \to D^0\rho^+$
$B^+ \to D^0a_1^+$

Table 17: Modes included in the charged B cocktail Monte Carlo sample

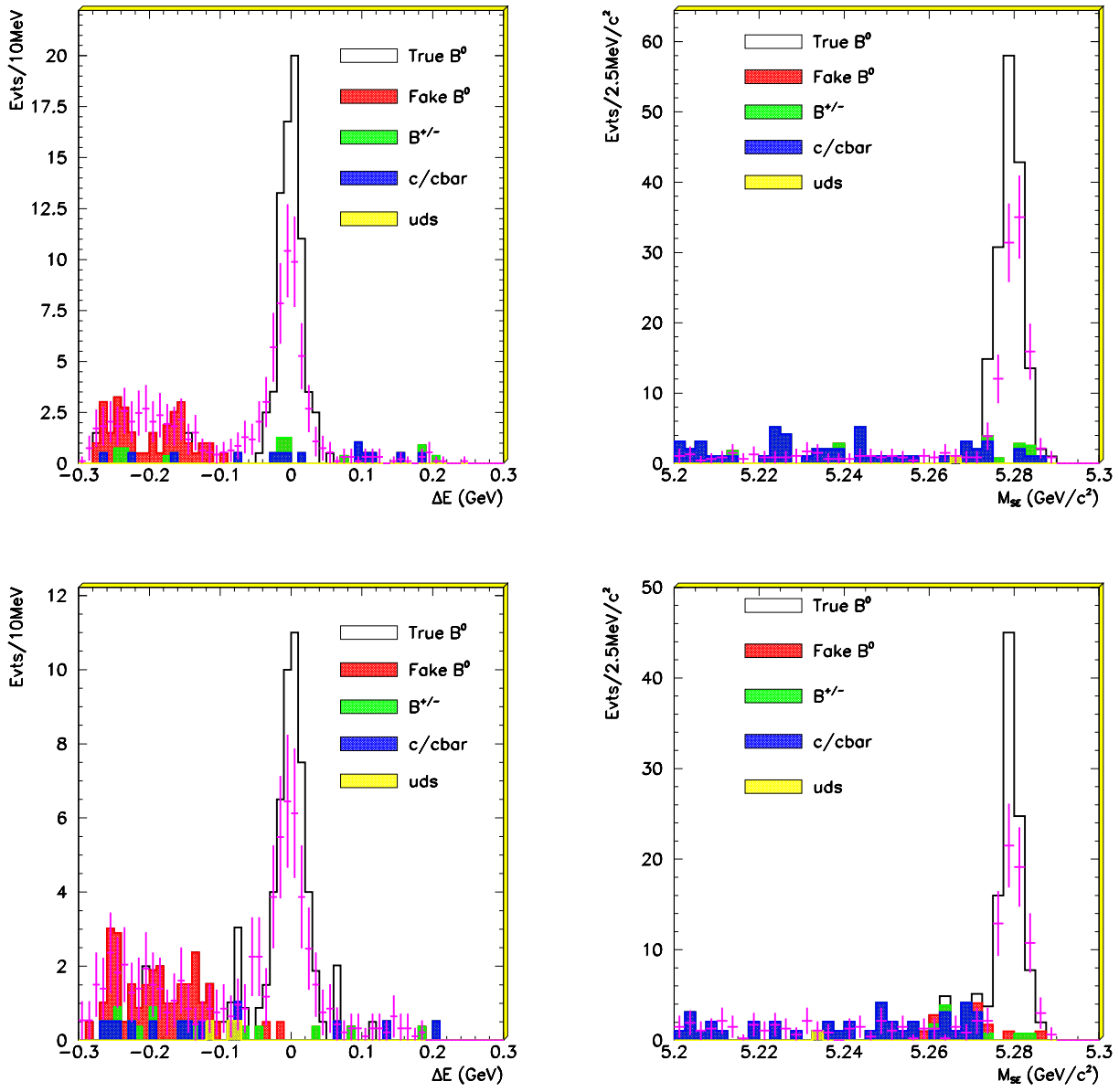

Figure 18: Generic MC studies of $\overline{B}^0 \to D^{*+}\pi^-$ for $D^0 \to K^-\pi^+$ (top) and $D^0 \to K^-\pi^+\pi^0$ (bottom). $m_{\rm ES}$ for $|\Delta E\ | < 2.5\sigma_{\Delta E}$ (right), ΔE for $|m_{\rm ES} - m_B| < 2.5\sigma m_{\rm ES}$ (left). Data normalized by luminosity is overlaid in purple.

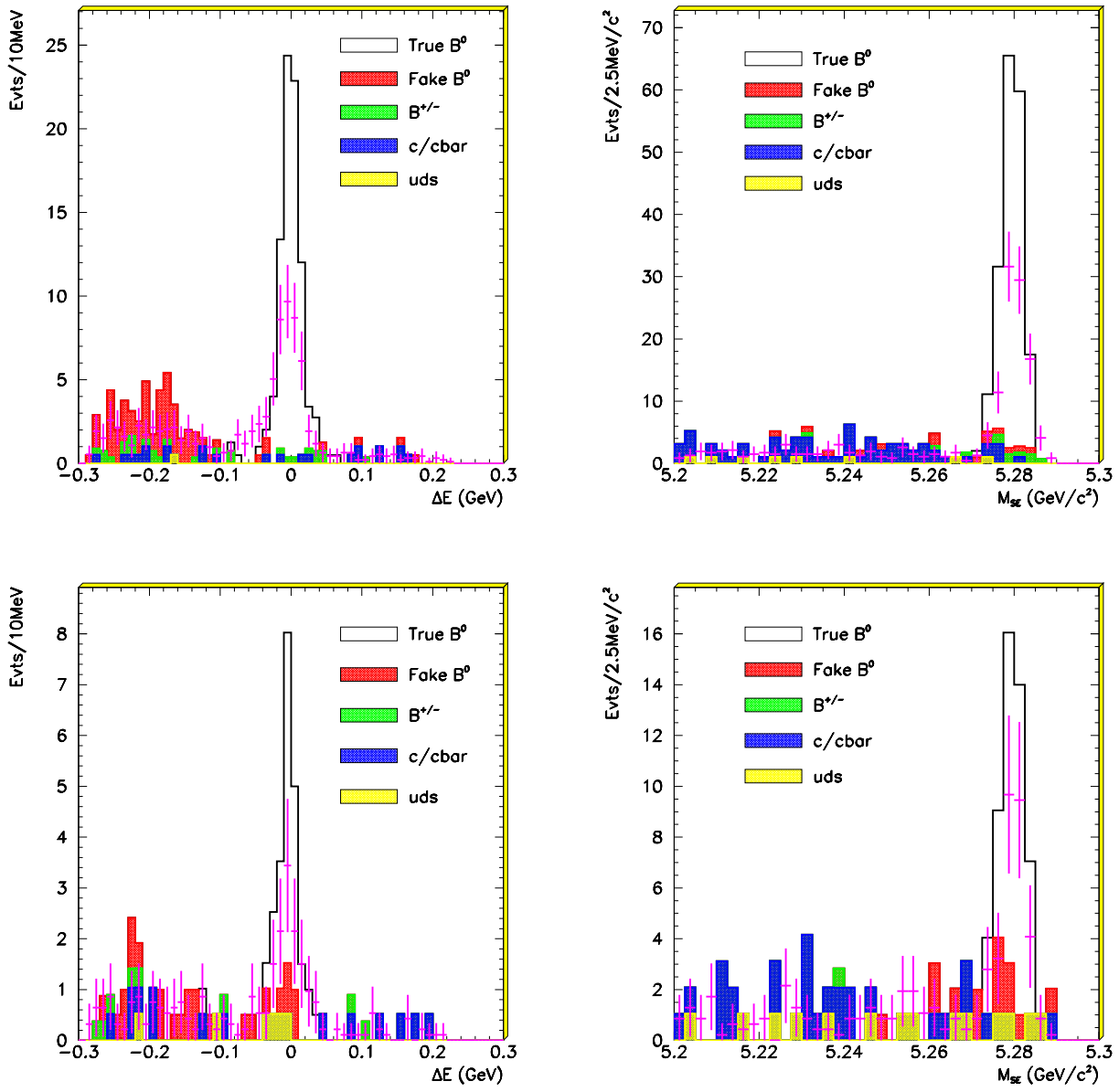

Figure 19: Generic MC studies of $\overline{B}^0 \to D^{*+}\pi^-$ for $D^0 \to K^-\pi^+\pi^-\pi^+$ (top) and $D^0 \to K^0_S\pi^+\pi^-$ (bottom). $m_{\rm ES}$ for $|\Delta E\ | < 2.5\sigma_{\Delta E}$ (right), ΔE for $|m_{\rm ES} - m_B| < 2.5\sigma m_{\rm ES}$ (left). Data normalized by luminosity is overlaid in purple.

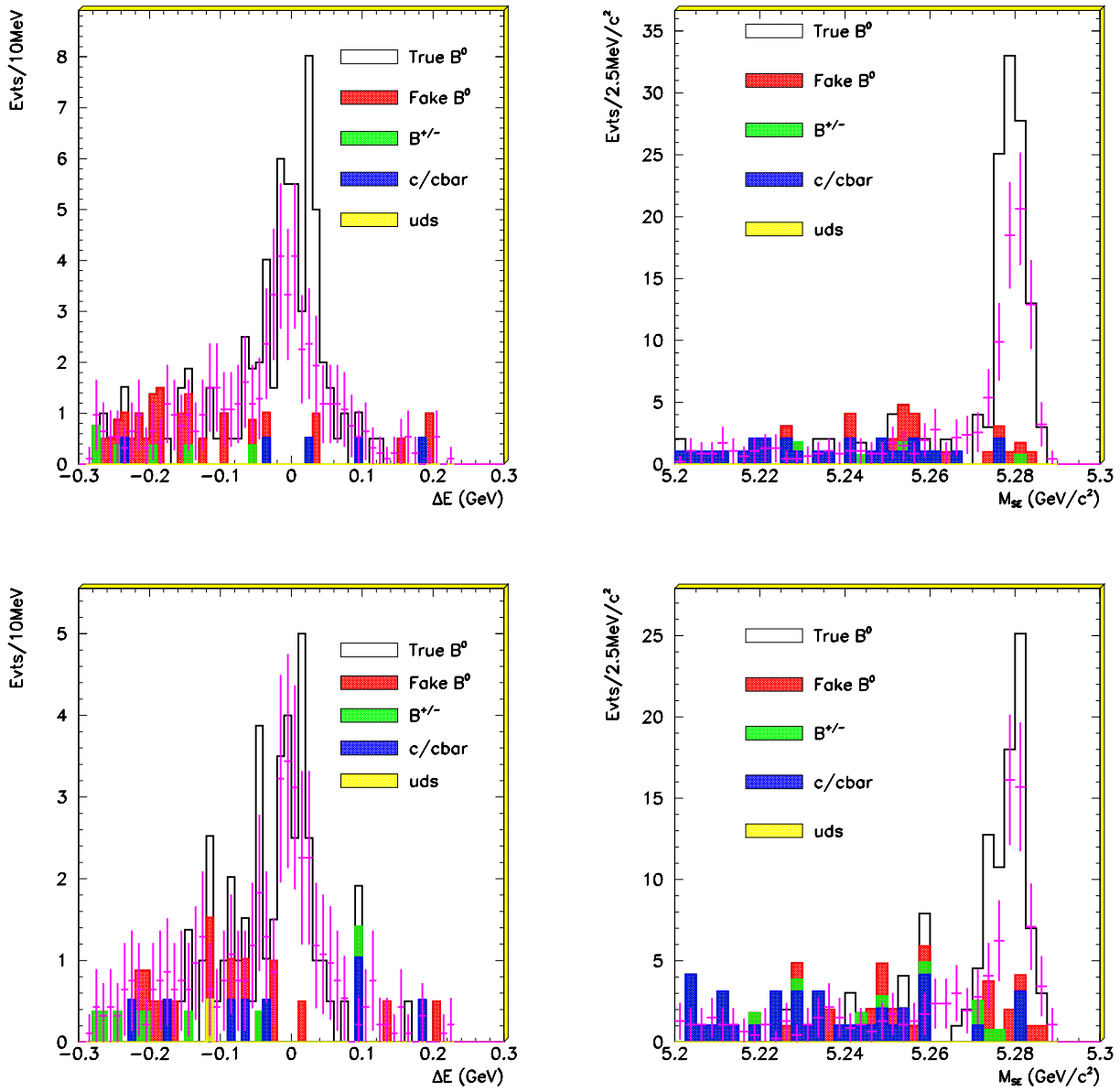

Figure 20: Generic MC studies of $\overline{B}^0 \to D^{*+}\rho^-$ for $D^0 \to K^-\pi^+$ (top) and $D^0 \to K^-\pi^+\pi^0$ (bottom). $m_{\rm ES}$ for $|\Delta E\ | < 2.5\sigma_{\Delta E}$ (right), ΔE for $|m_{\rm ES} - m_B| < 2.5\sigma m_{\rm ES}$ (left). Data normalized by luminosity is overlaid in purple.

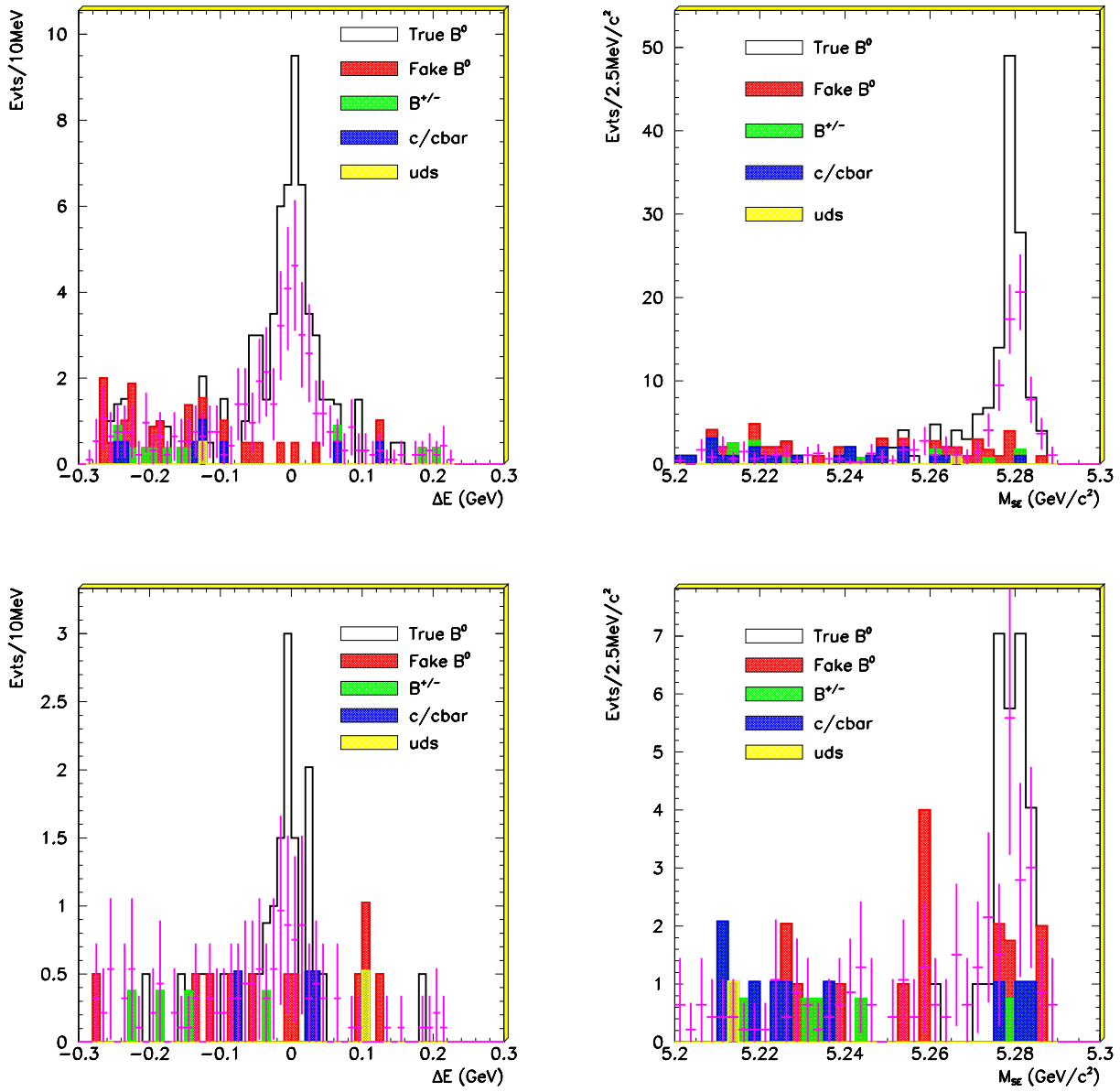

Figure 21: Generic MC studies of $\overline{B}^0 \to D^{*+}\rho^-$ for $D^0 \to K^-\pi^+\pi^-\pi^+$ (top) and $D^0 \to K^0_S\pi^+\pi^-$ (bottom). $m_{\rm ES}$ for $|\Delta E\ | < 2.5\sigma_{\Delta E}$ (right), ΔE for $|m_{\rm ES} - m_B| < 2.5\sigma m_{\rm ES}$ (left). Data normalized by luminosity is overlaid in purple.

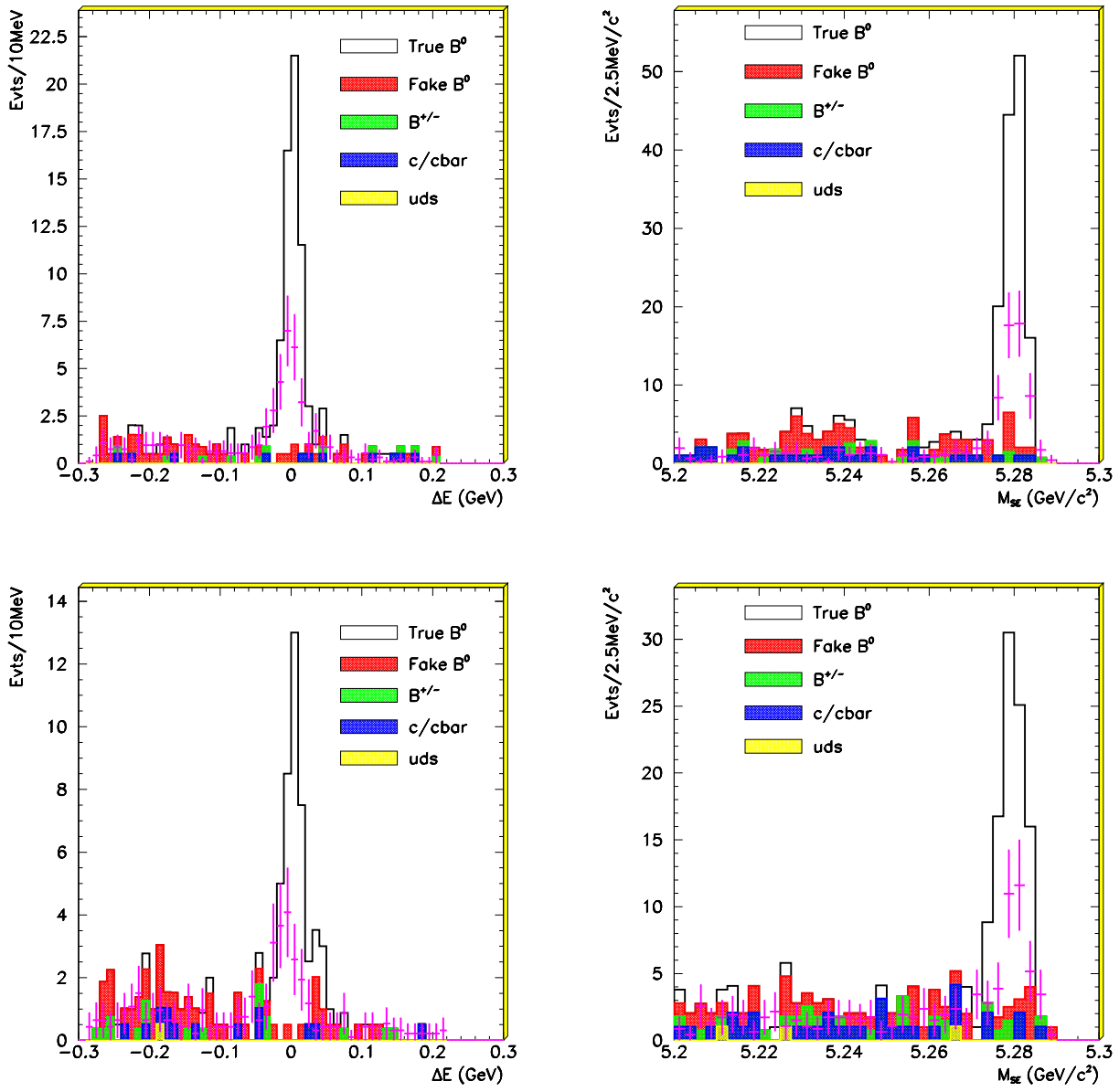

Figure 22: Generic MC studies of $\overline{B}^0 \to D^{*+}a_1^-1$ for $D^0 \to K^-\pi^+$ (top) and $D^0 \to K^-\pi^+\pi^0$ (bottom). $m_{\rm ES}$ for $|\Delta E\ | < 2.5\sigma_{\Delta E}$ (right), ΔE for $|m_{\rm ES} - m_B| < 2.5\sigma m_{\rm ES}$ (left). Data normalized by luminosity is overlaid in purple.

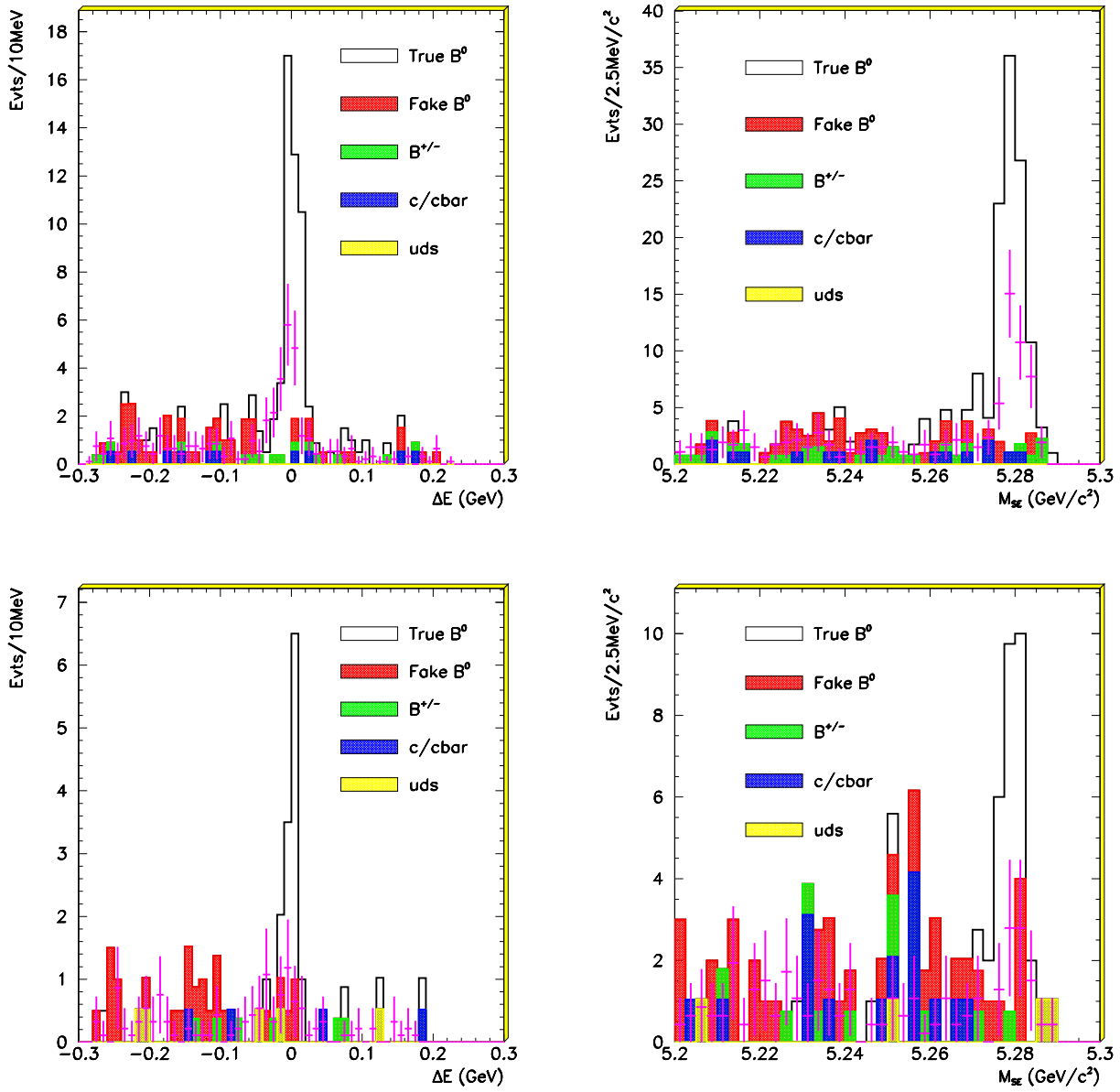

Figure 23: Generic MC studies of $\overline{B}^0 \to D^{*+}a_1^-1$ for $D^0 \to K^-\pi^+\pi^-\pi^+$ (top) and $D^0 \to K^0_S\pi^+\pi^-$ (bottom). $m_{\rm ES}$ for $|\Delta E\ | < 2.5\sigma_{\Delta E}$ (right), ΔE for $|m_{\rm ES} - m_B| < 2.5\sigma m_{\rm ES}$ (left). Data normalized by luminosity is overlaid in purple.

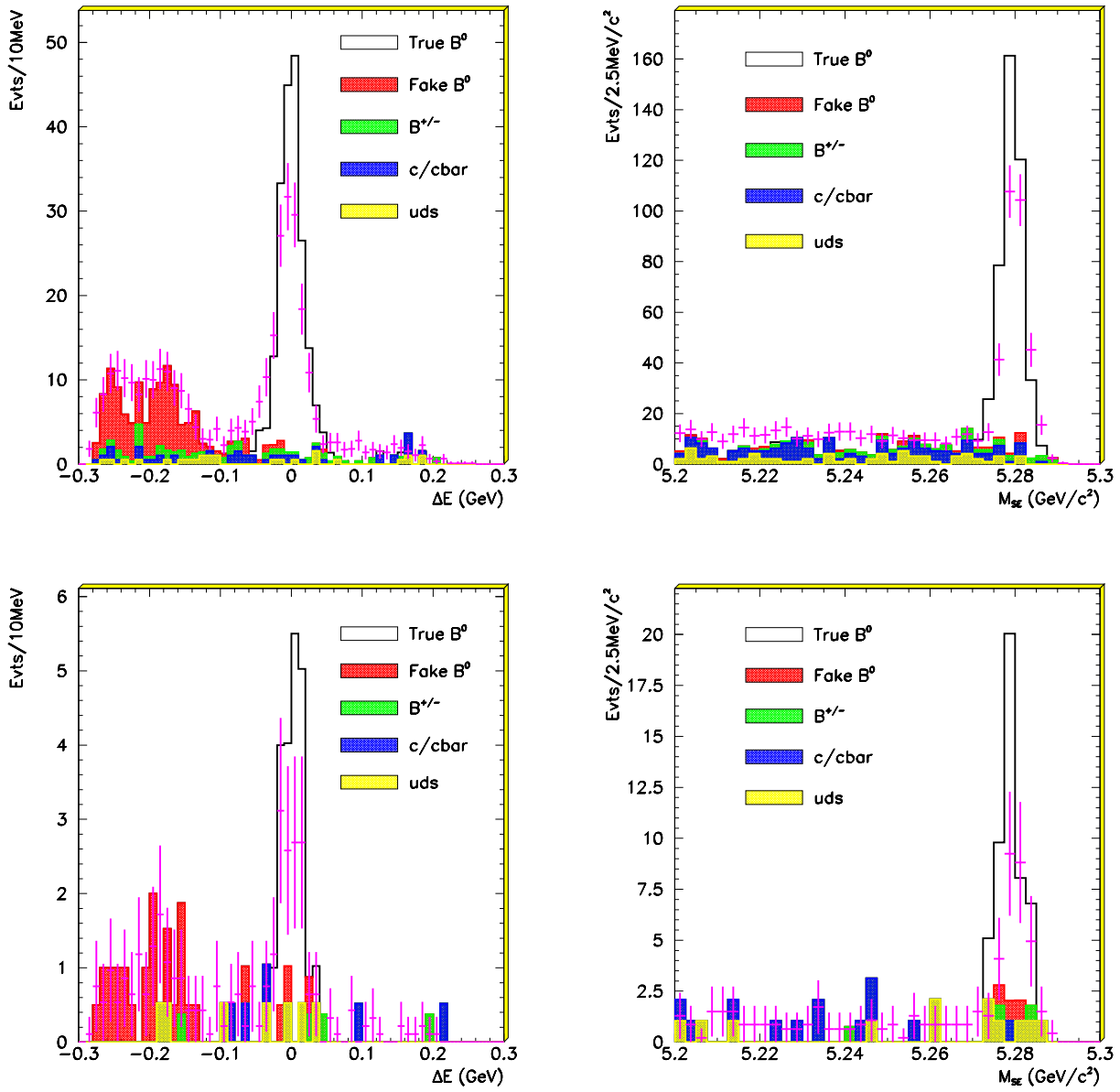

Figure 24: Generic MC studies of $\overline{B}^0 \to D^+\pi^-$ for $D^+ \to K^-\pi^+\pi^+$ (top) and $D^+ \to K^0_S\pi^+$ (bottom). $m_{\rm ES}$ for $|\Delta E\ | < 2.5\sigma_{\Delta E}$ (right), ΔE for $|m_{\rm ES} - m_B| < 2.5\sigma m_{\rm ES}$ (left). Data normalized by luminosity is overlaid in purple.

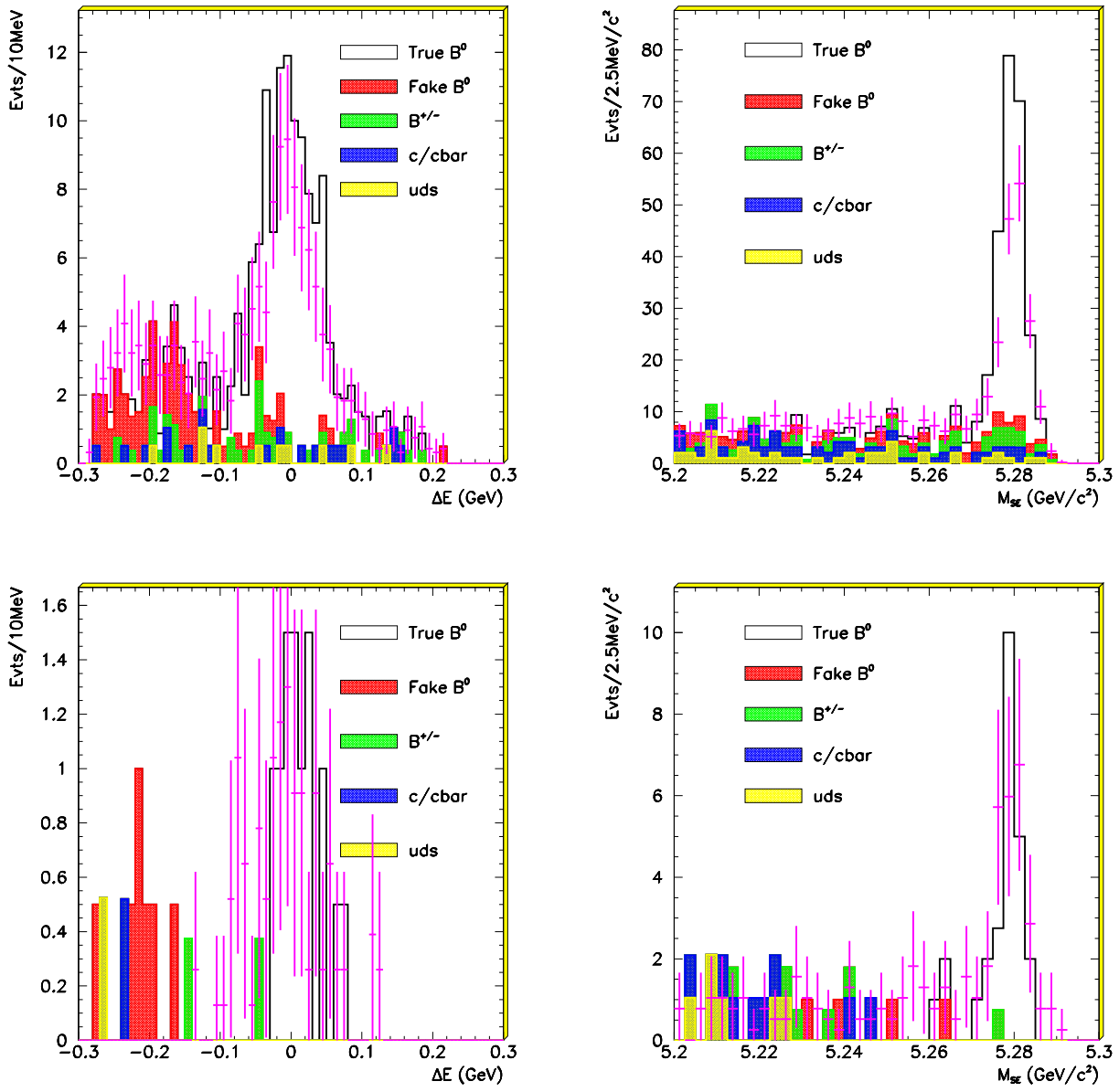

Figure 25: Generic MC studies of $\overline{B}^0 \to D^+\rho^-$ for $D^+ \to K^-\pi^+\pi^+$ (top) and $D^+ \to K^0_S\pi^+$ (bottom). $m_{\rm ES}$ for $|\Delta E\ | < 2.5\sigma_{\Delta E}$ (right), ΔE for $|m_{\rm ES} - m_B| < 2.5\sigma m_{\rm ES}$ (left). Data normalized by luminosity is overlaid in purple.

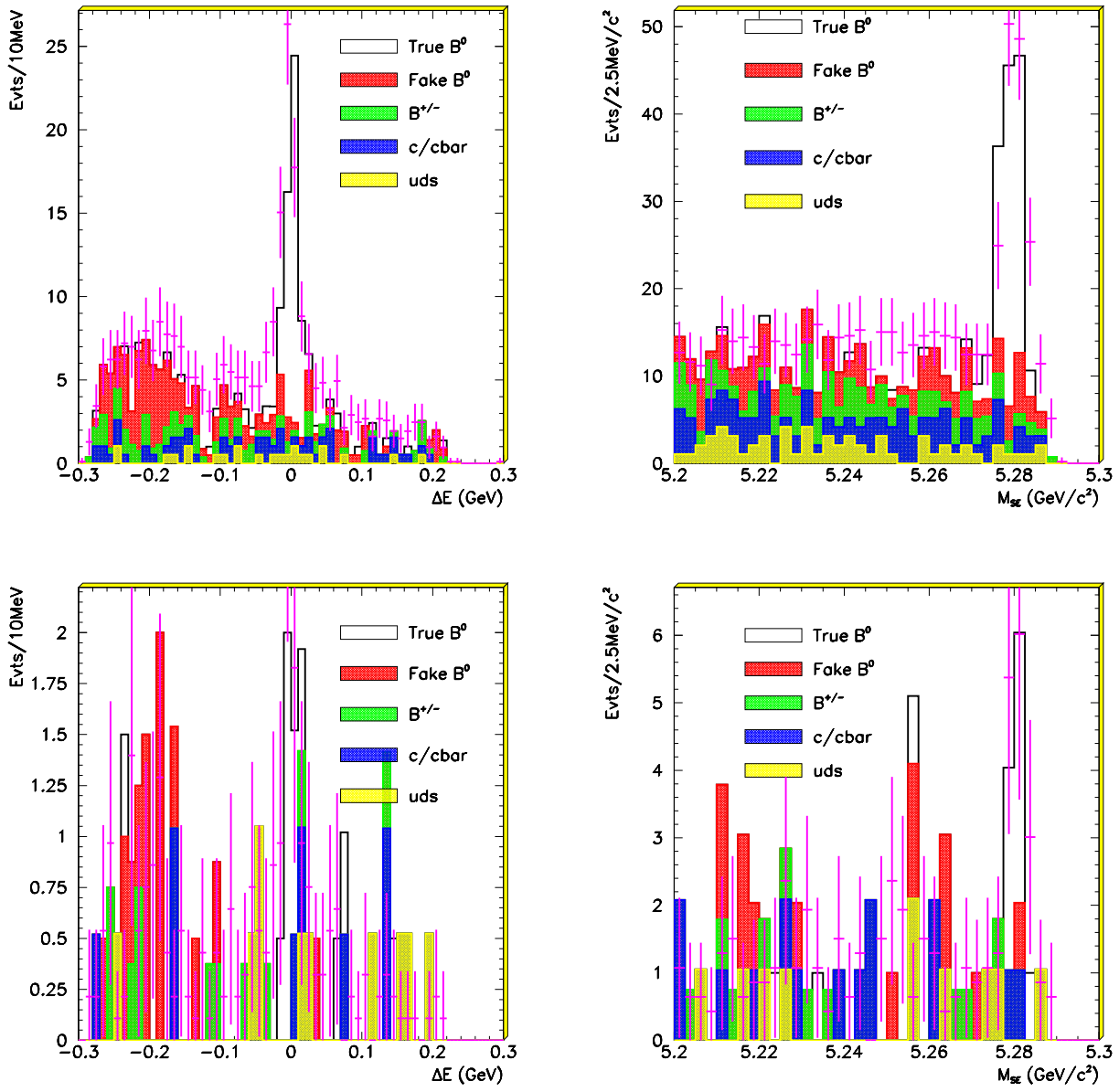

Figure 26: Generic MC studies of $\overline{B}^0 \to D^+ a_1^- 1$ for $D^+ \to K^- \pi^+ \pi^+$ (top) and $D^+ \to K_S^0 \pi^+$ (bottom). $m_{\rm ES}$ for $|\Delta E \ | < 2.5\sigma_{\Delta E}$ (right), ΔE for $|m_{\rm ES} - m_B| < 2.5\sigma m_{\rm ES}$ (left). Data normalized by luminosity is overlaid in purple.

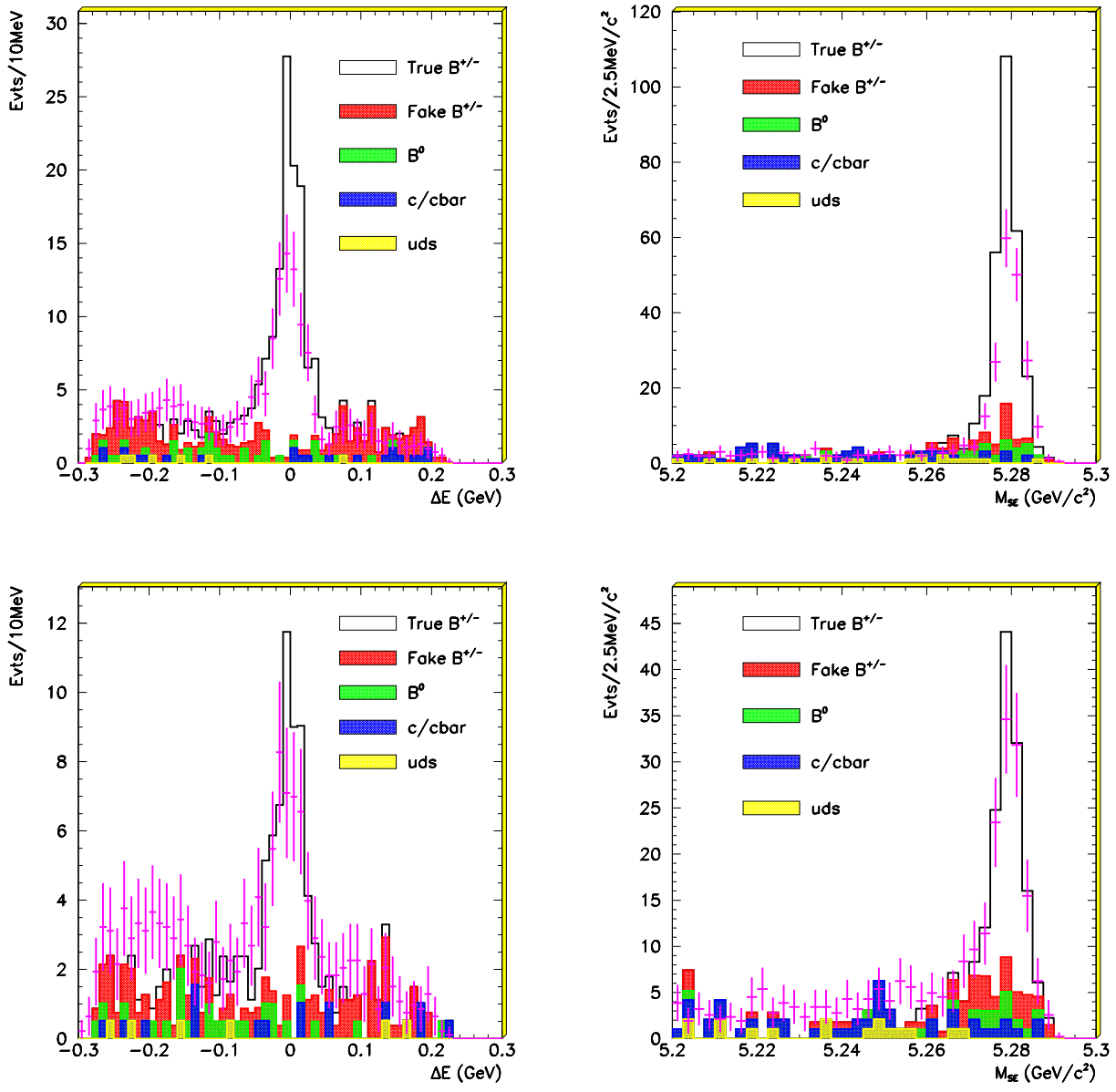

Figure 27: Generic MC studies of $B^- \to D^{*0}\pi^-$ for $D^0 \to K^-\pi^+$ (top) and $D^0 \to K^-\pi^+\pi^0$ (bottom). $m_{\rm ES}$ for $|\Delta E\ | < 2.5\sigma_{\Delta E}$ (right), ΔE for $|m_{\rm ES} - m_B| < 2.5\sigma m_{\rm ES}$ (left). Data normalized by luminosity is overlaid in purple.

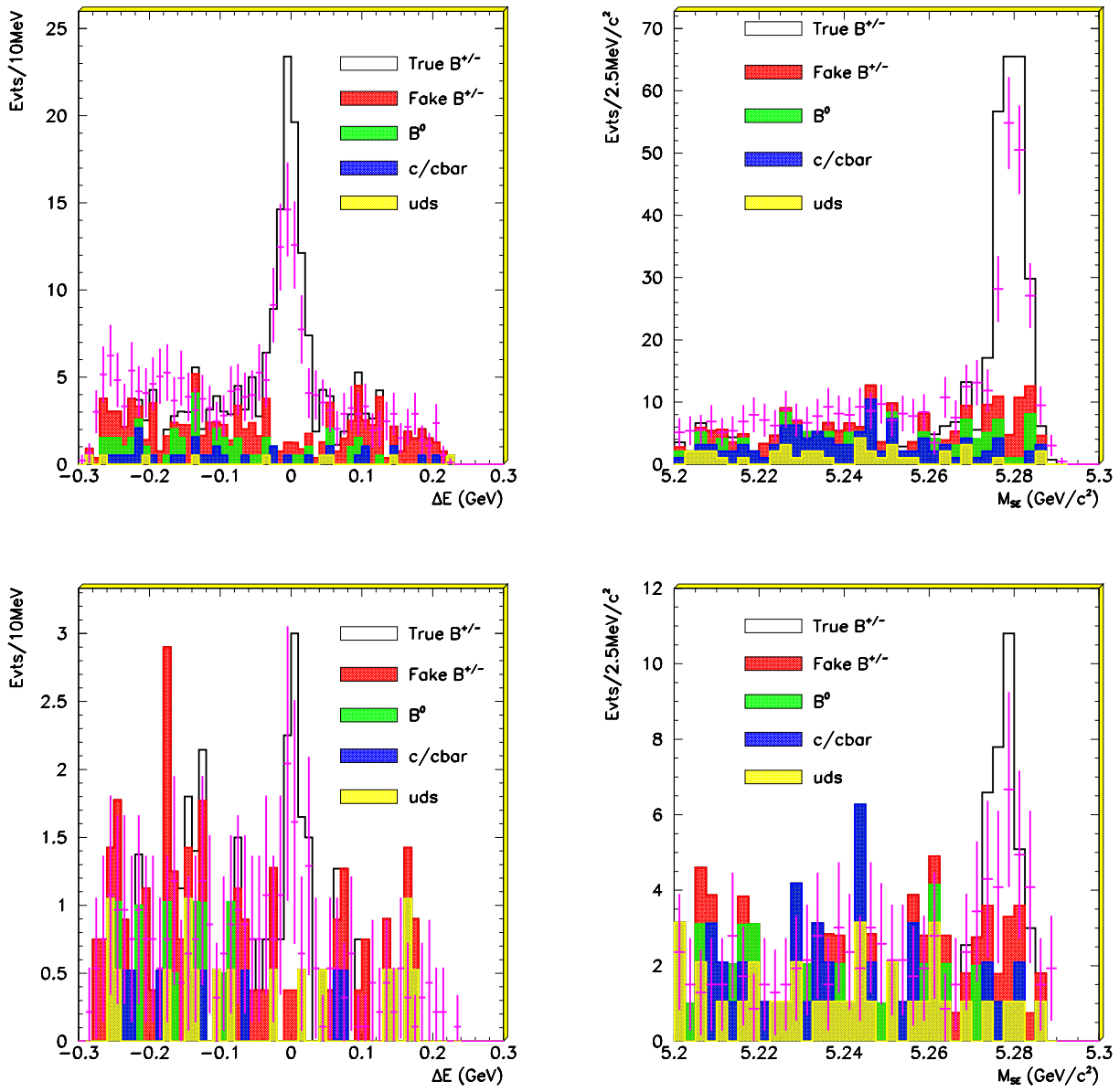

Figure 28: Generic MC studies of $B^- \to D^{*0}\pi^-$ for $D^0 \to K^-\pi^+\pi^-\pi^+$ (top) and $D^0 \to K^0_S\pi^+\pi^-$ (bottom). $m_{\rm ES}$ for $|\Delta E\ | < 2.5\sigma_{\Delta E}$ (right), ΔE for $|m_{\rm ES} - m_B| < 2.5\sigma m_{\rm ES}$ (left). Data normalized by luminosity is overlaid in purple.

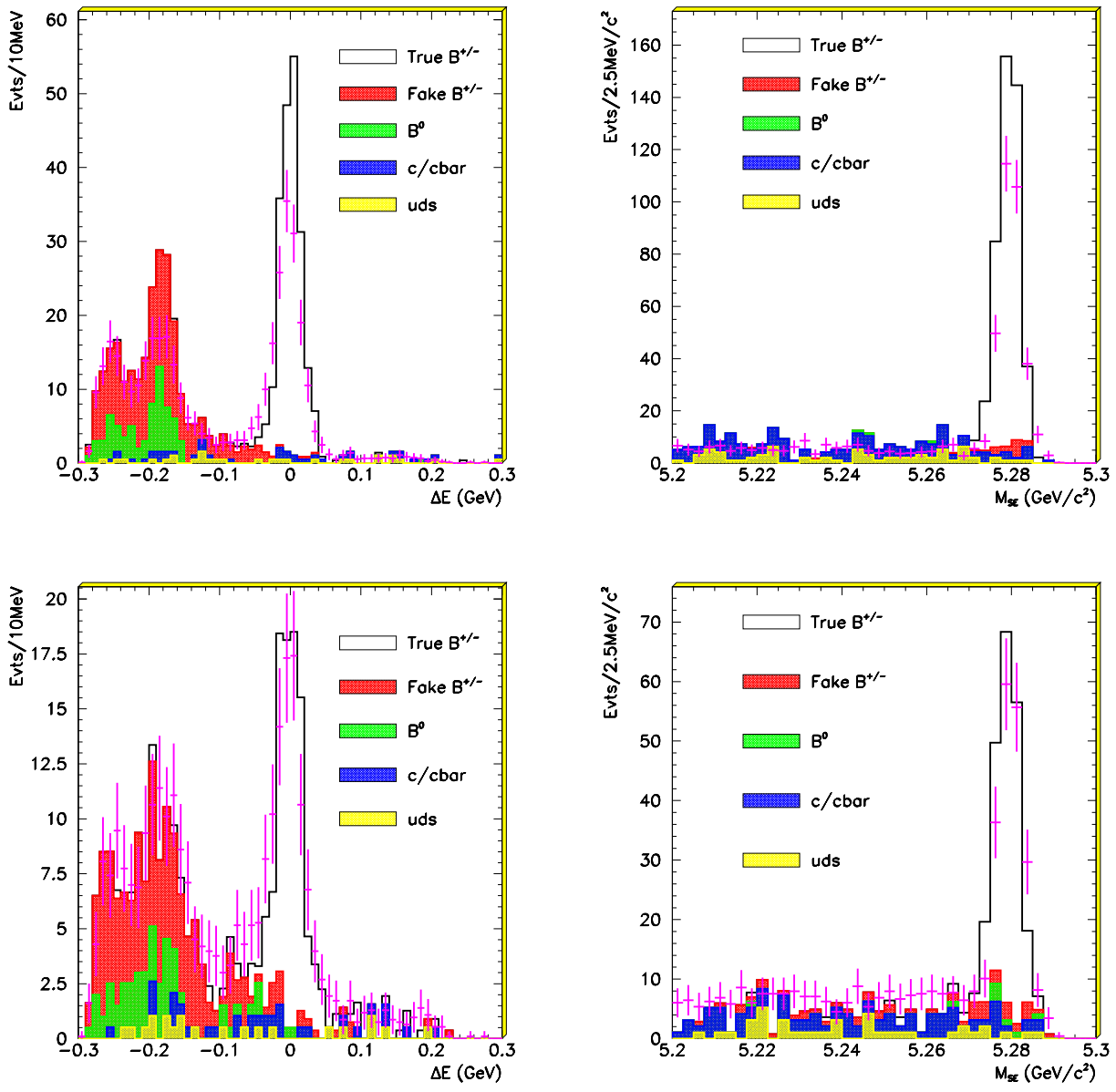

Figure 29: Generic MC studies of $B^- \to D^0\pi^-$ for $D^0 \to K^-\pi^+$ (top) and $D^0 \to K^-\pi^+\pi^0$ (bottom). $m_{\rm ES}$ for $|\Delta E\ | < 2.5\sigma_{\Delta E}$ (right), ΔE for $|m_{\rm ES} - m_B| < 2.5\sigma m_{\rm ES}$ (left). Data normalized by luminosity is overlaid in purple.

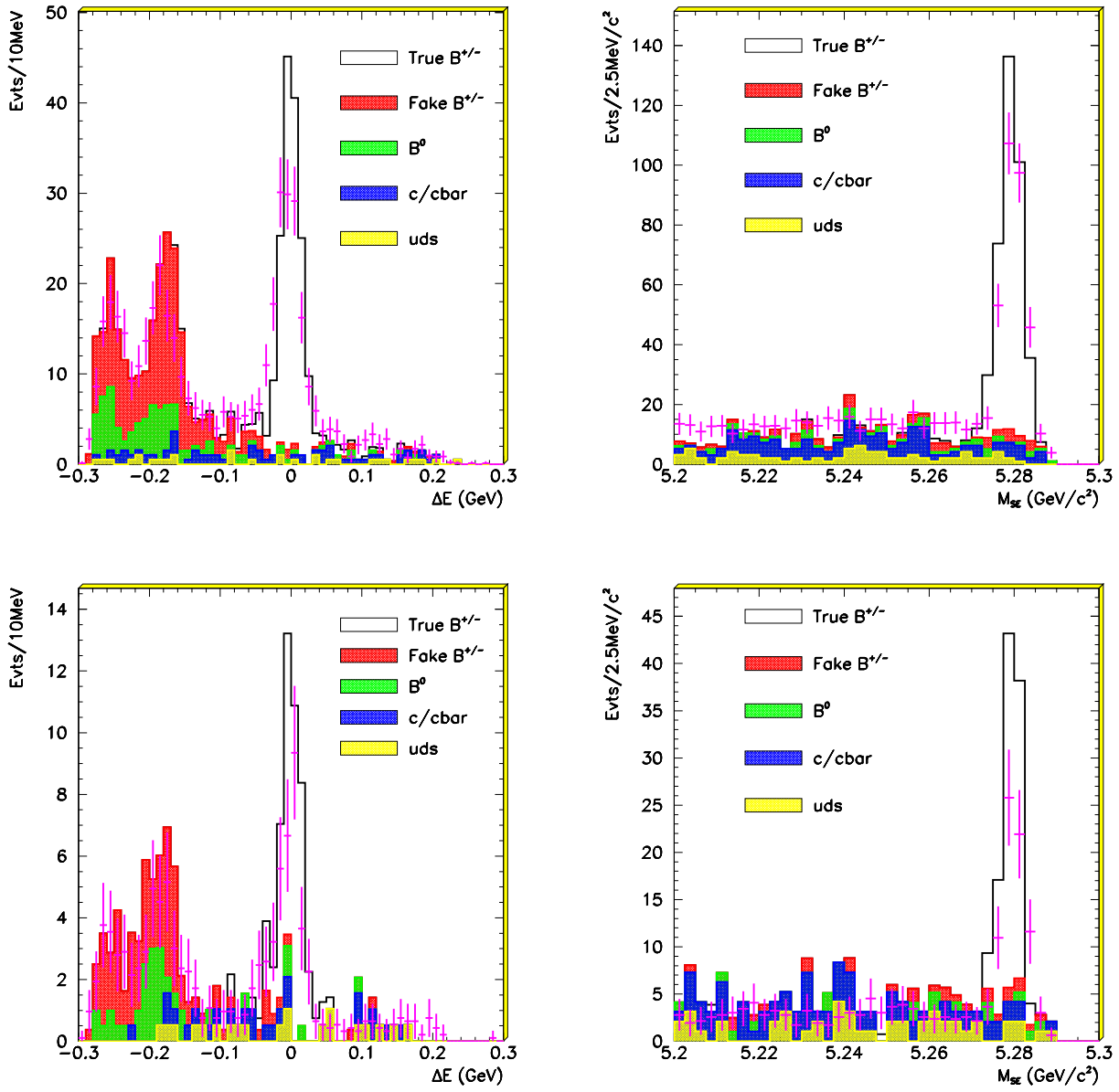

Figure 30: Generic MC studies of $B^- \to D^0\pi^-$ for $D^0 \to K^-\pi^+\pi^-\pi^+$ (top) and $D^0 \to K^0_S\pi^+\pi^-$ (bottom). $m_{\rm ES}$ for $|\Delta E\ | < 2.5\sigma_{\Delta E}$ (right), ΔE for $|m_{\rm ES} - m_B| < 2.5\sigma m_{\rm ES}$ (left). Data normalized by luminosity is overlaid in purple.

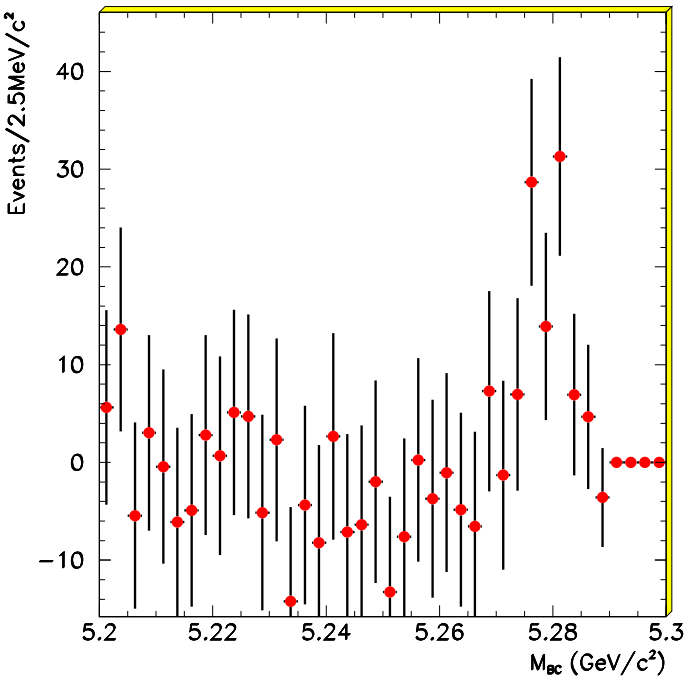

Figure 31: Generic MC studies of peaking bacground. Shown is $m_{\rm ES}$ distribution of all background types in the B^0 sample, after ARGUS subtraction.

4 B^0 Decays

Here we provide tables of resolutions and yields for the B^0 decay modes reconstructed.

A sample plot showing the ΔE versus $m_{\rm ES}$ distribution for $\overline{B}^0 \to D^{*+}\pi^-$, $D^0 \to K^-\pi^+$ is given in Figure 32

For each individual decay chain, the distribution of $m_{\rm ES}$ for $|\Delta E\ | < 2.5\sigma_{\Delta E}$ and ΔE for *check this!* $|m_{\rm ES} - {m_{\rm ES}}^0| < 3\sigma_{m_{\rm ES}}$ is provided. The same plots are also shown summed over D^0 or D^+ modes. These are shown as Figures 33 through 41

The fit results for $\sigma_{m_{\rm ES}}$ and $\sigma_{\Delta E}$ in Monte Carlo and data are summarized in Table 18. The fitted numbers of events are shown in Table 19.

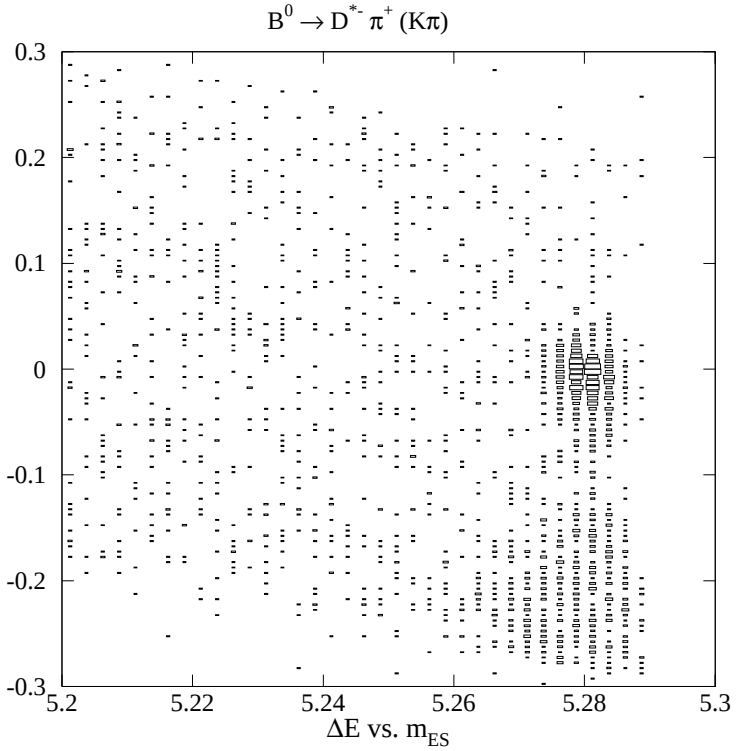

Figure 32: ΔE versus $m_{\rm ES}$ for the decay $\overline{B}^0 \to D^{*+}\pi^-$, $D^0 \to K^-\pi^+$.

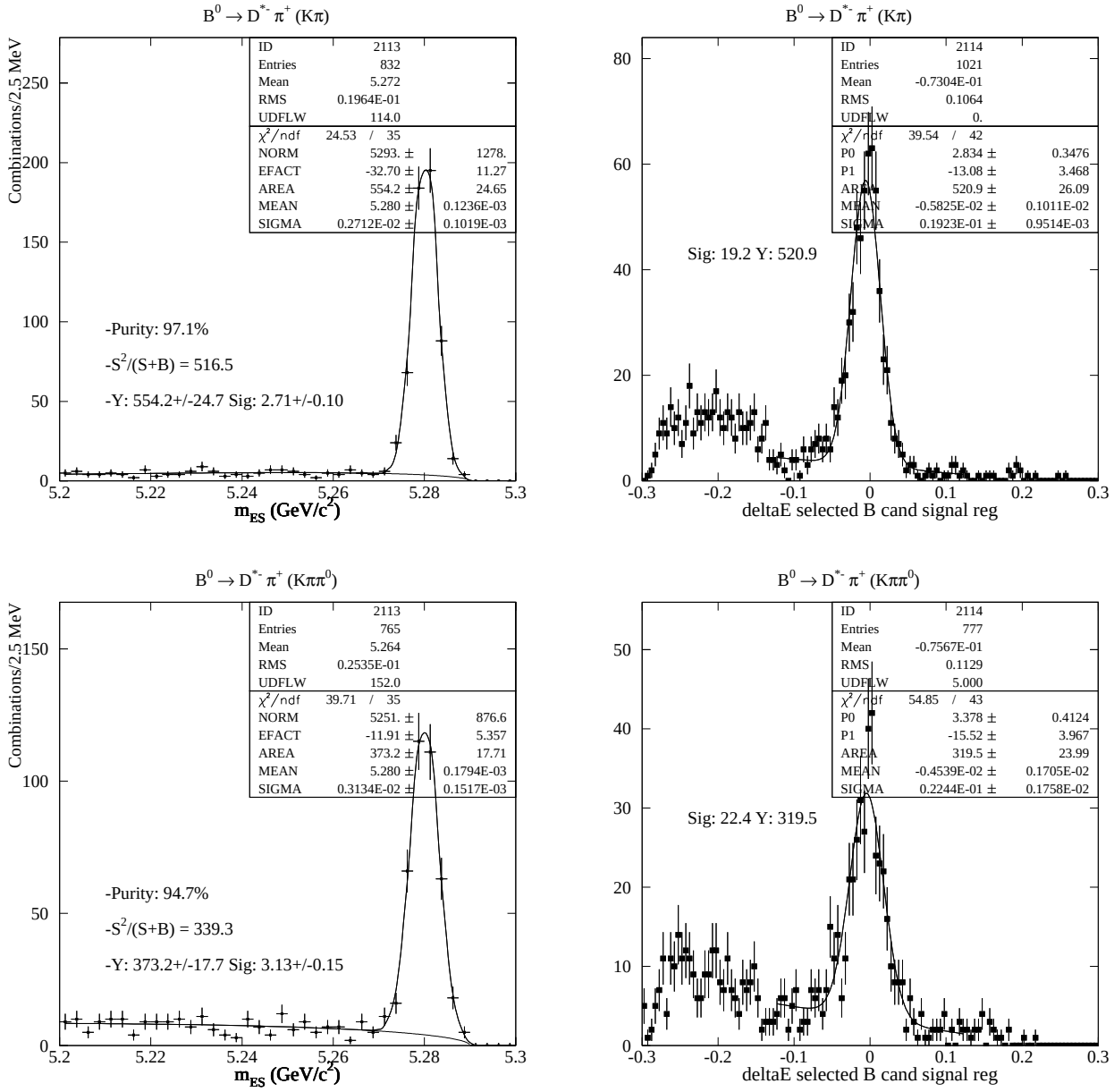

Figure 33: $\overline{B}^0 \to D^{*+}\pi^-$ for $D^0 \to K^-\pi^+$ (top) and $D^0 \to K^-\pi^+\pi^0$ (bottom). $m_{\rm ES}$ for $|\Delta E\ | < 2.5\sigma_{\Delta E}$ (left), ΔE for $|m_{\rm ES} - m_B| < 2.5\sigma_{m_{\rm ES}}$ (right).

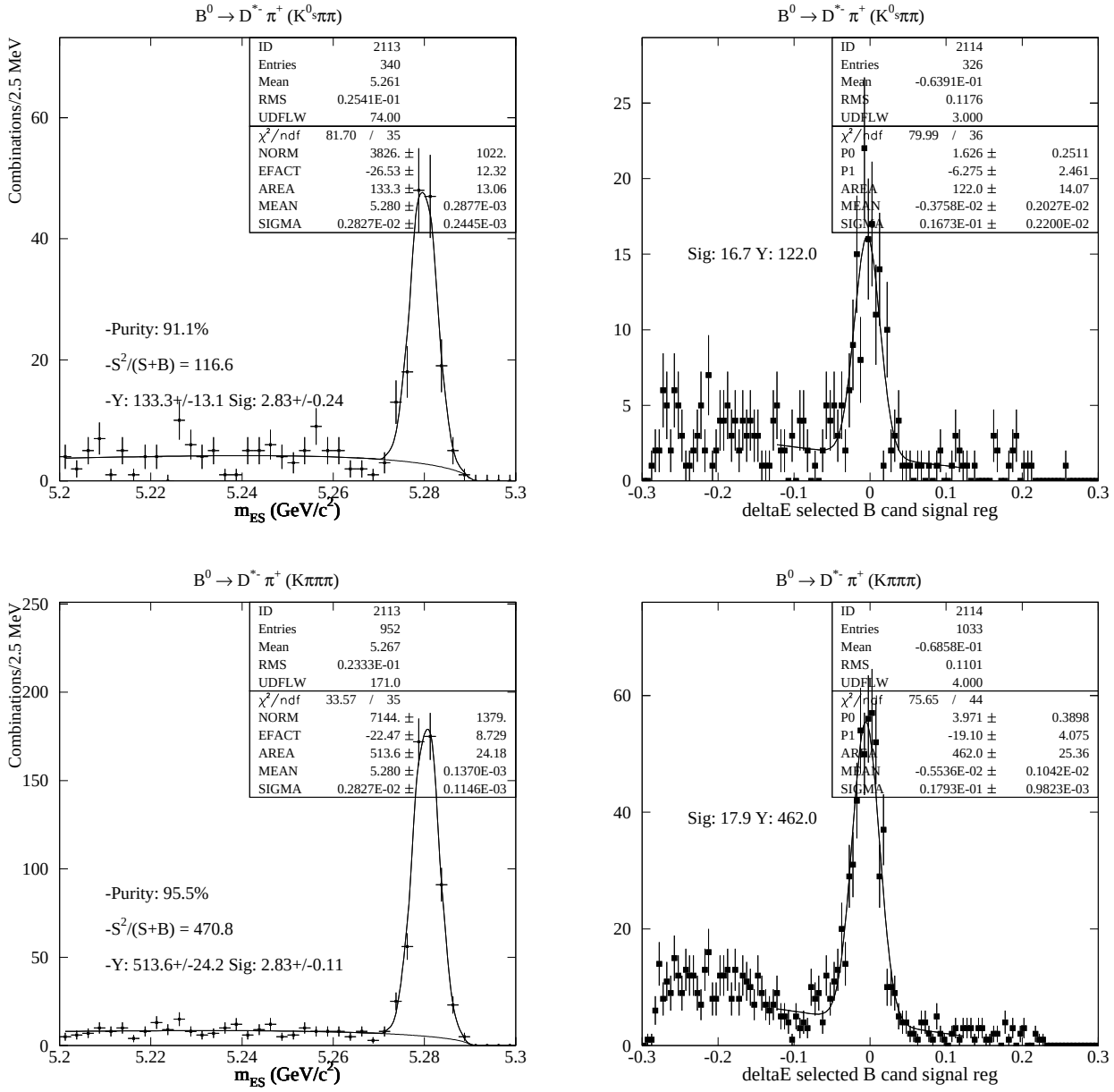

Figure 34: $\overline{B}^0 \to D^{*+}\pi^-$ for $D^0 \to K^0_S\pi^+\pi^-$ (top) and $D^0 \to K^-\pi^+\pi^-\pi^+$ (bottom). $m_{\rm ES}$ for $|\Delta E\ | < 2.5\sigma_{\Delta E}$ (left), ΔE for $|m_{\rm ES} - m_B| < 2.5\sigma_{m_{\rm ES}}$ (right).

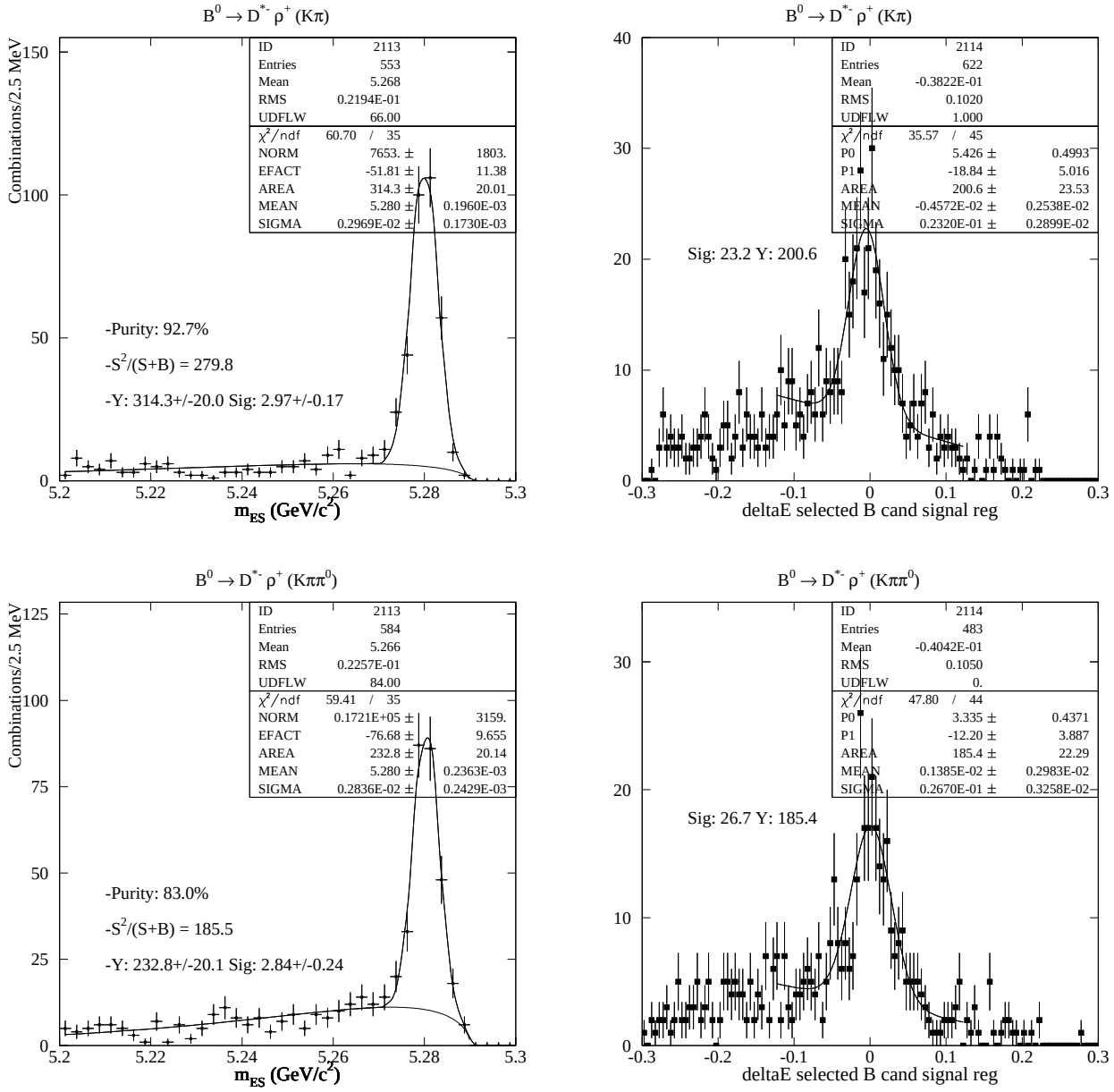

Figure 35: $\overline{B}^0 \to D^{*+}\rho^-$ for $D^0 \to K^-\pi^+$ (top) and $D^0 \to K^-\pi^+\pi^0$ (bottom). $m_{\rm ES}$ for $|\Delta E\ | < 2.5\sigma_{\Delta E}$ (left), ΔE for $|m_{\rm ES} - m_B| < 2.5\sigma_{m_{\rm ES}}$ (right).

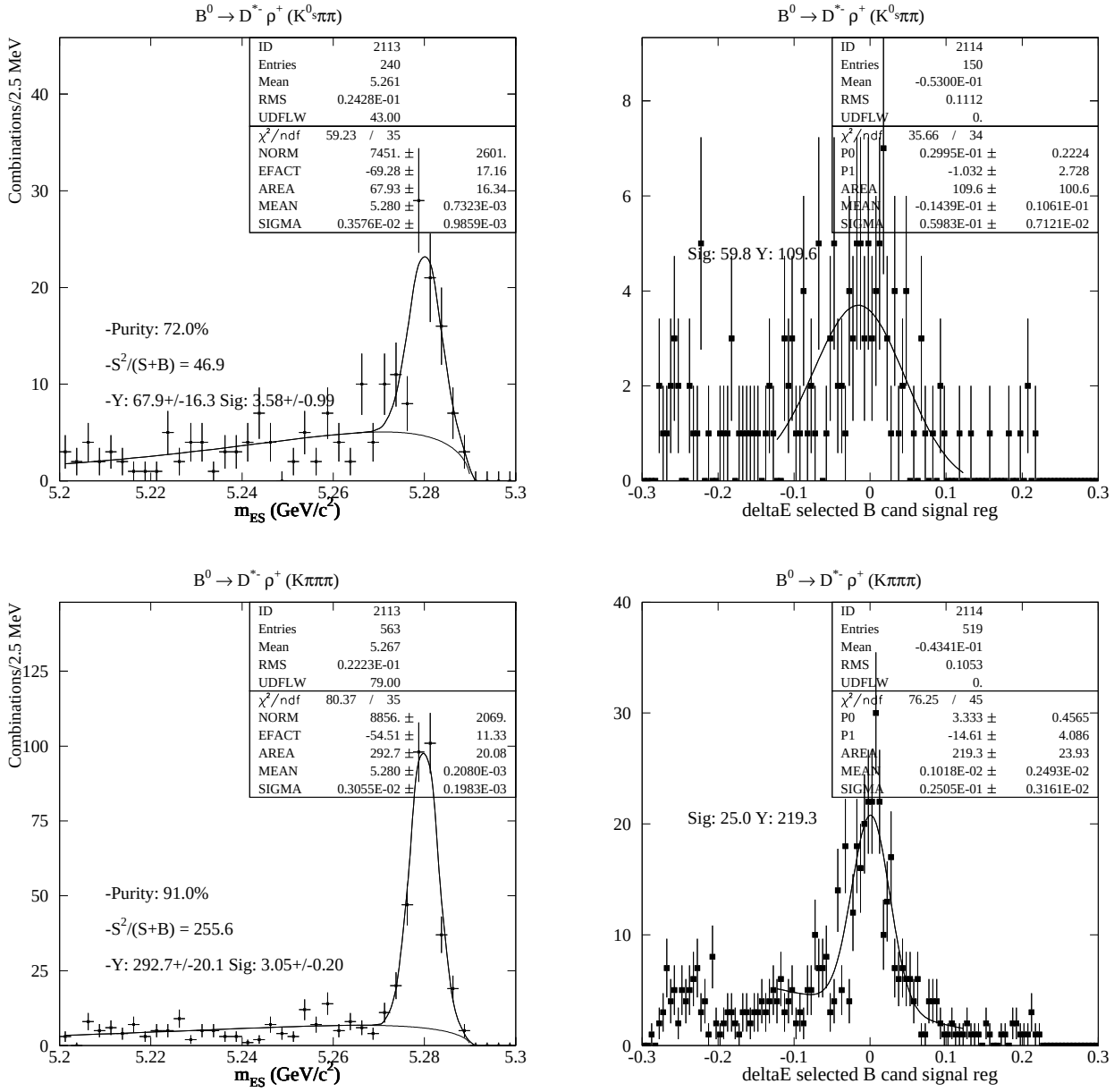

Figure 36: $\overline{B}^0 \to D^{*+}\rho^-$ for $D^0 \to K^0_S\pi^+\pi^-$ (top) and $D^0 \to K^-\pi^+\pi^-\pi^+$ (bottom). $m_{\rm ES}$ for $|\Delta E\ | < 2.5\sigma_{\Delta E}$ (left), ΔE for $|m_{\rm ES} - m_B| < 2.5\sigma_{m_{\rm ES}}$ (right).

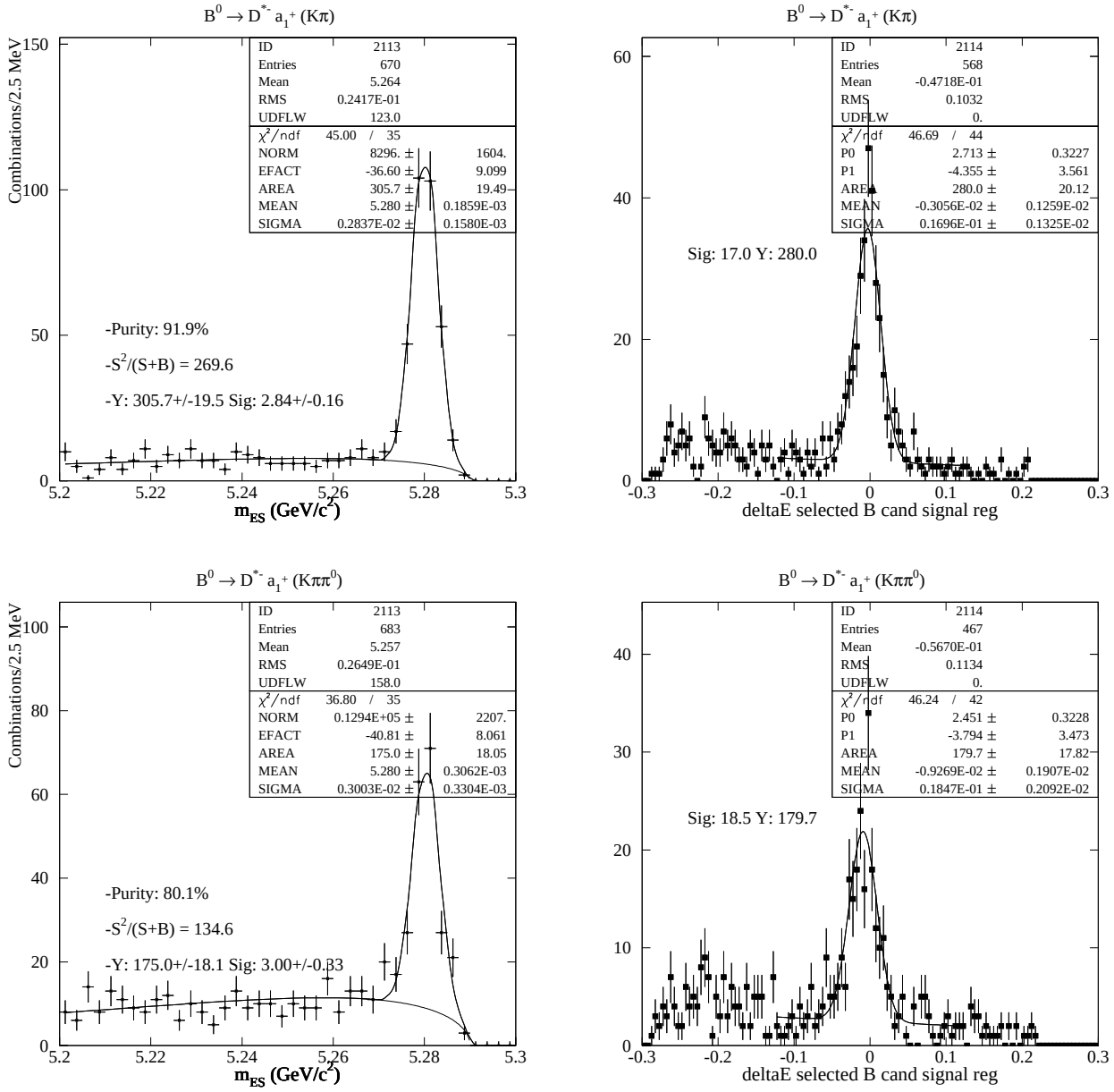

Figure 37: $\overline{B}^0 \to D^{*+}a_1^-$ for $D^0 \to K^-\pi^+$ (top) and $D^0 \to K^-\pi^+\pi^0$ (bottom). $m_{\rm ES}$ for $|\Delta E\ | < 3\sigma_{\Delta E}$ (left), ΔE for $|m_{\rm ES} - {m_{\rm ES}}^0| < 3\sigma m_{\rm ES}$ (right).

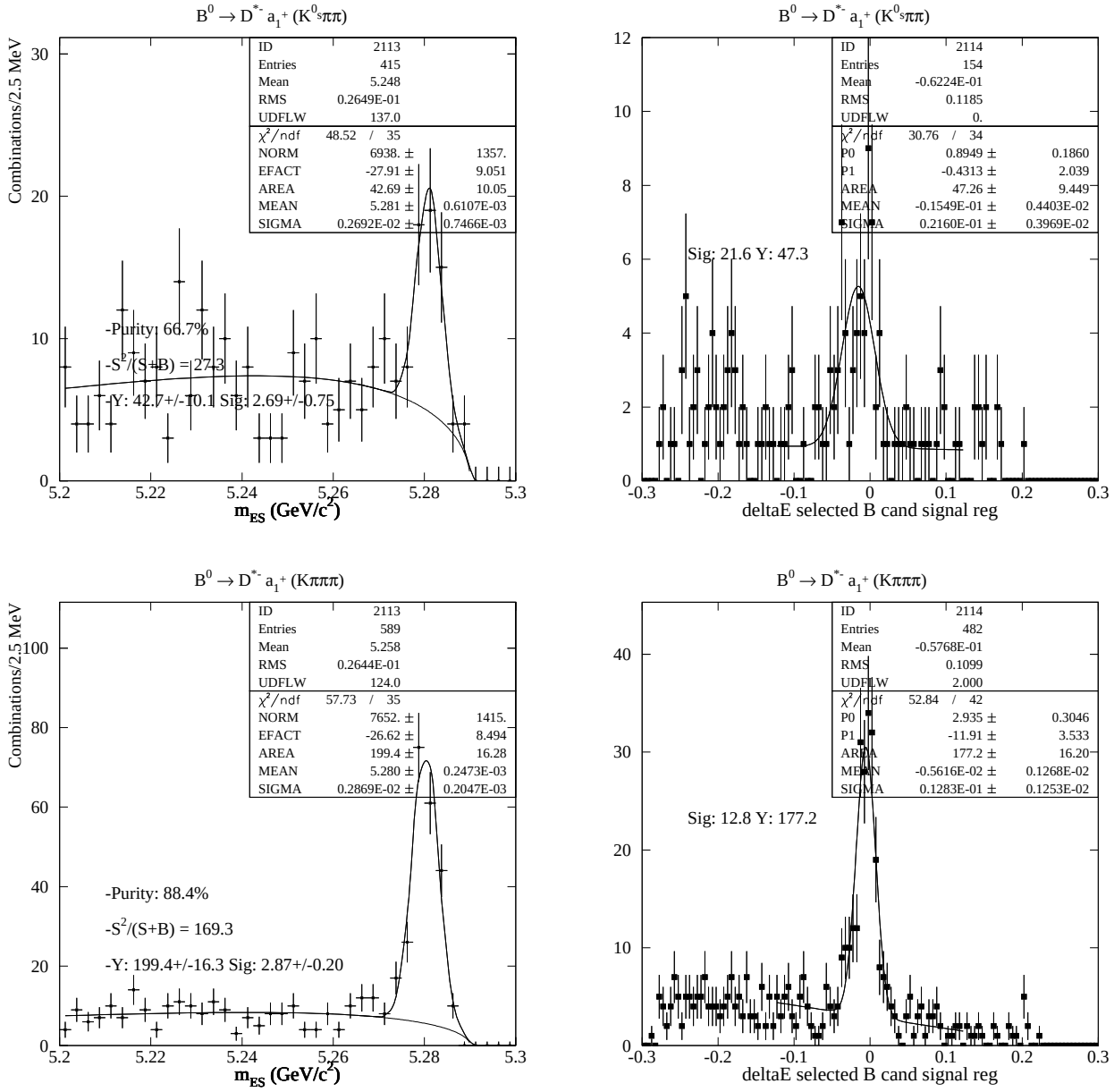

Figure 38: $\overline{B}^0 \to D^{*+}a_1^-$ for $D^0 \to K^0_S\pi^+\pi^-$ (top) and $D^0 \to K^-\pi^+\pi^-\pi^+$ (bottom). $m_{\rm ES}$ for $|\Delta E\ | < 3\sigma_{\Delta E}$ (left), ΔE for $|m_{\rm ES} - {m_{\rm ES}}^0| < 3\sigma m_{\rm ES}$ (right).

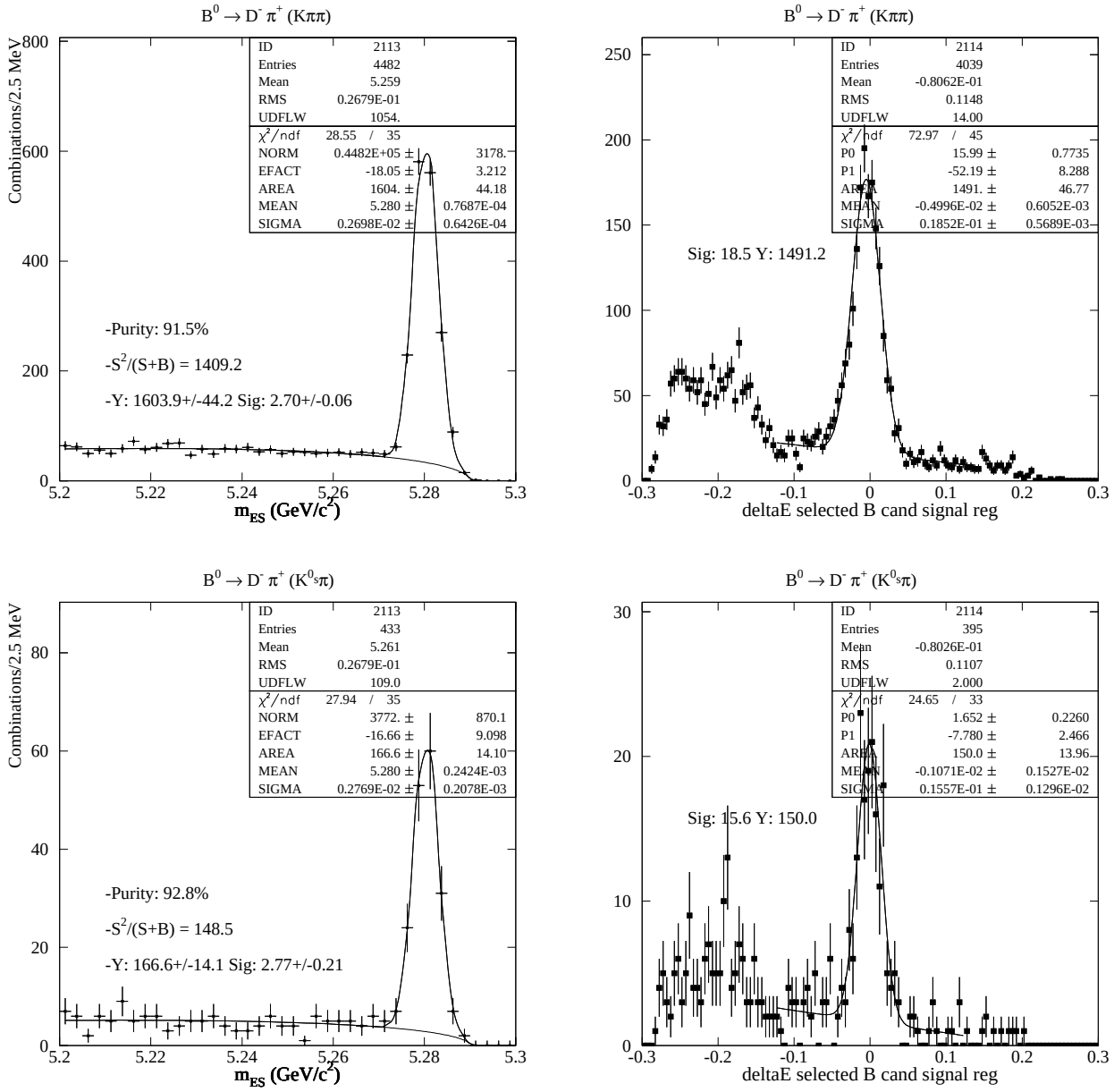

Figure 39: $\overline{B}^0 \to D^+\pi^-$ for $D^+ \to K^-\pi^+\pi^+$ (top) and $D^+ \to K^0_S\pi^+$ (bottom). $m_{\rm ES}$ for $|\Delta E\ | < 3\sigma_{\Delta E}$ (left), ΔE for $|m_{\rm ES} - {m_{\rm ES}}^0| < 3\sigma m_{\rm ES}$ (right).

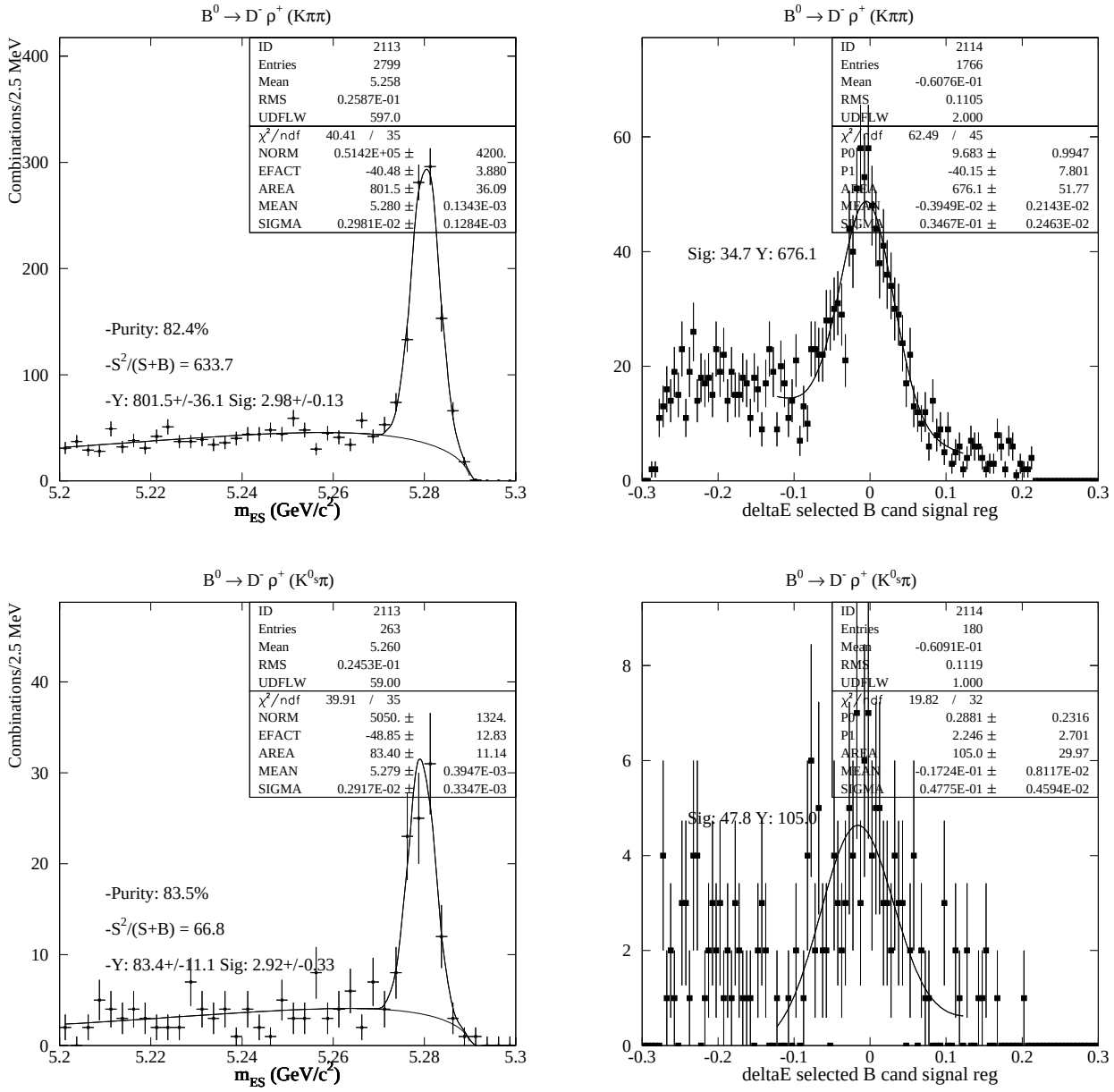

Figure 40: $\overline{B}^0 \to D^+\rho^-$ for $D^+ \to K^-\pi^+\pi^+$ (top) and $D^+ \to K^0_S\pi^+$ (bottom). $m_{\rm ES}$ for $|\Delta E\ | < 3\sigma_{\Delta E}$ (left), ΔE for $|m_{\rm ES} - {m_{\rm ES}}^0| < 3\sigma m_{\rm ES}$ (right).

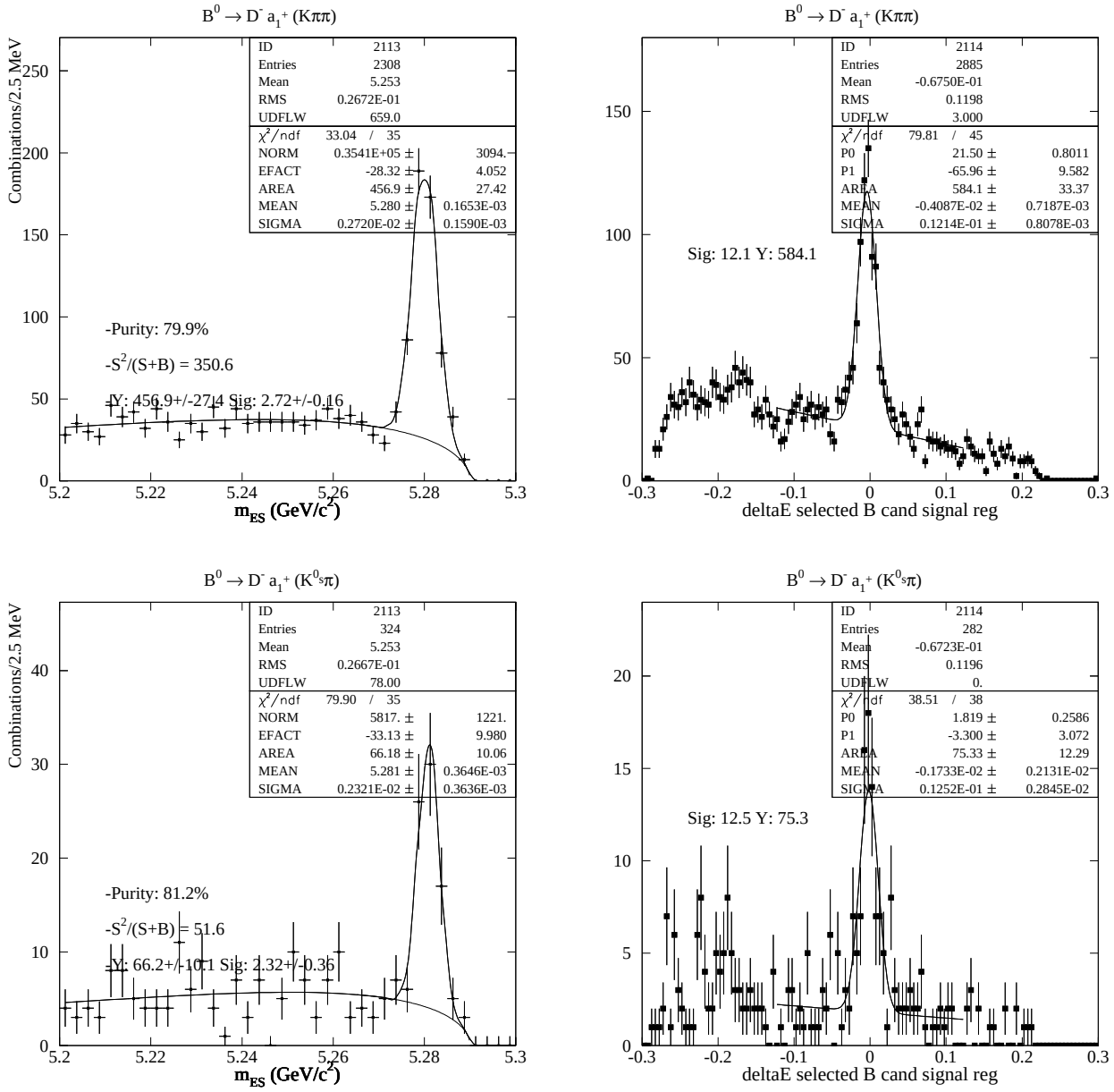

Figure 41: $\overline{B}^0 \to D^+ a_1^-$ for $D^+ \to K^-\pi^+\pi^+$ (top) and $D^+ \to K^0_S\pi^+$ (bottom). $m_{\rm ES}$ for $|\Delta E\ | < 3\sigma_{\Delta E}$ (left), ΔE for $|m_{\rm ES} - {m_{\rm ES}}^0| < 3\sigma m_{\rm ES}$ (right).

Table 18: Observed and predicted resolution for ΔE and $m_{\rm ES}$ for B^0 decay modes. In some cases, the fit results for individual decay chains suffer from inadequate statistics, particularly without full confidence in Monte Carlo predictions for signal widths.

B^0 mode	D mode	$\sigma_{\Delta E}$ Data (MeV)	ΔE offset (MeV)	$\sigma_{\Delta E}$ MC (MeV)	$\sigma_{m_{\rm ES}}$ Data (MeV)	$\sigma_{m_{\rm ES}}$ MC (MeV)
$D^{*-}\pi^+$	$K^-\pi^+$	19.2 ± 1.0	-5.8 ± 1.0	13.8 ± 0.3	2.7 ± 0.1	2.5 ± 0.1
	$K^-\pi^+\pi^0$	22.4 ± 1.7	-4.5 ± 1.7	15.8 ± 0.4	3.1 ± 0.2	2.7 ± 0.1
	$K^0_S\pi^+\pi^-$	16.7 ± 2.2	-3.8 ± 2.0	12.6 ± 0.6	2.8 ± 0.2	2.5 ± 0.1
	$K^-\pi^+\pi^+\pi^-$	18.0 ± 1.0	-5.5 ± 1.0	13.7 ± 0.3	2.8 ± 0.1	2.5 ± 0.1
$D^{*-}\rho^+$	$K^-\pi^+$	23.2 ± 2.9	-4.6 ± 2.5	26.3 ± 1.2	3.0 ± 0.2	2.8 ± 0.1
	$K^-\pi^+\pi^0$	26.7 ± 3.3	1.4 ± 3.0	27.6 ± 1.3	2.8 ± 0.2	2.8 ± 0.1
	$K^0_S\pi^+\pi^-$	$xx \pm xx$	$xx \pm xx$	27.9 ± 2.8	3.6 ± 0.1	2.9 ± 0.2
	$K^-\pi^+\pi^+\pi^-$	25.1 ± 3.2	1.0 ± 2.5	27.4 ± 1.3	3.1 ± 0.2	2.8 ± 0.1
$D^{*-}a_1^+$	$K^-\pi^+$	17.0 ± 1.3	-3.1 ± 1.3	10.4 ± 0.3	2.8 ± 0.2	2.4 ± 0.1
	$K^-\pi^+\pi^0$	18.5 ± 2.1	-9.2 ± 1.9	12.2 ± 0.5	3.0 ± 0.3	2.6 ± 0.1
	$K^0_S\pi^+\pi^-$	21.6 ± 4.0	-15.4 ± 4.4	12.6 ± 0.8	2.7 ± 0.7	2.6 ± 0.1
	$K^-\pi^+\pi^+\pi^-$	12.8 ± 1.3	-5.6 ± 1.3	9.8 ± 0.3	2.9 ± 0.2	2.5 ± 0.1
$D^-\pi^+$	$K^-\pi^+\pi^+$	18.5 ± 0.6	-5.0 ± 0.6	13.4 ± 0.1	2.7 ± 0.1	2.5 ± 0.1
	$K^0_S\pi^+$	15.6 ± 1.3	-1.1 ± 1.5	13.8 ± 0.3	2.8 ± 0.2	2.5 ± 0.1
$D^-\rho^+$	$K^-\pi^+\pi^+$	34.7 ± 2.5	-3.9 ± 2.1	28.4 ± 0.6	3.0 ± 0.1	2.8 ± 0.1
	$K^0_S\pi^+$	$xx \pm xx$	$xx \pm xx$	28.0 ± 1.8	2.9 ± 0.3	2.9 ± 0.1
$D^-a_1^+$	$K^-\pi^+\pi^+$	12.1 ± 0.8	-4.1 ± 0.7	9.4 ± 0.2	2.7 ± 0.2	2.4 ± 0.1
	$K^0_S\pi^+$	12.5 ± 2.8	-1.7 ± 2.1	9.1 ± 0.9	2.3 ± 0.4	2.3 ± 0.1

Table 19: Observed yields for B^0 decay modes.

B^0 mode	D mode	Observed Yield
$D^{*-}\pi^+$	$K^-\pi^+$	546 ± 25
	$K^-\pi^+\pi^0$	375 ± 21
	$K^0_S\pi^+\pi^-$	131 ± 13
	$K^-\pi^+\pi^+\pi^-$	504 ± 24
$D^{*-}\rho^+$	$K^-\pi^+$	305 ± 20
	$K^-\pi^+\pi^0$	232 ± 21
	$K^0_S\pi^+\pi^-$	68 ± 17
	$K^-\pi^+\pi^+\pi^-$	287 ± 20
$D^{*-}a_1^+$	$K^-\pi^+$	304 ± 20
	$K^-\pi^+\pi^0$	175 ± 18
	$K^0_S\pi^+\pi^-$	39 ± 11
	$K^-\pi^+\pi^+\pi^-$	196 ± 16
$D^-\pi^+$	$K^-\pi^+\pi^+$	1596 ± 44
	$K^0\pi^+$	165 ± 14
$D^-\rho^+$	$K^-\pi^+\pi^+$	809 ± 36
	$K^0\pi^+$	80 ± 11
$D^-a_1^+$	$K^-\pi^+\pi^+$	459 ± 28
	$K^0\pi^+$	66 ± 10
Total		6389 ± 93

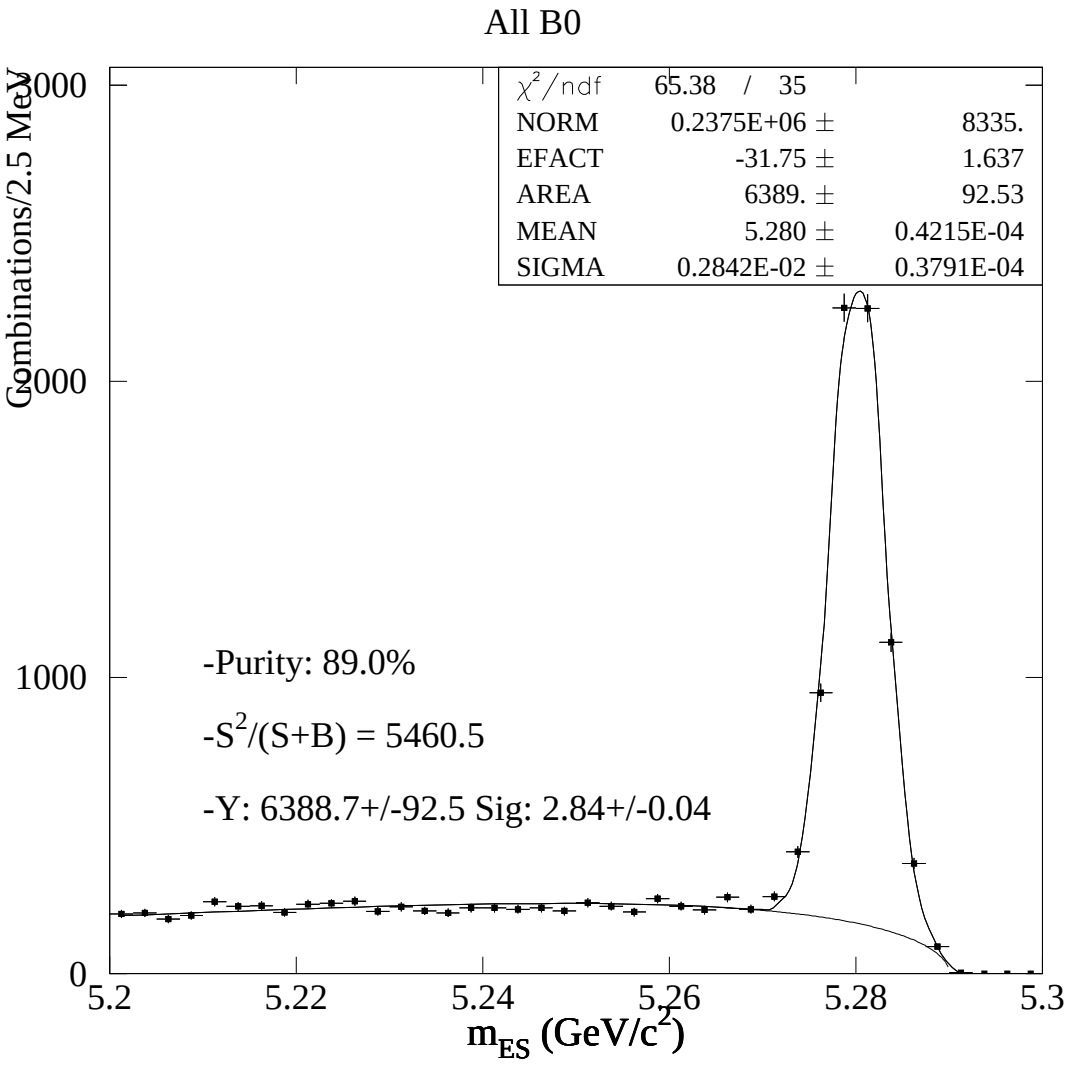

Figure 42: Combined distribution for $m_{\rm ES}$ from all hadronic B^0 modes.

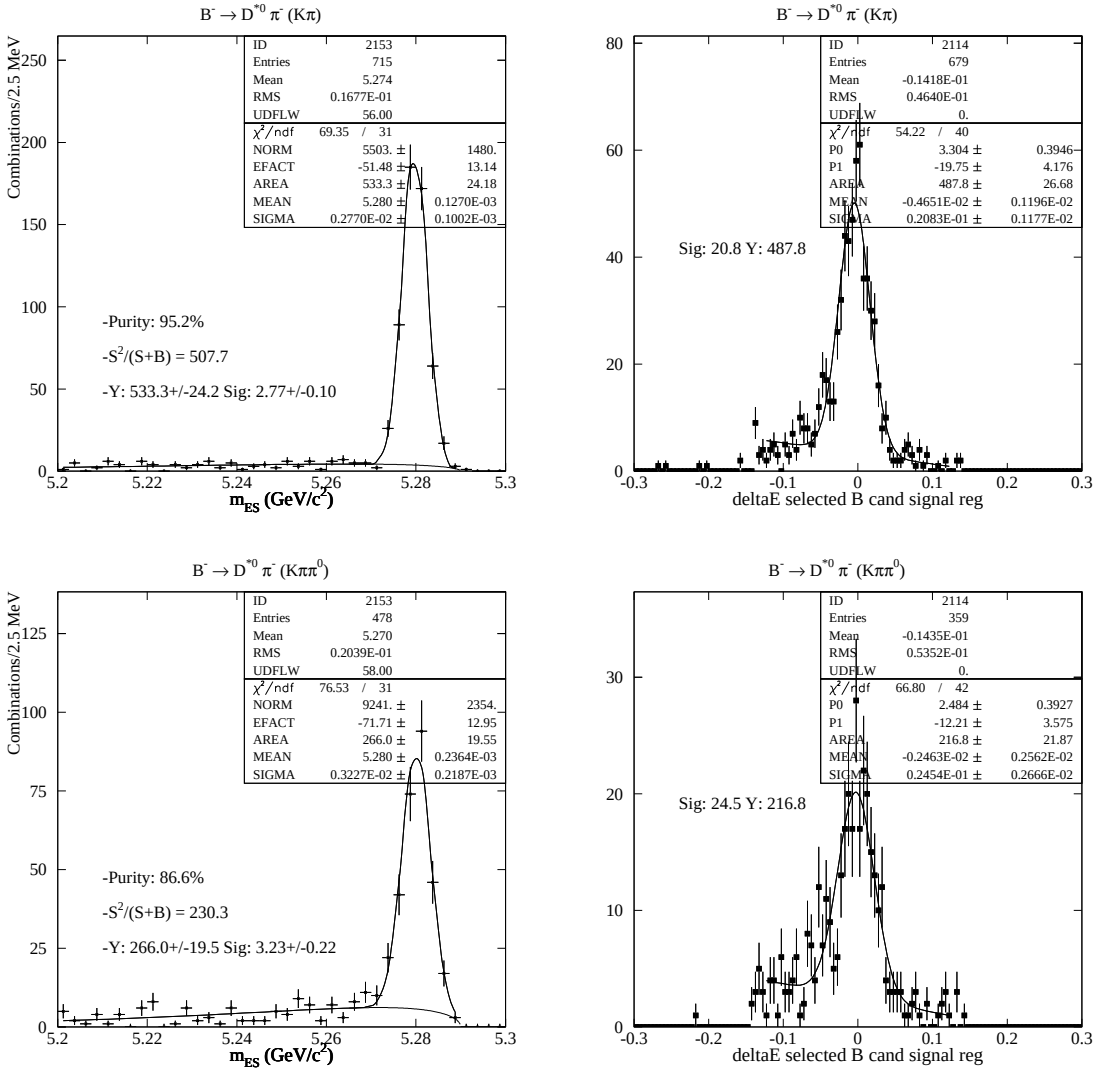

Figure 43: $B^- \to D^{*0}\pi$ for $D^0 \to K^-\pi^+$ (top) and $D^0 \to K^-\pi^+\pi^0$ (bottom). $m_{\rm ES}$ for $|\Delta E\ | < 3\sigma_{\Delta E}$ (left), ΔE for $|m_{\rm ES} - {m_{\rm ES}}^0| < 3\sigma_{m_{\rm ES}}$ (right).

5 B^- Decays

Here we provide tables of resolutions and yields for the B^0 decay modes reconstructed.

For each individual decay chain, the distribution of $m_{\rm ES}$ for $|\Delta E\ | < 3\sigma_{\Delta E}$ and ΔE for $|m_{\rm ES} - {m_{\rm ES}}^0| < 3\sigma_{m_{\rm ES}}$ is provided. The same plots are also shown summed over D^0 or D^+ modes. These are shown as Figures 43 through 46.

The fit results for $\sigma_{m_{\rm ES}}$ and $\sigma_{\Delta E}$ in Monte Carlo and data are summarized in Table 18. The fitted numbers of events are shown in Table 19.

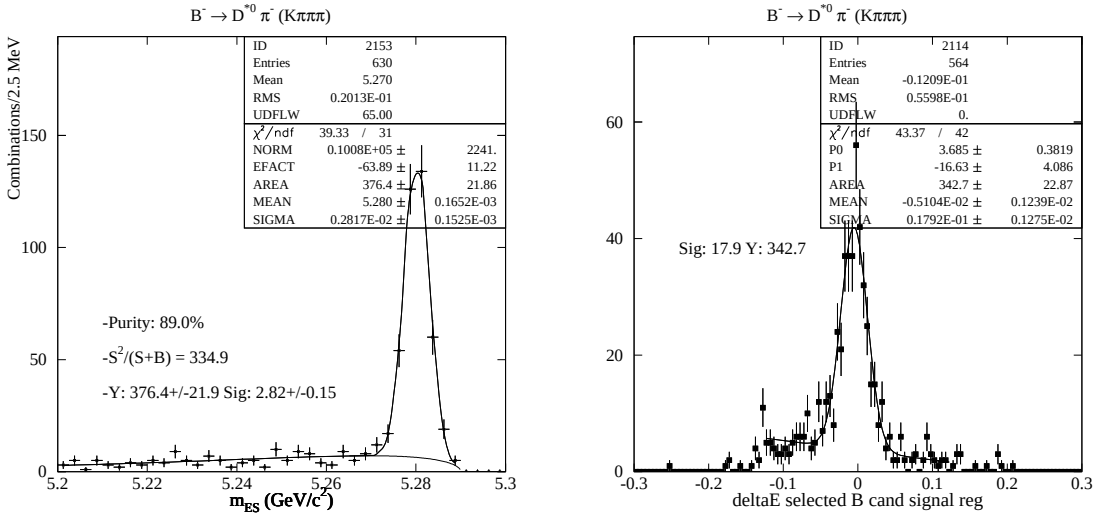

Figure 44: $B^- \to D^{*0}\pi$ for $D^0 \to K^-\pi^+\pi^-\pi^+$. $m_{\rm ES}$ for $|\Delta E\ | < 3\sigma_{\Delta E}$ (left), ΔE for $|m_{\rm ES} - {m_{\rm ES}}^0| < 3\sigma m_{\rm ES}$ (right).

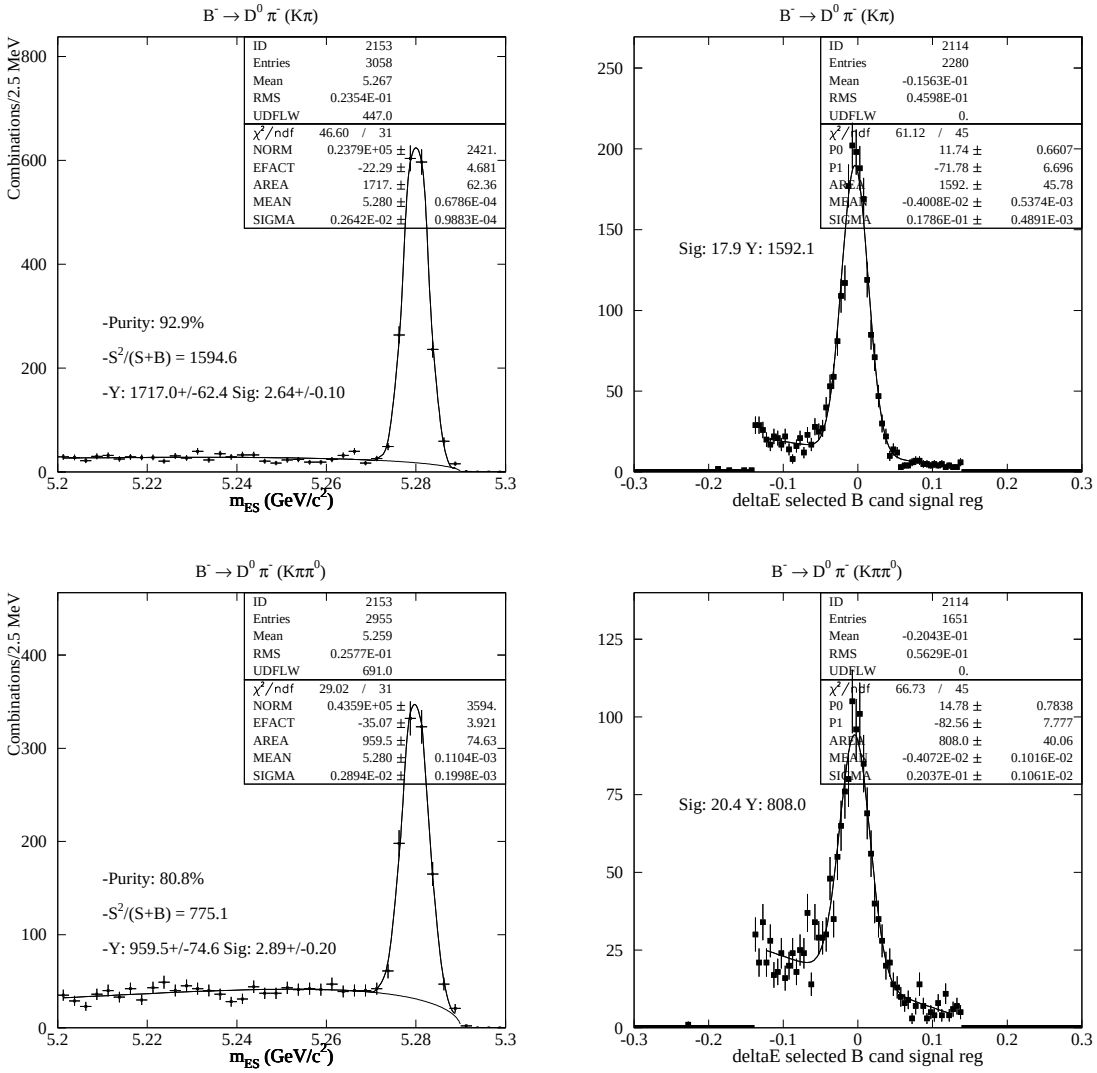

Figure 45: $B^- \to D^0\pi$ for $D^0 \to K^-\pi^+$ (top) and $D^0 \to K^-\pi^+\pi^0$ (bottom). $m_{\rm ES}$ for $|\Delta E\ | < 3\sigma_{\Delta E}$ (left), ΔE for $|m_{\rm ES} - {m_{\rm ES}}^0| < 3\sigma_{m_{\rm ES}}$ (right).

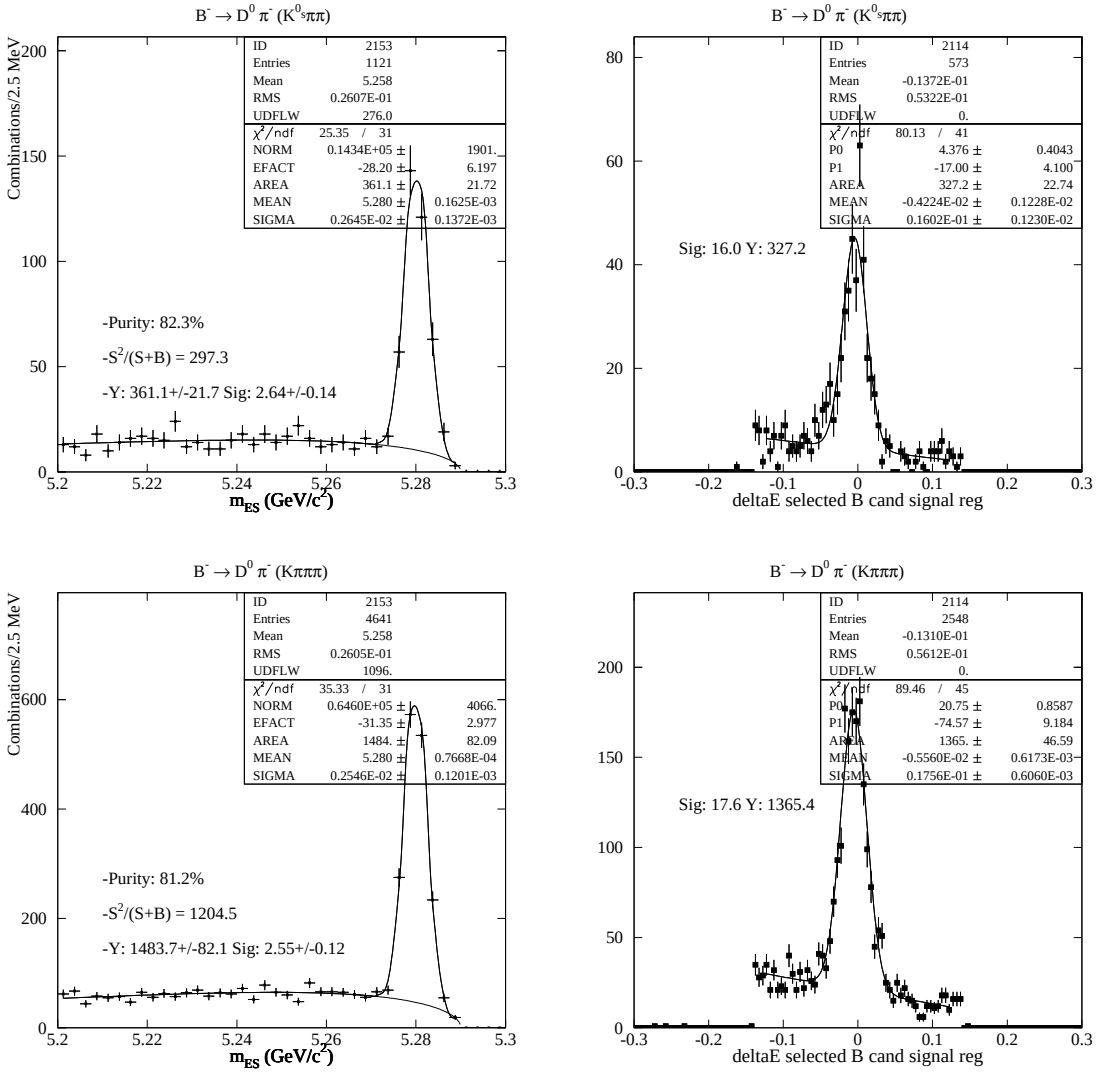

Figure 46: $B^- \to D^0\pi$ for $D^0 \to K^0_S\pi^+\pi^-$ (top) and $D^0 \to K^-\pi^+\pi^-\pi^+$ (bottom). $m_{\rm ES}$ for $|\Delta E\ | < 3\sigma_{\Delta E}$ (left), ΔE for $|m_{\rm ES} - {m_{\rm ES}}^0| < 3\sigma m_{\rm ES}$ (right).

Table 20: Observed and predicted resolution for ΔE and $m_{\rm ES}$ for B^- decay modes.

B mode	D mode	$\sigma_{\Delta E}$ data	ΔE offset	$\sigma_{\Delta E}$ MC	$\sigma_{m_{\rm ES}}$ data	$\sigma_{m_{\rm ES}}$ mc
$D^{*0}\pi^+$	$K^-\pi^+$	19.2 ± 1.0	-4.1 ± 1.0	19.2 ± 1.0	3.1 ± 0.1	3.1 ± 0.1
	$K^-\pi^+\pi^0$	21.2 ± 2.0	-4.2 ± 1.8	21.3 ± 1.9	3.4 ± 0.2	3.4 ± 0.2
	$K^-\pi^+\pi^+\pi^-$	15.7 ± 0.9	-5.4 ± 0.9	15.7 ± 0.9	3.0 ± 0.1	3.0 ± 0.1
$D^0\pi^+$	$K^-\pi^+$	17.9 ± 0.5	-4.0 ± 0.5	17.9 ± 0.5	2.6 ± 0.1	2.6 ± 0.1
	$K^-\pi^+\pi^0$	20.2 ± 1.0	-3.5 ± 1.0	20.2 ± 1.0	2.9 ± 0.1	2.9 ± 0.1
	$K^0_S\pi^+\pi^-$	16.3 ± 1.2	-4.5 ± 1.3	16.3 ± 1.2	2.6 ± 0.1	2.6 ± 0.1
	$K^-\pi^+\pi^+\pi^-$	17.3 ± 0.6	-5.4 ± 0.6	17.3 ± 0.6	2.5 ± 0.1	2.5 ± 0.1

Table 21: Observed yields for B^- decay modes.

B^+ mode	D mode	Observed Yield
$D^{*0}\pi^+$	$K^-\pi^+$	533 ± 24
	$K^-\pi^+\pi^0$	266 ± 20
	$K^-\pi^+\pi^+\pi^-$	377 ± 22
$D^0\pi^+$	$K^-\pi^+$	1716 ± 44
	$K^-\pi^+\pi^0$	960 ± 37
	$K^0_S\pi^+\pi^-$	361 ± 22
	$K^-\pi^+\pi^+\pi^-$	1484 ± 44
Total		5686 ± 155

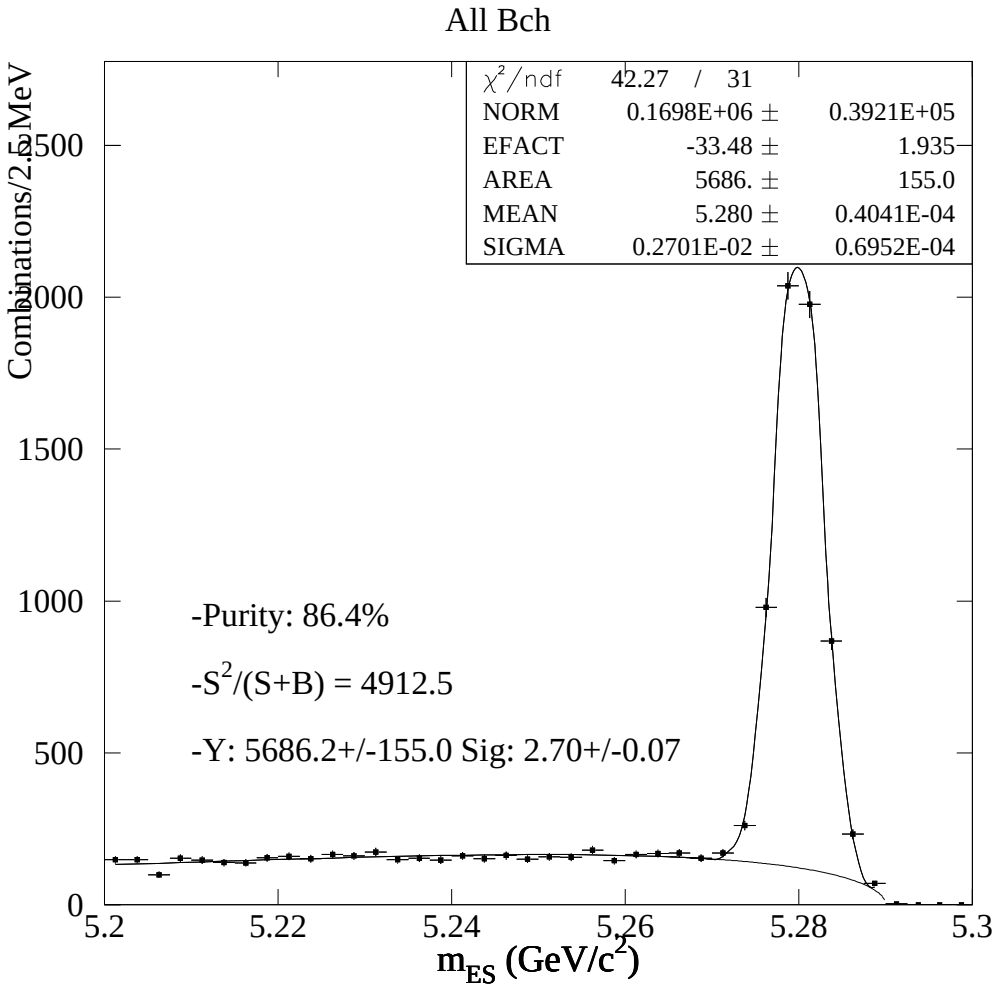

Figure 47: Combined distribution for $m_{\rm ES}$ from all hadronic B^- modes.

6 Conclusions

conclusions

References

[1] "Review of Particle Properties", European Physical Journal C3, Number 1–4 (1998).

[2] Charmonium AWG and Tracking Group, "Studies on $K^0_S \to \pi^+\pi^-$ Reconstruction: Status Report", BaBar Analysis Document 019, Version 1 (2000).

[3] Neutral Identification and Reconstruction AWG, "Studies on π^0 Reconstruction: Status Report", BaBar Analysis Document 020, Version 1 (2000).

[4] C.Hearty, "Hadronic Event Selection and B-Counting for Inclusive Charmonium Measurements", *BABAR* Analysis Document 30 (2000).

[5] W.T.Ford, "Choice of Kinematic Variables in B Meson Reconstruction—Take 3", *BABAR* Analysis Document 53 (2000); ΔE is a Lorentz invariant, and could be calculated using lab frame 4-vectors.

[6] O.Long, "Measurement of the slow pion relative efficiency using helicity distributions", *BABAR* Analysis Document 54 (2000).

[7] G.Raven, "Determination of the tracking efficiency for high momentum tracks", *BABAR* Analysis Document 61 (2000).

[8] J.Smith, A.Soffer, and R.Waldi, "Recommendation for Exclsuive B Reconstruction Analysis Variables", *BABAR* Note 497 (1999).

[9] Philip Hart, "Elements of Selecting Good Runs", `http://www.slac.stanford.edu/~philiph/rqm/7mar.pdf` (2000).

[10] `http://www.slac.stanford.edu/BFROOT/www/doc/workbook/nanomicro/v8.6/Micro/Cand_Lists.html`

[11] `http://www.slac.stanford.edu/BFROOT/www/Physics/BaBarData/ChangesSince8.6.2a.html`

[12] M.S. Alam *et al.*, Phys. Rev. **D50** (1994) 43.

[13] E691 Collab., J. C. Anjos *et al.*, Phys. Rev. **D48** (1993) 56.

[14] `http://www.slac.stanford.edu/~chcheng/talk/kpipi0DalitzFunc/index.html`

[15] Presentations of B. Brau and P. Robbe, `http://babar-hn.slac.stanford.edu:5090/HyperNews/get/EHBDOC/241/1.html`

[16] BaBar Analysis Document #105, *BRecoUser User's Guide.*

[17] BaBar Analysis Document #102, *The BaBar Vertexing.*

[18] BaBar Analysis Document #130, *Vertexing Performances and systematic checks with fully reconstructed B events.*